BINDING SERVICES
Tel +44 (0)29 2087 4949
Fax +44 (0)29 20371921
e-mail bindery@cardiff.ac.uk

Low Complexity Channel Shortening and Equalization for Multi-Carrier Systems

Thesis submitted to the University of Cardiff in candidature for the degree of Doctor of Philosophy.

Rab Nawaz

Center of Digital Signal Processing
Cardiff University
2006

ProQuest LLC
789 East Eisenhower Parkway
P.O. Box 1346
Ann Arbor, MI 48106-1346

DECLARATION

This work has not previously been accepted in substance for any degree and is not being concurrently submitted in candidature for any degree.

Signed ..... (candidate)
Date 19-09-06

STATEMENT 1

This thesis is the result of my own investigation, except where otherwise stated. Other sources are acknowledged by giving explicit reference. A bibliography is appended.

Signed ..... (candidate)
Date ...19-09-06...

STATEMENT 2

I hereby give consent for my thesis, if accepted, to be available for photocopying and for inter-library loan, and for the title and summary to be made available to outside organizations.

Signed ..... (candidate)
Date 19-09-06

ABSTRACT

A new time domain blind adaptive channel shortening algorithm for Discrete Multi Tone (DMT)-based multicarrier systems is first proposed. It is computationally less expensive, and more robust to non-Gaussian impulsive noise environments than a recently reported Sum squared Autocorrelation Minimization (SAM) algorithm. A "left" initialization scheme is also suggested for Carrier Serving Area (CSA) loop Asymmetric Digital Subscriber Line (ADSL) channels. Simulation studies show that by a proper selection of the learning parameter i.e., the step size, the bit rates achieved by the SAM algorithm when operating in an environment contaminated by Additive White Gaussian Noise (AWGN) can be further improved.

Next a novel time domain low complexity blind adaptive channel shortening algorithm called Single Lag Autocorrelation Minimization (SLAM) is introduced. The algorithm is totally blind in the sense that it does not require a prior knowledge about the length of the channel impulse response. The proposed novel stopping criterion freezes the adaptation of the SLAM algorithm when the maximum amount of Inter Symbol Interference (ISI) is cancelled. As such, the stopping criterion can also be used with SAM.

An attractive alternate frequency domain equalization approach for multicarrier systems is Per Tone Equalization (PTEQ). This scheme en-

ables true signal-to-noise ratio optimization to be implemented for each tone and it always achieves higher bit rates than Time domain Equalizer (TEQ) based channel shortening schemes but at the price of increased computational complexity and higher memory requirements. A low complexity (PTEQ) scheme is, therefore, finally proposed. The complexity of the PTEQ can be traded off with the complexity of the timing synchronization within the system. In particular, it is shown that the use of more than one difference terms and hence a long equalizer in the PTEQ scheme is generally redundant. The PTEQ scheme assumes knowledge of the channel impulse response. In this case synchronization is trivial and it is possible to use only a length two PTEQ equalizer and attain essentially identical bit rate performance to a PTEQ equalizer with length matched to the cyclic prefix. This observation allows for a substantial reduction in computational complexity of the PTEQ scheme in both initialization and data transmission modes. For a reasonable range of values of synchronization error, δ, around the optimal value of $\delta = 0$, the performance of this length two equalizer is shown to remain relatively constant. For positive synchronization errors, however, the required PTEQ equalizer length is proportional to the synchronization error. A low complexity blind synchronization method is ultimately suggested which is based on the construction of the difference terms of the PTEQ scheme.

To my loving wife Iram

ACKNOWLEDGEMENTS

I would like to thank my thesis advisor Prof. Jonathon Chambers, without his invaluable support and mentoring this thesis would have not been accomplished. He manages to strike the perfect balance between providing direction and encouraging independence. He has contributed to all papers and the thesis with a major impact. He has my deepest respect professionally and personally. Dr. Rick Martin from the Cornell University USA, contributed greatly to my understanding of the material in this thesis. I also thank Prof. Brian Evans of the University of Texas, Austin for the DMT simulation toolbox. I am grateful to Dr. Andreas Jakobsson for his guidance with the issues in LaTeX. Financial support for this research was provided by grants from the Teachers and Researchers Overseas Scholarship Scheme (TROSS) of the Ministry of Science & Technology, Govt. of Pakistan; many thanks go to Mr. Amjad Hussain for administering this scheme. The research office staff within the School of Engineering have also been extremely helpful. Other friends whose encouragement and moral support have remained constant are Dr. Waseem and Dr. Qaisar. I thank my wife Iram for her support during the write up stage. Finally, I would like to thank my family for their patience and encouragement while we have been separated for many years.

PUBLICATIONS

- R. Nawaz and J. A. Chambers,"Robust blind adaptive channel shortening in impulsive noise environments," *12th European Signal Processing Conf. (Eusipco)*, Vienna, Austria, Sep. 2004.

- R. Nawaz and J. A. Chambers, "Partial equalization of multicarrier systems in non-Gaussian noise," *Institute of Mathematics & its applications (IMA) conf. on Mathematics in Signal Processing VI*, Cirencester, UK, Dec. 2004.

- R. Nawaz and J. A. Chambers, "Blind adaptive channel shortening by single lag auto-correlation minimization (SLAM)," *Electronics Letters*, vol. 40, pp. 1609-1611, Dec. 2004.

- R. Nawaz and J. A. Chambers, "A novel single lag auto-correlation minimization (SLAM) algorithm for blind adaptive channel shortening," *in Proc. IEEE Int. Conf. on Acoustics, Speech, and Signal Processing*, Philadelphia, Mar. 2005.

- R. Nawaz and J. A. Chambers, "Low complexity Per Tone equalization for DMT-based systems," *The Eighth IASTED International Conf. on Signal and Image Processing (SIP 2006)*, Honolulu, Hawaii, USA, Aug. 2006.

Acronyms

4G	Fourth Generation
ADSL	Asymmetric Digital Subscriber Line
AR	Auto Regressive
AWGN	Additive White Gaussian Noise
CLT	Central Limit Theorem
CMA	Constant Modulus Algorithm
CP	Cyclic Prefix
CSA	Carrier Serving Area
DAB	Digital Audio Broadcast
dB	deci-Bel
DD-LMS	Decision-Directed LMS
DFT	Discrete Fourier Transform
DMT	Discrete Multitone
DS-CDMA	Direct Sequence Code Division Multiple Access
DVB	Digital Video Broadcast

EC-ADSL	Echo Cancelled ADSL EC-ADSL
FDM-ADSL	Frequency Division Multiplexed ADSL
FEQ	Frequency domain Equalizer
FFT	Fast Fourier Transform
FIR	Finite Impulse Response
FLOMs	Fractional Lower Order Moments
FRODO	Forced Redundancy with Optional Data Omission
G-SNR	Geometric-SNR
ICI	Inter Carrier Interference
ISI	Inter Symbol Interference
LMS	Least Mean Square
MA	Moving Average
MBR	Maximum Bit Rate
MD	Minimum Dispersion
MERRY	Multicarrier Equalization by Restoration of Redundancy
MFB	Matched Filter Bound
MIMO	Multiple Input Multiple Output
MLSE	Maximum Likelihood Sequence Estimation
MMSE	Minimum Mean Squared Error
MSSNR	Maximum Shortening Signal to Noise Ratio

NEXT	Near End Crosstalk
OFDM	Orthogonal Frequency Division Multiplexing
POTS	Plain Old Telephone Service
PTEQ	Per Tone Equalization
QAM	Quadrature Amplitude Modulation
RF	Radio Frequency
RLS	Recursive Least Squares
SαS	Symmetric Alpha Stable
SAAM-C	SAAM with Center spike initialization
SAAM-L	SAAM with Left initialization
SAAM	Sum-Absolute Autocorrelation Minimization
SAM-opt	SAM with optimal step size
SAM	Sum-squared Autocorrelation Minimization
SISO	Single Input Single Output
SLAM	Single Lag Autocorrelation Minimization
SNR	Signal to Noise Ratio
TEQ-FB	TEQ-Filter Bank
TEQ	Time domain Equalizer
TIR	Target Impulse Response
VDSL	Very high bit rate DSL

WSS Wide Sense Stationary

CONTENTS

List of Figures

List of Tables

Chapter 1

INTRODUCTION

1.1 Introduction and Motivation

Orthogonal Frequency Division Multiplexing (OFDM) is a multicarrier modulation scheme for wireless systems. OFDM systems efficiently deal with large channel delay spreads with a reasonable implementation complexity as compared to single carrier systems. The basic principle of OFDM is to split a high-rate data stream into a number of lower rate streams that are transmitted simultaneously over a number of subcarriers or subchannels. Because the symbol duration increases for the lower rate parallel subcarriers, the relative amount of dispersion in time caused by multipath delay spread is decreased. ISI is eliminated almost completely by introducing a guard time equal to the order of the channel impulse response in every OFDM symbol. In the guard time, the OFDM symbol is cyclically extended to avoid Intercarrier Interference (ICI). That is why the guard time is also called the cyclic prefix (CP). Due to ISI and ICI free transmission, the equalization in OFDM is trivial and is performed by a bank of single tap Frequency domain Equalizers (FEQs) after the Fast Fourier Transform (FFT) to compensate for the amplitude and phase distortion within each subchannel. The complexity of an OFDM system is largely de-

termined by the FFT in contrast to single-carrier systems where the implementation complexity is dominated by equalization. The processing complexity of an OFDM system is significantly less than that of a single carrier system for the same amount of delay spread [1]. In the wireline counterparts of OFDM, the multicarrier modulation is named DMT. DMT modulation is standardized for ADSL and Very-high-bit-rate DSL (VDSL) systems. ADSL and VDSL provide high speed data service to residences and offices on the existing coppers wires of the telephone network. The data rates of latest versions of ADSL systems are up to 10Mbps and 1Mbps for the downstream and upstream transmission respectively. VDSL systems provide data rates up to 13 Mbps and 3 Mbps for the downstream and upstream transmission respectively [2]. Compared to OFDM, DMT modulation has an extra ability to perform bit loading due to the slow varying subchannel Signal to Noise Ratio (SNR) of the wireline channel [3]. The signal constellations used for different carriers can be independently selected in accordance with the channel attenuation and interference at the corresponding frequencies. The other difference is that, the transmitted signal is at baseband and must be real. The symmetry property of the FFT is exploited by using $N/2$ instead of N inputs, and then conjugating and mirroring the first half of the tones such that the resulting N IFFT inputs obey conjugate symmetry. This results in a real IFFT output [4].

If v is the length of CP and N is the actual data symbol duration, the bandwidth loss due to the insertion of CP is v/N. In order to minimize this bandwidth loss, it is desirable to have the symbol duration much larger than the CP. It cannot be arbitrarily large, as a large symbol duration means more carriers with a smaller carrier spacing reducing

the tolerance to the channel time variations, a larger implementation complexity, and more sensitivity to phase noise and frequency offset, as well as an increased peak-to-average power ratio [1]. In practical applications, the CP is chosen to be equal to the channel impulse response length minus 1, and the symbol duration is then selected so as to keep the bandwidth loss below 25%. The insertion of CP is shown in Figure (1.1) for the length of the channel 4 and the actual data symbol duration of 12.

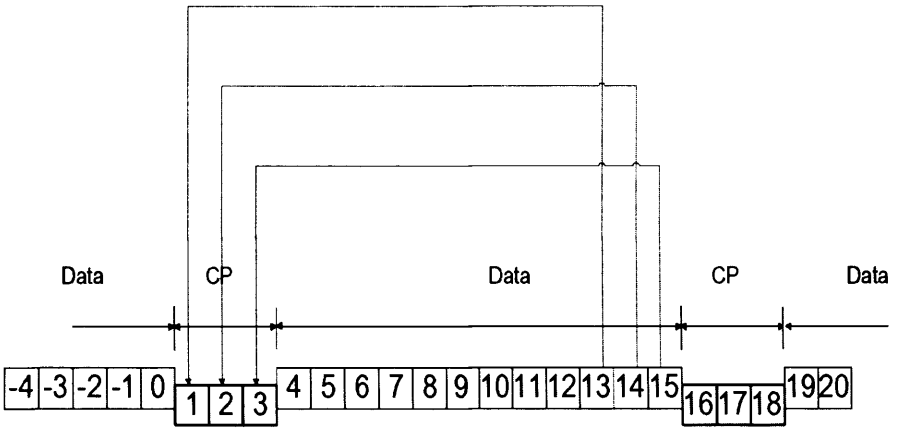

Figure 1.1. Loss of throughput due to insertion of the CP.

For long impulse response channels, the insertion of the CP becomes prohibitive. The symbol duration has to be impractically large to keep bandwidth loss small. What is done instead, is that a small value of CP is chosen so that a practical value of symbol duration can be used to keep the bandwidth loss small. Further, TEQ, usually an FIR filter, is inserted at the receiver front end. The convolution of the TEQ and the actual channel yields an effective channel, having significant components in a contiguous length window equal to the $v + 1$ length. In this way, ISI and ICI is combated while keeping the loss in bandwidth at a minimum whilst using a practical value of N. Channel shortening

in multicarrier systems should be termed as "partial equalization" as compared to equalization in single carrier communication systems, because here the channel impulse response need only be shortened to the $(v+1)$ length samples rather than to one sample [5].

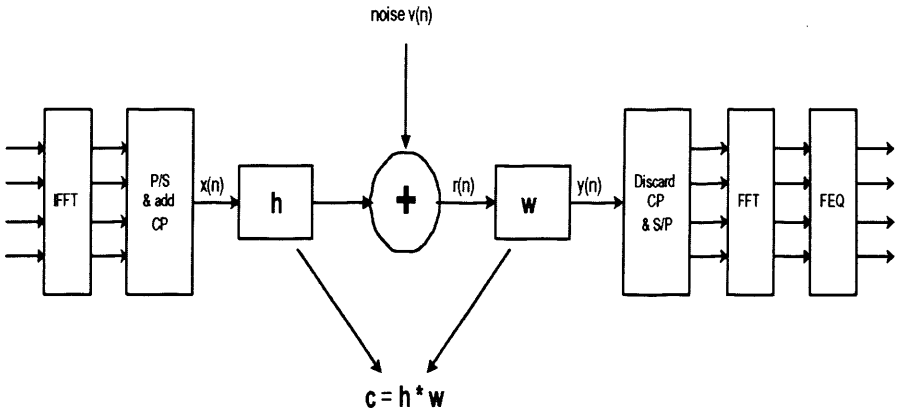

Figure 1.2. OFDM baseband system model. (I)FFT: (inverse) fast Fourier transform, P/S: parallel to serial, S/P: serial to parallel, CP: cyclic prefix, FEQ: Frequency domain Equalizer, **w**: TEQ

The baseband OFDM multicarrier model along with the TEQ is shown in Figure (1.2). The frequency-selective channel is divided into N subchannels. The input bits stream is first divided into blocks of N Quadrature Amplitude Modulation (QAM) symbols. These QAM symbols are modulated onto N subchannels. An efficient means of implementing the modulation in discrete time is to use an inverse fast Fourier transform (IFFT). The output of the IFFT is converted from parallel to serial and CP is inserted. The data are then serially transmitted. At the receiver the ISI corrupted CP is discarded and an FFT is used to demodulate the signal. Because of the nature and length of the CP, the linear convolution between the effective channel $\mathbf{c} = \mathbf{h} * \mathbf{w}$ and the transmitted signal becomes circular. Therefore, the output of the FFT at each subchannel is the multiplication of the symbol sent on that

subchannel and the frequency response of the effective channel at the subchannel plus the noise at that subchannel. Finally, the transmitted symbols are retrieved by dividing this output by the one-tap FEQs which are actually the frequency response of the effective channel at respective subcarriers.

Channel shortening was first used in the 1970's to reduce the complexity of Maximum Likelihood Sequence Estimation (MLSE) in single carrier communication systems [6, 7]. For an alphabet size $\mathcal{A}$ and effective channel length $L_c + 1$, the complexity of an MLSE grows as $\mathcal{A}^{(L_c+1)}$. The approach was to employ a prefilter to shorten the effective channel to a manageable length and then apply the MLSE algorithm.

Channel shortening has been proposed for use in multiuser detection [8] in Direct Sequence Code Division Multiple Access (DS-CDMA) systems. The complexity of the MLSE grows exponentially with the number of users. "Channel shortening" can be implemented to suppress L-K of the scalar channels and retain the other K channels, effectively reducing the number of users from L to K. Then the MLSE can be implemented to recover the signals of the remaining K users. In this context, "channel shortening" means reducing the number of scalar channels rather than reducing the number of channel taps, and the mathematical structure is similar to channel shortening for MLSE applications [9].

Channel shortening can be used to reduce the complexity of ultra wideband systems [10]. Yet another application is in acoustics. Psychoacoustics defines the D50-measure for intelligibility speech as the ratio of energy in a 50 ms window of the room impulse response to the total energy of the impulse response, and optimization of this measure can

be performed by a channel shortener [11].

Channel shortening has found its revival and main use in multicarrier communication systems [12]. Examples of multicarrier communication systems include wireless local area networks (IEEE 802.11 a/g, HIPERLAN/2) [13], wireless metropolitan area networks (IEEE 802.16) [14], Digital Audio Broadcast (DAB) [15] and Digital Video Broadcast (DVB) [16] in Europe, satellite radio (Sirius and XM Radio) [17], and the proposed standard for multiband ultra wideband (IEEE 802.15.3a). Examples of wireline multicarrier systems include power line communications (HomePlug) [18] and digital subscriber lines (DSL) [19]. OFDM in combination with MIMO technology is also being investigated for the Fourth Generation (4G) mobile phone systems [20]. There has been extensive research in proposing the TEQ algorithms. A literature survey of TEQ design methods is given in Chapter 2. However there remains need for further work to reduce the computational complexity of previously proposed algorithms and also to mitigate the effects of impulsive noise for the channel shortening algorithms. This is the focus of the thesis. Channel shortening has also been used in the context of Multiple Input Multiple Output (MIMO) systems. However, these works only extend the channel shortening algorithms previously proposed for Single Input Single Output (SISO) system models to the MIMO case. Hence, this thesis considers only SISO systems, as the work can potentially be extended to MIMO systems.

1.2 Organization of the thesis

The remainder of the thesis is organized as follows. Chapter 2 presents a literature survey of the previous TEQ design methods for multicarrier

systems.

Chapter 3 proposes a robust blind adaptive channel shortening algorithm. The algorithm is based on the Sum-Absolute Autocorrelation Minimization (SAAM) of the effective channel outside the window of desired length. The algorithm approaches the Maximum Shortening Signal to Noise Ratio (MSSNR) solution of [21] in AWGN conditions. It is computationally less expensive, and more robust to non-Gaussian impulsive noise environments than a recently reported SAM algorithm [22]. The non-Gaussian impulsive noise has been modeled as Gaussian-mixture and as α-stable distributions. Due to the *quasi* minimum phase nature of the channel impulse response of ADSL, a "left" initialization scheme is suggested which further enhances the convergence performance of SAAM. Additional studies have been undertaken showing that by a proper selection of parameters e.g., the step size, the bit rates achieved by SAM in AWGN conditions can be improved as well.

Chapter 4 addresses the complexity reduction and convergence issues with SAM [22]. The drawback with SAM is that it has a significantly higher computational complexity and it does not have any stopping criterion to freeze the TEQ when the shortening signal to noise ratio (SSNR) of the effective channel reaches its maximum. The main argument of this chapter is that identical channel shortening can be achieved by minimizing a single autocorrelation. The proposed SLAM algorithm has, therefore, relatively low complexity and unlike SAM, it does not require, a priori, the knowledge of the length of the original channel. The novel stopping criterion freezes the adaptation of the TEQ when maximum SSNR has been achieved. As such, the stopping criterion

can be used with SAM as well.

Chapter 5 discusses the alternate equalization scheme called PTEQ for multicarrier systems. Van Acker et al. [23] proposed PTEQ, where equalization is performed with a T-tap equalizer after the FFT-demodulation for each tone separately. This scheme enables true signal-to-noise ratio optimization to be implemented for each tone. The resulting capacity of the PTEQ scheme is always higher and a smoother function of the synchronization delay as compared to the TEQ scheme [23]. Although the complexities of the PTEQ and the TEQ schemes are approximately the same during data transmission modes [23], the PTEQ scheme has very large complexity during the initialization mode. This problem is addressed in this chapter. A low complexity PTEQ scheme for DMT-based systems is, therefore, proposed. It is shown that the use of more than one difference term in the PTEQ scheme is generally redundant. The PTEQ scheme assumes knowledge of the channel impulse response. In this case synchronization is trivial and it is possible to use only a length two PTEQ equalizer and attain essentially identical bit rate performance as a PTEQ equalizer with length matched to the cyclic prefix. This observation allows for a substantial reduction in computational complexity of the PTEQ scheme in both initialization and data transmission modes. Simulations also show that for a reasonable range of values of synchronization error, δ around the optimal values of $\delta = 0$, the performance of this length two equalizer is relatively insensitive. For positive synchronization errors, however, the required PTEQ equalizer length is proportional to the synchronization error, which is a consequence of strong intercarrier interference ICI in the received signal. A low complexity blind synchronization method

is also suggested which is intuitively based on the construction of the difference terms of the PTEQ scheme.

Chapter 6 concludes this thesis and points out possible areas for further research.

Chapter 2

LITERATURE SURVEY

This chapter surveys different TEQ design structures.

2.1 Minimum Mean-Squared Error Method

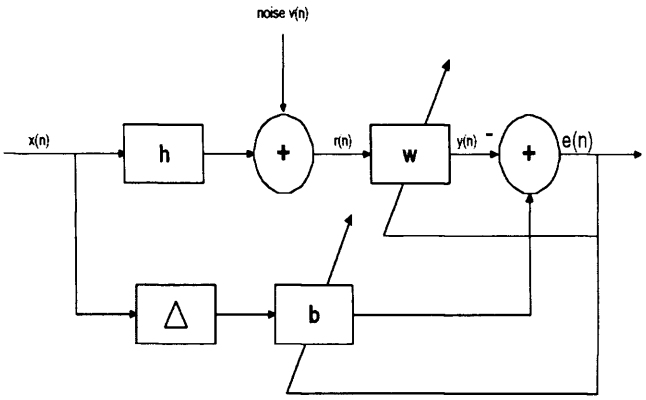

Figure 2.1. MMSE channel shortening

In [24] the Minimum Mean Squared Error (MMSE) TEQ design method is proposed. Its block diagram is shown in Figure (2.1). Here $\mathbf{b}$ is a $(v + 1)$ tap long Target Impulse Response (TIR). The TEQ $\mathbf{w}$ is designed to minimize the mean squared error between its output and the Δ delayed output of $\mathbf{b}$. In [25] an iterative implementation of the MMSE channel shortening algorithm is detailed. The error as in Equation (2.1.1) is defined in [26] and also includes the signal and noise

autocorrelation matrices in the MMSE channel shortening framework

$$\begin{aligned} E[e^2] &= E\left(\mathbf{w}^T\mathbf{r} - \mathbf{b}^T\mathbf{x}\right)^2 \\ &= \mathbf{w}^T\mathbf{R}_{rr}\mathbf{w} + \mathbf{b}^T\mathbf{R}_{xx}\mathbf{b} - 2\mathbf{w}^T\mathbf{R}_{rx}\mathbf{b} \end{aligned} \tag{2.1.1}$$

where $\mathbf{R}_{xx}$, $\mathbf{R}_{rx}$ and $\mathbf{R}_{rr}$ are the transmitted signal auto-correlation, channel input-output cross-correlation and the channel output auto-correlations matrices, respectively. For a given Δ, the optimal TEQ is given by

$$\mathbf{w}_{opt} = \mathbf{R}_{rr}^{-1}\mathbf{R}_{rx}\mathbf{b} \tag{2.1.2}$$

Substituting Equation (2.1.2) into Equation (2.1.1)

$$E[e^2] = \mathbf{b}^T.(\mathbf{R}_{xx} - \mathbf{R}_{rx}^T\left(\mathbf{R}_{rr}^{-1}\right)^T\mathbf{R}_{rx}).\mathbf{b} = \mathbf{b}^T.O.\mathbf{b} \tag{2.1.3}$$

Minimizing this expression, the target impulse response $\mathbf{b}$ is calculated, which is the eigenvector corresponding to the minimum eigenvalue of the matrix O then the TEQ $\mathbf{w}$ is designed using Equation (2.1.2). A unit tap or unit norm constraint is imposed on $\mathbf{b}$ to avoid the trivial solution $\mathbf{w} = 0$. There has been a flurry of research in designing MMSE TEQ. In [27] a good literature survey of the MMSE TEQ design methods is given. Most of these approaches try to minimize the complexity of the MMSE channel shortening.

The TEQ design for Frequency Division Multiplexed ADSL (FDM-ADSL) is somewhat different than that for Echo Cancelled ADSL (EC-ADSL). The FDM-ADSL allocates separate frequency bands for the down- and upstream transmission. To achieve this, it uses sharp filters at the analogue front end of the receiver. The EC-ADSL uses

overlapping spectra for up-and downstream transmission and applies Echo-Canceling [5]. The authors in [28] note that the MMSE TEQ can have high gain in the FDM-ADSL stopband region i.e., the upstream transmission band. The Discrete Fourier Transform which comes after the TEQ, has relatively high spectral sidelobes [5]. Due to these sidelobes, spreading of noise or leakage occurs at the receiver. A TEQ, that boosts the stop band noise or the near end cross talk from the local upstream transmission, significantly drops the SNR of the used subcarriers. The authors modify the MMSE cost function to include suppression of the TEQ energy in the stop band. Their simulations demonstrate a 35% increase in the bit rate of the system.

A detailed comment in [29] about MMSE channel shortening is worth highlighting. The MMSE method minimizes the difference between the TIR and the effective impulse response. It minimizes both the difference inside the target window and outside the target window. However, the difference between the effective impulse response and TIR inside the target window does not cause any ISI. Furthermore, the TIR and effective impulse responses generally have larger magnitude inside the target window than outside, which means that the difference between them inside the window causes the major part of the error. This means that the MMSE method primarily tries to minimize the difference inside the window, which does not cause ISI, than outside the window, which causes ISI. Therefore, minimizing the MSE to remove ISI is not a good choice to design a TEQ for discrete multitone modulation.

2.2 Maximum Shortening Signal-to-Noise Ratio Method

It is generally not possible to shorten the impulse response perfectly. Some energy will lie outside the largest $v+1$ consecutive samples of the effective channel. What is required is to force as much of the effective channel's impulse response as possible to lie in $v+1$ consecutive samples. The MSSNR TEQ design method of [21] maximizes the ratio of the effective channel impulse response energy within a target window length $v+1$ samples to the energy of the channel outside of the window. With reference to Figure (1.2), the effective channel impulse response is given by

$$\mathbf{h}_{eff} = \mathbf{c} = \mathbf{h} * \mathbf{w} \tag{2.2.1}$$

where $*$ denotes linear convolution. The shape of the resulting impulse response of the effective channel $\mathbf{h}_{eff}$ is usually unimportant; what is important is that the SSNR be maximized. The MSSNR channel shortening is shown in Figure (2.2).

If $\mathbf{H}$ denotes the convolution matrix of the original channel $\mathbf{h}$, then the

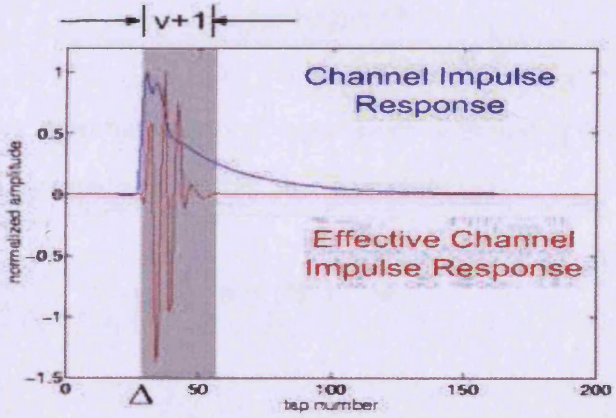

Figure 2.2. MSSNR channel shortening, showing original (blue) and the effective (pink) channel impulse responses

effective channel $\mathbf{h}_{eff} = \mathbf{Hw}$ [21]. In [21], the effective channel has

been partitioned into two parts. (1) The part of the channel samples lying within the desired $(v+1)$ window are denoted by $\mathbf{h}_{win} = \mathbf{H}_{win}\mathbf{w}$. (2) The part of the channel samples lying outside this desired window are denoted by $\mathbf{h}_{wall} = \mathbf{H}_{wall}\mathbf{w}$. $\mathbf{H}_{win}$ consists of $(v+1)$ rows of $\mathbf{H}$ starting from position $\triangle$ where $\triangle$ is the transmission delay, and $\mathbf{H}_{wall}$ consists of the remaining rows of $\mathbf{H}$. The SSNR is defined as

$$SSNR = \frac{\mathbf{w}^T\mathbf{H}_{win}^T\mathbf{H}_{win}\mathbf{w}}{\mathbf{w}^T\mathbf{H}_{wall}^T\mathbf{H}_{wall}\mathbf{w}} = \frac{\mathbf{w}^T\mathbf{B}\mathbf{w}}{\mathbf{w}^T\mathbf{A}\mathbf{w}} \tag{2.2.2}$$

The shortening is achieved by minimizing the wall energy (the denominator) while keeping the window energy (the numerator) equal to unity. If the length of the TEQ is smaller than $(v+1)$, matrix $\mathbf{B}$ is positive definite and can be decomposed by Cholesky decomposition [30]

$$\begin{aligned} B &= \mathbf{Q}\mathbf{\Lambda}\mathbf{Q}^T \\ &= (\mathbf{Q}\mathbf{\Lambda}^{1/2})(\mathbf{\Lambda}^{1/2}\mathbf{Q}^T) \\ &= (\mathbf{Q}\mathbf{\Lambda}^{1/2})(\mathbf{Q}\mathbf{\Lambda}^{1/2})^T \\ &= (\mathbf{B}^{1/2})(\mathbf{B}^T)^{1/2} \end{aligned} \tag{2.2.3}$$

where $\mathbf{\Lambda}$ is a diagonal matrix of eigenvalues of $\mathbf{B}$ and $\mathbf{Q}$ is a matrix of orthogonal eigenvectors vectors. Let us denote

$$\mathbf{s} = \left(\mathbf{B}^T\right)^{1/2}\mathbf{w} \tag{2.2.4}$$

then

$$\mathbf{w} = \left(\mathbf{B}^T\right)^{-1/2}\mathbf{s} \tag{2.2.5}$$

Then substituting Equation (2.2.5) into Equation (2.2.2)

$$SSNR = \frac{\mathbf{s}^T\mathbf{s}}{\mathbf{s}^T\mathbf{C}\,\mathbf{s}} \tag{2.2.6}$$

where $\mathbf{C} = (\mathbf{B}^{-1/2})\mathbf{A}(\mathbf{B}^T)^{-1/2}$. The MSSNR TEQ method minimizes the denominator of Equation (2.2.6) while setting its numerator equal to unity. This minimization gives the eigenvector $\mathbf{s}_{min}$ corresponding to the minimum eigenvalue of the matrix $\mathbf{C}$. The resulting TEQ is given by Equation (2.2.5)

$$\mathbf{w}_{opt} = \left(\mathbf{B}^T\right)^{-1/2}\mathbf{s}_{min} \tag{2.2.7}$$

The MSSNR method requires the knowledge of the channel and it does not take into account the noise present in the channel. Maximizing SSNR does not necessarily maximize the data rate [21]. The choice of the transmission delay, Δ which gives the best SSNR is computationally very expensive. There is a difference between the MMSE method and the MSSNR method. As mentioned before, the error definition in MMSE method also includes the difference between the effective channel and the target channel inside the window of interest. Therefore minimizing the MSE does not necessarily minimize the wall energy of the effective channel.

When the length of $\mathbf{w}$ exceeds the length of the cyclic prefix, the matrix $\mathbf{B}$ becomes singular and $(\mathbf{B})^{-1/2}$ does not exist. In [31] it was suggested to maximize the energy inside the window i.e., $\mathbf{w}^T\mathbf{B}\mathbf{w}$ while keeping the energy outside the window i.e., $\mathbf{w}^T\mathbf{A}\mathbf{w}$ equal to unity. The matrix $\mathbf{A}$ is always positive definite and the arbitrary length TEQ can be designed to obtain performance gains. The authors of [32] investigate further the work of [31] in the presence of white Gaussian and near-

and far-end crosstalk. Though their simulations show that a longer length TEQ increases the SSNR; it may not necessarily improve the subchannel SNR which is proportional to the data rate. It again shows the inadequacy of increasing the SSNR to maximize the bit rate of the system.

A low complexity sub-optimal divide and conquer TEQ design algorithm is proposed in [33]. This method separates the designing of a long length TEQ into a series of two-tap TEQs. The cost function at each iteration is the energy of the channel outside the window of interest and is changed at each iteration by the two-tap TEQ designed at the previous iteration [27]. This cost function is the same as the denominator of SSNR. The final TEQ is the convolution of all the TEQs designed at each step. This method eliminates the need for matrix inversion as in the MSSNR method and hence is less complex.

According to [34], the part of the channel response exceeding the CP length which causes ISI and ICI depends not only on its energy but also on its distance from the guard interval. Therefore, their cost function not only includes the energy of the taps of the channel outside the window of interest but also their distances from the time center of the original channel impulse response. They use the term "delay spread equalizer" as opposed to calling the MSSNR method as "energy equalizer". Their simulations show improvement in that the SNR distribution and the noise shaping by the TEQ at the subchannels does not have notches. The delay spread "equalizer" also has less sensitivity to the symbol synchronization errors. However, there is no explicit dependency on the inclusion of the channel-induced additive noise or the synchronization error in their design framework.

In [35] the algorithm of [34] is extended. Their formulation of a TEQ algorithm explicitly includes the noise and gives new penalizing functions for the delay spread of the effective channel. The objective function J is a combination of the channel shortening objective and noise-to-signal objective i.e.,

$$\begin{aligned} J &= \alpha J_{short} + (1-\alpha) J_{noise} \\ &= \alpha \frac{\sum_n f(n-n_{mid})|\mathbf{h}_{eff}|^2}{\sum_n |\mathbf{h}_{eff}|^2} \\ &\quad +(1-\alpha)\frac{\sigma^2_{noise}}{\sigma^2_{signal}\sum_n |\mathbf{h}_{eff}|^2} \end{aligned} \tag{2.2.8}$$

Here n_{mid} is the time center of $\mathbf{h}_{eff}$. $f(n)$ is a penalty function which penalizes the effective channel taps away from the time center n_{mid}. The shortening cost function penalizes all of the taps and not only the taps outside the window. The simulations show some improvement in the achievable data rates over those of [34] but there again appear notches in the subchannel SNR plot. In [36] the authors extend their work to MIMO implementation and the penalizing function is also changed to take into account only the taps outside the window.

The spectral flatness of the TEQ in the MSSNR cost function is included in [37]. The implicit flatness measure is the distance of the effective channel impulse response $\mathbf{h}_{eff}$ from the original channel impulse response $\mathbf{h}$. It seems strange though; one would not expect the effective channel to be the same as the original channel. The TEQ so designed does not have nulls in the frequency domain. Although this method shows lower SSNRs achieved as compared to the original MSSNR method, it results in higher data rates. The authors also suggest that the selection of the transmission delay should be to maximize

the SSNR rather than to maximize the SSNR as well as the flatness. In [38] a blind adaptive channel shortening algorithm based on the redundancy due to the CP in the transmitted signal is proposed. The algorithm is called MERRY (Multicarrier Equalization by Restoration of Redundancy). The following is true for the transmitted OFDM symbol in Figure (1.2)

$$x[(N+v)\cdot k+i] = x[(N+v)\cdot k+N+i] \quad i \in \{1,2,\ldots,v\} \quad (2.2.9)$$

where k is the symbol index. The input of the TEQ, $r(n)$ is given by

$$r(n) = \sum_{j=0}^{L_h} h(j)x(n-j) + v(n) \quad (2.2.10)$$

where L_h+1 is the length of the channel impulse response. $v(n)$ is the noise sample at index n. The output of the TEQ, $y(n)$, is given by

$$y(n) = \sum_{j=0}^{L_w} w(j)r(n-j) \quad (2.2.11)$$

Here L_w+1 is the length of the TEQ. The ISI destroys the relationship in Equation (2.2.9) because a channel that is longer than v samples will introduce energy into the sample $x[(N+v)\cdot k+v]$ at the receiver that is not equal to the energy received by its dual $x[(N+v)\cdot k+v+N]$ at the end of the DMT frame. Ignoring the symbol index k for simplicity, the cost function is defined as

$$J_{merry}(\triangle) = E\left(y(v+\triangle) - y(v+N+\triangle)\right)^2 \quad (2.2.12)$$

Here Δ is the transmission delay. MERRY only updates once per symbol and its cost function depends on Δ. It shortens the channel to v rather than $v+1$ samples. That is not a problem though; the ISI free transmission is guaranteed as long as the effective channel is smaller than or equal to $v+1$. The cost function analysis of the MERRY algorithm given in [38] shows that it minimizes the energy outside of a length v window plus the energy of the filtered noise. In contrast, the MSSNR design minimizes the energy of the combined impulse response outside of a window of length $v+1$ without taking into account the noise. MERRY is generalized to the so called FRODO (Forced Redundancy with Optional Data Omission) [39] algorithm. FRODO uses more than one sample in the update rule and allows for channel shortening of variable window lengths. The cost function is given by

$$J_{frodo}(\Delta) = \sum_{i \in S_f} E\left(y(i+\Delta) - y(i+N+\Delta)\right)^2 \qquad (2.2.13)$$

where $S_f \subset \{1, \ldots, v\}$. For MERRY $S_f = \{v\}$. The MERRY cost function analysis in [9] shows that it represents the effective channel energy outside a window of length v starting from the transmission delay Δ. It has been further suggested that if the number of comparisons made is more than one (the basic MERRY algorithm), say equal to the value of CP, then this "full" FRODO algorithm tries to suppress all of the channel taps except one. This is against the very idea of channel shortening to a desired window and actually tries to shorten the channel to an impulse. Their simulation results also show that although using more than one term increases the convergence rate of the FRODO algorithm, it degrades its asymptotic performance. The MERRY and

FRODO algorithms have also been applied to the MIMO case in [39]. Both MERRY and FRODO cost functions depend upon the choice of the transmission delay Δ which the authors suggest to calculate by the following heuristic i.e.,

$$\Delta = \Delta_{peak} + \frac{L_w}{2} \tag{2.2.14}$$

Δ_{peak} is the delay which maximizes the energy of the (unshortened) channel in a window of length $v+1$. As was mentioned earlier, the MERRY cost function represents the energy of the *effective* channel outside a window of length v. If there is no TEQ used, the cost function will represent the energy of the *original* channel outside a window of length v. The index Δ_{peak} in which the energy of the channel inside the window is maximum is the index in which the energy of the channel outside the window will be minimum. Therefore Δ_{peak} can be estimated by transmitting $\mathcal{K}$ symbols and calculating [39]

$$\hat{\Delta}_{peak} = \min_{0 \le d \le s-1} \sum_{k=1}^{\mathcal{K}} (r(k \cdot s + v + d) - r(k \cdot s + v + N + d))^2 \tag{2.2.15}$$

where $s = N + v$ is the OFDM symbol duration. Substitution of Equation (2.2.15) in Equation (2.2.14) gives an estimate for the transmission delay Δ for MERRY and FRODO algorithms. This is a low complexity method to avoid the global search over the transmission delay parameter Δ and can be used for other TEQ methods as well.

My experience with other TEQ design methods e.g., the MSSNR [21] method shows that Δ stays in the vicinity of Δ_{peak}. It has also been shown in [37] that Δ within ± 10 taps from Δ_{peak} proved sufficient to give good results to maximize the SSNR. I will elaborate more on Δ_{peak}

in multicarrier systems later in this chapter and in chapter 5.

The authors in [22] propose a blind, adaptive channel shortening algorithm SAM. SAM is based on minimizing the autocorrelation of the signal outside a window of length v at the output of the TEQ. The cost function is given by

$$J_{sam} = \sum_{l=v+1}^{L_c} (R_{yy}(l))^2 \tag{2.2.16}$$

where $R_{yy}(l)$ is the autocorrelation of the output of TEQ at lag l and L_c is the length of the effective channel ($\mathbf{c} = \mathbf{h} * \mathbf{w}$) minus one. Assuming an uncorrelated transmitted signal at the output of the IFFT block in Figure (1.2), if the channel is short the autocorrelation of the output of the channel should also be short. The good things about SAM are, it is blind, adaptive and independent of the transmission delay Δ. SAM converges faster than MERRY. SAM can track channel variations within a symbol because it can update once per sample while MERRY updates once every symbol. However, SAM has higher complexity than MERRY [22]. I shall discuss the SAM algorithm in detail in chapter 3 and 4.

In [29, 40] a subchannel SNR model is proposed

$$SNR_k = \frac{S_{x,k}|H_k^{signal}|^2}{S_{n,k}|H_k^{noise}|^2 + S_{x,k}|H_k^{ISI}|^2} \tag{2.2.17}$$

where H_k^{signal}, H_k^{noise} and H_k^{ISI} are the kth coefficients of the N point FFT of $\mathbf{h}_{win}$, $\mathbf{h}_{wall}$ and the TEQ $\mathbf{w}$ respectively and $S_{x,k}$ and $S_{n,k}$ are the kth subchannel power spectral densities of the signal and the noise before the equalizer. The numerator contains the portion of the resulting transmission channel that contributes to the useful signal and the denominator includes the contribution of the ISI noise of the shortened

channel impulse response outside of the desired window.

Define the following

$$\begin{aligned} H_k^{signal} &= \mathbf{q}_k^H \mathbf{GHw} \\ H_k^{ISI} &= \mathbf{q}_k^H \mathbf{DHw} \\ H_k^{noise} &= \mathbf{q}_k^H \mathbf{Fw} \end{aligned} \tag{2.2.18}$$

where the $N \times T$ matrix $\mathbf{H}$ is the first N rows of the convolutional matrix of the transmission channel, T denotes here the length of the TEQ. $N \times N$ diagonal matrices $\mathbf{G}$ and $\mathbf{D}$ give the rows of the vector $\mathbf{Hw}$ corresponding to the desired $v+1$ window and outside of it, respectively, and $N \times T$ matrix $\mathbf{F}$ when multiplied with $\mathbf{w}$ gives the TEQ vector $\mathbf{w}$ plus padding it with $N - T$ zeros. Multiplication with the vector $\mathbf{q}_k^H$ gives the k-th coefficient of the N point FFT. The subchannel SNR would then be

$$\begin{aligned} SNR_k &= \frac{\mathbf{w}^T\mathbf{H}^T\mathbf{G}^T\mathbf{q}_k S_{x,k}\mathbf{q}_k^H\mathbf{GHw}}{\mathbf{w}^T\mathbf{F}^T\mathbf{q}_k S_{n,k}\mathbf{q}_k^H\mathbf{Fw} + \mathbf{w}^T\mathbf{H}^T\mathbf{D}^T\mathbf{q}_k S_{x,k}\mathbf{q}_k^H\mathbf{DHw}} \\ &= \frac{\mathbf{w}^T\mathbf{A}_k\mathbf{w}}{\mathbf{w}^T\mathbf{B}_k\mathbf{w}} \end{aligned} \tag{2.2.19}$$

The bit rate of the DMT system is given by

$$b_{dmt} = \sum_{k=usedtone} \log_2\left(1 + \frac{SNR_k}{\Gamma}\right) \tag{2.2.20}$$

$$= \sum_{k=usedtone} \log_2\left(1 + \frac{1}{\Gamma}\frac{\mathbf{w}^T\mathbf{A}_k\mathbf{w}}{\mathbf{w}^T\mathbf{B}_k\mathbf{w}}\right) \tag{2.2.21}$$

Here Γ denotes SNR gap of the system and is assumed to be constant over all subchannels. The subchannel SNR model of Equation (2.2.17) and the Equation (2.2.20) are used to evaluate the performance of the

channel shortening algorithms presented in chapter 3 and 4.

The Maximum Bit Rate (MBR) algorithm [29] maximizes the non-linear bit rate Equation (2.2.21) using Matlab's optimization toolbox and achieves the Matched Filter Bound (MFB). However, the authors conclude that the MBR method is computationally very expensive. Therefore they propose a low complexity near optimal min-ISI method. The min-ISI method [29] introduces the idea of frequency weighting in the form of subchannels. It shapes the frequency response of the TEQ. Specifically, it results in increased minimization of ISI noise on the subchannels with higher SNRs. The simulations show that the min-ISI method achieves almost the same data rates as that of MBR method. The min-ISI TEQ is given by

$$\mathbf{w} = \arg \min_{\mathbf{w}:\mathbf{w}^T\mathbf{H}^T\mathbf{G}^T\mathbf{G}\mathbf{H}\mathbf{w}=1} \left[\mathbf{w}^T\mathbf{H}^T\mathbf{D}^T \sum_k \left(\mathbf{q}_k \frac{S_{x,k}}{S_{n,k}} \mathbf{q}_k^H \right) \mathbf{D}\mathbf{H}\mathbf{w} \right] \tag{2.2.22}$$

The value of the cost function increases in favor of the subchannels with higher SNRs. A small reduction in ISI power in these subchannels will increase the bit rate. While in low SNR subchannels, the noise is so dominant that decrease of ISI power does not have a big effect on the bit rate. The min-ISI method is a generalization of the MSSNR method. The min-ISI method takes into account the frequency response of the $\mathbf{h}_{wall}$ while the MSSNR method only looks at its energy.

Another interesting point to note is that the min-ISI method achieves almost 96% of the matched filter bound data (MFB) rates with a TEQ length of only 3 taps. The authors then get maximum data rates with the min-ISI method using a small value of the CP and a longer TEQ. In this way they are successful in trading off the reduction in the through-

put of the system due to CP with the complexity of the TEQ. The initial review of the TEQ is complete and I progress to the frequency domain equalization methods.

2.3 Per Tone Equalization Scheme

In [23] an alternate equalization structure for multicarrier systems is proposed where equalization is performed with a T-tap equalizer after the FFT for each tone/subcarrier separately, hence the name Per Tone Equalization (PTEQ). A TEQ equalizes all the tones of a multicarrier system in a combined fashion. The PTEQ scheme enables true signal-to-noise ratio (SNR) optimization to be implemented for each tone. Their simulation results have compared the performance of the PTEQ scheme with the MMSE TEQ scheme. The achievable data rates are always higher and a smoother function of the transmission delay $\triangle$ as compared to the MMSE TEQ scheme. Therefore, PTEQ is not that sensitive to the symbol timing synchronization ($\triangle_{peak}$ estimation) error. The PTEQ scheme has very large complexity during the initialization mode. For DMT-based systems, this scheme requires initialization of $T \times N/2$ filter taps instead of only T taps as in the TEQ scheme. This also increases the memory requirements of the PTEQ scheme as compared to the TEQ scheme. The symbol timing synchronization in TEQ schemes involves searching for the optimal delay around $\triangle_{peak}$ while it is equal to $\triangle_{peak}$ in the PTEQ scheme. Chapter 5 addresses the complexity problem and contains more on estimation of the symbol timing synchronization as well. The PTEQ scheme is generalized to MIMO in [41]. PTEQ has been considered for channel shortening and equalization over doubly selective OFDM channels in [42]. The non-adaptive

implementation of the PTEQ scheme in [23] requires knowledge of the channel and the signal and noise statistics. Recursive Least Squares (RLS) and Least Mean Square (LMS) adaptive implementations of the PTEQ scheme, which need training, have been suggested in [43]. The blind, adaptive version of the PTEQ scheme is discussed in [44] by using the Constant Modulus Algorithm (CMA) and the Decision-Directed LMS (DD-LMS) algorithm. For example the per tone DD-LMS algorithm is given in [9] as

$$\begin{aligned} z_i(k) &= \overline{\mathbf{v}}_i^T(k)\mathbf{F}_i\mathbf{r}(k) \\ e_i(k) &= Q[z_i(k)] - z_i(k) \\ \overline{\mathbf{v}}_i(k+1) &= \overline{\mathbf{v}}_i(k) + \mu e_i(k)\mathbf{F}_i^*\mathbf{r}^*(k) \end{aligned}$$

where $i = 1, \ldots, N$ is the subchannel index, $k = 1, 2, 3 \ldots$ is the symbol index, and $Q[\cdot]$ is the quantization or decision device. $z_i(k)$ is the equalized output for subchannel i. $\overline{\mathbf{v}}_i^T = [v_{i,T-1} \ldots v_{i,0}]$ is the T-tap reversed PTEQ equalizer for the subchannel i. The vector $\mathbf{F}_i \cdot \mathbf{r}(k)$ contains in reverse order $(T-1)$ required difference terms extracted from the received vector $\mathbf{r}(k)$ in its first $(T-1)$ entries, and the ith value of the FFT in its last entry. For more details of the variables definitions please refer to chapter 5. The authors of [44] suggest to use first the CMA PTEQ and then the DD-LMS PTEQ during the initialization of the equalizer. The simulations show the characteristics of the SNR distribution on one of the subchannels as a function of the symbol timing synchronization error. The SNR distribution is relatively constant over a range of negative synchronization error δ values and drops in magnitude for the positive synchronization errors. The results are very

much in agreement to the ones presented in chapter 5.

The SNR improvement by the PTEQ scheme over TEQ schemes is more pronounced at higher SNR subchannels of the unequalized channel. To find a better tradeoff between complexity and bit rate, [45] propose a dual-path TEQ scheme. Two TEQ filters are designed such that one TEQ equalizes over the entire bandwidth while the other one optimizes over a selected frequency band. The dual-path TEQ structure passes the received data through two paths instead of one path. Each path have its own TEQ, FFT and the one-tap FEQ. The selective band TEQ is focused on the subchannels with higher initial pre-TEQ SNR. The TEQ that equalizes over the entire bandwidth can be designed using any of the TEQ design methods such as MMSE or MSSNR. The selective band TEQ would need to be designed using a method that allows frequency selective weighting such as Min-ISI. The simulations show a 4% increase in bit rates over a single path TEQ.

The TEQ-Filter Bank (TEQ-FB) of [46] is another algorithm similar to the PTEQ scheme where each subchannel has its own filter but in the time domain. After the TEQs, the transfer to the frequency domain is performed using a bank of Goertzel filters, each one tuned to the frequency of the desired subchannel and computing a single point DFT coefficient. This method may have lower memory needs than the PTEQ scheme but its computational requirements are significantly higher during data transmission mode [46]. Their simulations show a slightly better performance than PTEQ. I restrict my thesis to channel shortening in the applications using the FFT block approach instead of a bank of Goertzel filters.

In [47] a blind adaptive equalization algorithm for OFDM systems

which exploits the null carriers present in the system is proposed. This carrier nulling algorithm is based on minimizing a quadratic criterion based on the energy of the null carriers.

$$J = \sum_{i=nullcarriers} E[|\mathbf{Y}_i|^2] \tag{2.3.1}$$

where $\mathbf{Y}_i$ is the received signal after the FFT in the i subchannel. A unit norm constraint is imposed on the equalizer to avoid the trivial solution. It shortens the channel to a single spike i.e., complete equalization. The algorithm does not require the transmission of CP. The use of the blind term for this algorithm is debatable; as transmission of zeros on certain carriers could be thought of as training signal consisting of zeros [22]. This concludes the literature review and I continue to my contributions to the field.

Chapter 3

ROBUST BLIND ADAPTIVE CHANNEL SHORTENING FOR IMPULSIVE NOISE ENVIRONMENTS

As noted in the previous chapter, the good things about the SAM algorithm are, it is blind, adaptive and does not depend on the choice of the transmission delay Δ. It converges faster than another blind adaptive algorithm MERRY and can track channel variations within a symbol because it can update once every sample. This chapter proposes a blind adaptive channel shortening algorithm, SAAM, for multicarrier modulation systems. The algorithm is based on the sum-absolute autocorrelation minimization (SAAM) of the effective channel outside a window of desired length. The algorithm is robust to impulsive noise impairment found in the ADSL channels. The algorithm is computationally less expensive as well. Due to the *quasi* minimum phase nature of the channel impulse response of Asymmetric Digital Subscriber Digital Lines (ADSL), a "left" initialization scheme is suggested for blind adaptive channel shortening equalizers which further enhances

the convergence performance of SAAM. Additional studies have also been undertaken showing that by a proper selection of parameters e.g., the step size, the bit rates achieved by SAM in AWGN conditions can be improved.

3.1 Gaussian Noise Model

The Gaussian noise model [48] has widespread use in the design and analysis of signal processing systems. The probability density function of a zero mean Gaussian random variable is given by

$$f_n(x) = \frac{1}{\sqrt{2\pi}\sigma} exp\left\{-\frac{x^2}{2\sigma^2}\right\}$$

where σ^2 is the variance of the distribution. Due to its mathematical form, the Gaussian assumption for additive noise in signal processing and communication systems greatly simplifies the design and analysis of receiver structures. The Gaussian noise assumption can be justified by the following theorem [49].

Theorem 3.1.1. ***(Central Limit Theorem, CLT)***
Given $x_1, x_2, \ldots, x_N$ a sequence of independent identically distributed (i.i.d.) random variables with mean μ and variance σ^2. Then, as $N \rightarrow \infty$, the distribution of the normalized sum

$$S_N = \frac{1}{N}\sum_{j=1}^{N} x_j$$

converges almost surely to a Gaussian process with the same mean and variance as x_j.

Therefore, many of the theorems of communication, estimation and

detection theory have been formulated based on the Gaussian noise assumption [50]. This is appropriate in Gaussian noise environments but even mild deviations from the Gaussian assumption have detrimental effects [51–53]. Noise sources encountered in physical environments e.g., underwater acoustic noise, urban and man-made RF noise, atmospheric noise, radar clutter noise and telephone circuit noise are decidedly non-Gaussian. They are impulsive, i.e., having higher probability of producing outliers than predicted by an additive Gaussian noise model [54–57].

3.2 Impulse noise in ADSL

Impulse noise is generated in ADSL systems from nonstationary crosstalk due to temporary electromagnetic events in the vicinity of telephone lines. Examples of impulse generators are as diverse as the opening of the refrigerator door, control voltages to elevators, and ringing of phones on lines sharing the same binder. Numerous studies of impulses have resulted in analytical models based on the statistical analysis of over 100,000 impulses by various groups [19]. The most widely used analytical model is the Cook pulse [58]. In [59] a method to simulate the amplitude, length, inter arrival times and the spectral characteristics of the impulses was proposed. The parameters of their model were based on the statistics derived from observations of impulse noise on the telephone networks of British Telecom (BT) and Deutsche Telekom (DT). It is noteworthy that it has also been argued that impulses defy analysis and people sometimes use representative worst case waveforms e.g., the ADSL standard [60] itself uses two measured impulses. However, in common with other researchers, Gaussian mixture and α-stable

distributions are considered appropriate in this thesis for modelling the impulsive noise.

3.2.1 Gaussian-mixture noise model

An analytically simple impulse noise model is the Gaussian mixture model [52, 61, 62]. It is popular due to its mathematical tractability. The probability density function has the form

$$f_n(x) = (1-p)f_v(x) + pf_i(x)$$

where f_v represents the nominal Gaussian pdf with variance $\sigma_v^2 > 0$ and f_i is also a Gaussian pdf with higher variance $k^2\sigma_v^2$. The parameter $p \in [0, 1]$ is the probability of contribution of the components from this high variance distribution. The parameter $k \geq 1$ is the ratio of the standard deviations of the two variances. By varying p and k, the effect of different shapes of Gaussian mixture noise density can be simulated to evaluate the algorithm performance.

3.2.2 Properties of Stable processes

The impulsive noise can be represented by another model called the α-stable distribution [63]. This distribution also shares several desirable properties with the Gaussian model, such as the *stability property* and *generalized* form of the *Central Limit Theorem* [50]. In fact α-stable distributions include the Gaussian density as a special case and have other useful properties as explained below.

A random variable x is said to have a stable distribution, denoted by $x \sim S_\alpha(\gamma, \beta, a)$, if the Fourier Transform of its pdf, also called its

characteristic function, has the following form [64].

$$\varphi(t) = exp\{jat - \gamma|t|^{\alpha}[1 + j\beta sign(t)w(t,\alpha)]\} \tag{3.2.1}$$

where

$$w(t,\alpha) = \begin{cases} tan\frac{\alpha\pi}{2}, & if\ \alpha \neq 1 \\ \frac{2}{\pi}\ log|t|, & if\ \alpha = 1 \end{cases}$$

$$sign(t) = \begin{cases} 1, & if\ t > 0 \\ 0, & if\ t = 0 \\ -1, & if\ t < 0 \end{cases} \tag{3.2.2}$$

Thus the four parameters $-\infty < a < \infty$, $\gamma > 0$, $0 < \alpha \leq 2$, $-1 \leq \beta \leq 1$ describing the stable distribution are [64]

- α which is called the *characteristic exponent* and determines the thickness of the tails of the distribution. Smaller values of α correspond to heavier tailed distributions and vice versa. An $\alpha = 2$ corresponds to a Gaussian distribution. Another special case is the Cauchy distribution when $\alpha = 1$ and $\beta = 0$.

- γ which is a scale parameter called the *dispersion.* It is similar to variance of a Gaussian distribution and equals half the variance in the Gaussian case.

- β which is a *symmetry* parameter. When $\beta = 0$, it corresponds to a symmetric distribution. The resulting distribution is called a Symmetric α-Stable (SαS) distribution.

- a which is the *location* parameter. It is the mean if $1 < \alpha \leq 2$ and the median if $0 < \alpha < 1$.

The pdf of a stable distribution is obtained by taking the inverse Fourier transform of the characteristic function in Equation (3.2.1). No closed form expression exists for the stable density, except for Gaussian ($\alpha = 2$), Cauchy ($\alpha = 1, \beta = 0$), and Pearson($\alpha = 1/2, \beta = -1$) [50].
If it is assumed that SαS distributions have a zero location parameter i.e., $a = 0$, the resulting characteristic function only depends on α and γ, i.e.

$$\varphi(t) = exp\,(-\gamma|t|^{\alpha})$$

whose pdf is given by

$$S_{\alpha}(\gamma,0,0) = \begin{cases} \frac{1}{\pi\gamma^{1/\alpha}} \sum_{k=1}^{\infty} \frac{(-1)^{k-1}}{k!} \Gamma(\alpha k+1) sin\left(\frac{k\alpha\pi}{2}\right) \left(\frac{|x|}{\gamma^{1/\alpha}}\right)^{-\alpha k-1} \\ ,0<\alpha<1 \\ \frac{\gamma}{\pi(x^2+\gamma^2)}, \quad \alpha = 1 \\ \frac{1}{\pi\alpha\gamma^{1/\alpha}} \sum_{k=0}^{\infty} \frac{(-1)^k}{(2k)!} \Gamma\left(\frac{sk+1}{\alpha}\right) \left(\frac{x}{\gamma^{1/\alpha}}\right)^{2k} 1<\alpha<2 \\ \frac{1}{2\sqrt{\gamma\pi}} exp\left(-\frac{x^2}{4\gamma}\right) \alpha = 2 \end{cases}$$

where $\Gamma(\cdot)$ is the usual gamma function defined by

$$\Gamma(x) = \int_0^{\infty} t^{x-1} e^{-t} dt \tag{3.2.3}$$

The pdfs of zero-mean SαS distributions with different values of α are shown in Figure (3.1) [65]. The value of the dispersion γ is equal to unity. It is clear that the non-Gaussian stable density functions differ from the corresponding Gaussian density in the following ways. For small values of x, the SαS densities are more peaked than the Normal densities. For intermediate ranges of $|x|$, the SαS distributions have lower values than the Normal density. But unlike the Gaussian density

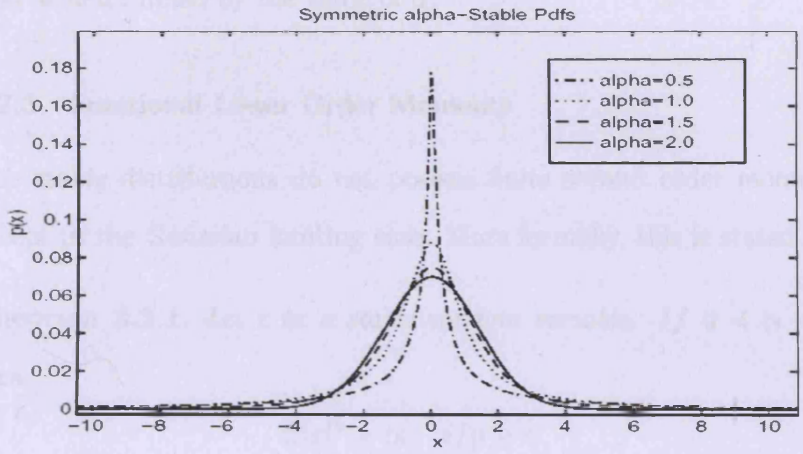

Figure 3.1. Effect of α on the pdf of an alpha-stable distribution with $\beta = 0$, $a = 0$ and $\gamma = 1$.

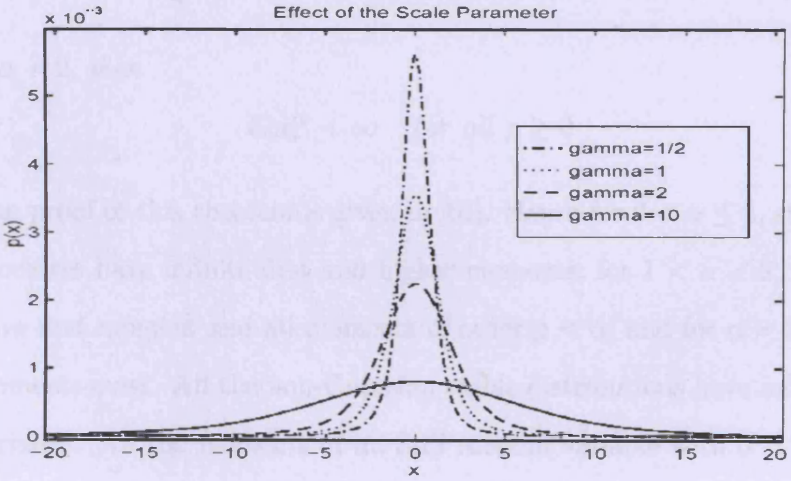

Figure 3.2. Effect of γ on the pdf of an alpha-stable distribution with $\beta = 0$, $a = 0$ and $\alpha = 1$.

which has exponential tails, the SαS distributions have heavier, i.e., algebraic tails. The effect of γ on the pdf of an zero-mean SαS distribution is shown in Figure (3.2) [65]. The value of the characteristic exponent α is equal to 1. It shows that the effect of γ is analogous to variance in the Gaussian density case and it determines the spread of the samples around the location parameter at the respective impulsive-

ness as determined by the value of α.

3.2.3 Fractional Lower Order Moments

The stable distributions do not possess finite second order moments except in the Gaussian limiting case. More formally, this is stated as

Theorem 3.2.1. *Let x be a stable random variable. If $0 < \alpha < 2$, then*

$$E|x|^p = \infty \quad if p \geq \alpha$$

and

$$E|x|^p < \infty \quad if\ 0 < p < \alpha$$

if $\alpha = 2$, then

$$E|x|^p < \infty \quad for\ all\ p \geq 0$$

The proof of this theorem is given in [64]. Hence for $0 < \alpha \leq 1$, stable processes have infinite first and higher moments; for $1 < \alpha < 2$, they have first moment and all moments of order $p < \alpha$; and for $\alpha = 2$, all moments exist. All the non-Gaussian stable distributions have infinite variance. All the moments of an SαS random variable with $0 < \alpha < 2$ of order less than α are termed Fractional Lower Order Moments (FLOMs). The relationships between the FLOMs of an SαS random variable and its dispersion and its characteristic exponent are given by the following preposition [64].

Proposition 3.2.1. *Let $x \sim S_\alpha(\gamma, 0, 0)$. Then*

$$E(|x|^p) = C(p, \alpha)\gamma^{p/\alpha} \quad if\ 0 < p < \alpha$$

where

$$C(p,\alpha) = \frac{2^{p+1}\Gamma\left(\frac{p+1}{2}\right)\Gamma(-p/\alpha)}{\alpha\sqrt{\pi}\Gamma(-p/2)}$$

is a function of α and p and is independent of x.

Most of the research in the area of modeling noise by α-stable distributions has concentrated on the design of near-optimum receivers operating in impulsive noise environments, blind channel estimation, parameter estimation of linear processes, direction of arrival estimation, bearing estimation and other problems related to radar and signal modeling. For a comprehensive list see the bibliographies in [50, 65]. In [66] it was found that noise over telephone lines can be non-Gaussian and the outliers in the noise can be best described by α-stable distributions. The value of α was found to be in the range $1.9 < \alpha < 2$. Stuck [67] also introduced the concept of *minimum dispersion* (MD) criterion for non-Gaussian stable models as a direct generalization of the MMSE criterion which is optimal for Gaussian models. The important observation from the proposition (3.2.1) is that FLOMs are related to the dispersion γ, through only a constant. Therefore the MD criterion dictates that the p-th lower order moment should be minimized, where $0 < p < \alpha$. The range of α found in [66] and mathematical convenience dictates the use of the l_1-norm for the case of noise on telephone lines. Therefore the new algorithm proposed in this chapter will be derived from sum-absolute autocorrelation minimization (SAAM). For ADSL channel noise, without loss of generality, a zero-mean symmetric α-stable (SαS) distribution is assumed, where $0 < \alpha \leq 2$ controls the impulsiveness of the distribution.

3.2.4 Geometric Power of Stable Noise

Due to the infinite variance of stable distributions, the standard SNR definition based on noise variance cannot be used. Instead, a Geometric-SNR (G-SNR) definition has been used [68]. If A is the amplitude of a signal in additive SαS noise of geometric power S_o^2, then the G-SNR in dB is defined as

$$G - SNR = 10 \log \left[\frac{1}{2C_g} \left(\frac{A}{S_o} \right)^2 \right] \tag{3.2.4}$$

where $C_g \cong 1.98$ is the exponential of the Euler constant and

$$S_o = \frac{(C_g \gamma)^{\frac{1}{\alpha}}}{C_g} \tag{3.2.5}$$

Here α is the characteristic exponent and γ is the dispersion of the $S\alpha S$ noise. The normalized constant $2C_g$ in Equation (3.2.4) ensures that for the Gaussian case ($\alpha = 2$), the definition of G-SNR coincides with that of the standard SNR. SαS noise is generated in this work by modifying the Matlab code available at [68] which is based on the Chambers-Mallows-Stuck Method [69]. Figure (3.3) shows samples of SαS noise at G-SNR of 40dB and at different values of α. The signal amplitude is kept at unity. The impulse noise in plot (b) shows that for an $\alpha = 1.99$ value close to 2, the noise samples characterized by G-SNR possess almost the same strength as the Gaussian noise samples of plot (a) where the value of α is 2. Nonetheless, the concept of variance can lead to the misleading conclusion that the stable noise with $\alpha = 1.99$ has infinite strength, although this is clearly not the case in plot (b). As the value of α is decreased to 1.5, the noise becomes impulsive in

nature having samples of larger amplitude as shown in plot (c). The number of outliers and their amplitude/strength is more visible in plot (d) where plot (c) is magnified on the y-axis.

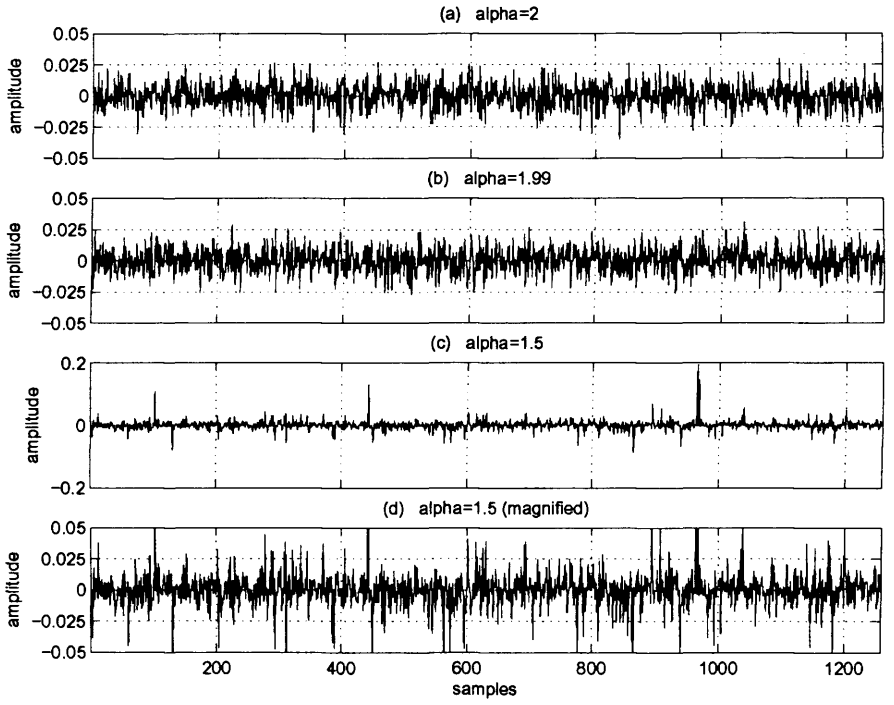

Figure 3.3. Gaussian and impulsive noise at GSNR=40dB. The signal amplitude is unity. (a) Gaussian noise $\alpha = 2$, (b) impulse noise $\alpha = 1.95$, (c) more impulsive noise $\alpha = 1.5$, and (d) magnified view of (c).

3.3 System Model

The system model of blind adaptive channel shortening is shown in Figure (3.4). In multicarrier systems, the input vector $X(k)$ to the IFFT is a white, zero-mean and Wide-Sense Stationary (WSS) complex sequence which is drawn from a finite alphabet QAM constellation. The transmitted baseband sequence $x(n)$ in Figure (3.4) is the output of the unitary transformation IFFT matrix block in Figure (1.2). This sequence is assumed to be white, zero-mean and WSS. This unit variance,

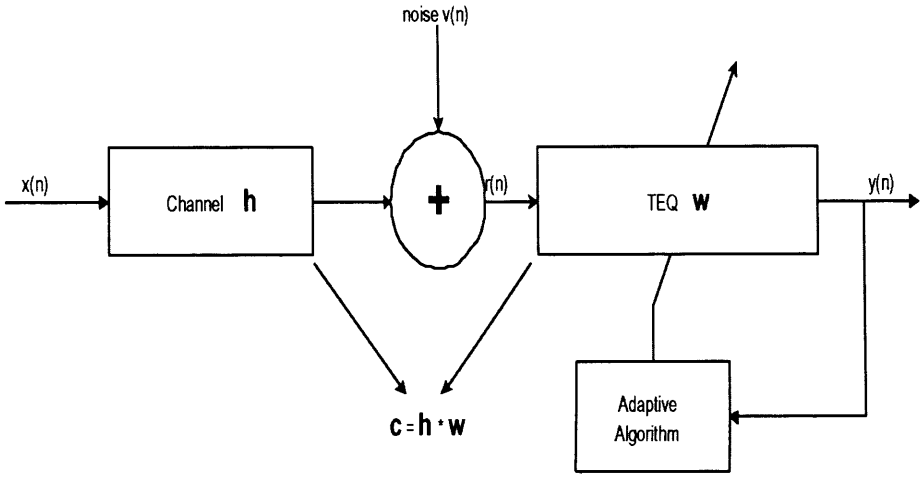

Figure 3.4. System model for blind adaptive channel shortening.

$\sigma_x^2 = 1$, source sequence is transmitted through the linear FIR channel $\mathbf{h} = [h(0)h(1), \ldots, h(L_h)]^T$. Here $v(n)$ is a zero-mean, i.i.d., noise sequence uncorrelated with the source sequence and has a variance σ_v^2. The received signal $r(n)$ at the input of the TEQ is

$$r(n) = \sum_{k=0}^{L_h} h(k)x(n-k) + v(n) \tag{3.3.1}$$

and $y(n)$, the output of the TEQ is given by

$$y(n) = \sum_{k=0}^{L_w} w(k)r(n-k) = \mathbf{w}^T\mathbf{r}_n \tag{3.3.2}$$

where $\mathbf{w} = [w(0)w(1), \ldots, w(L_w)]^T$ is the impulse response vector of the TEQ and $\mathbf{r}_n = [r(n)\ r(n-1)\ \ldots\ r(n-L_w)]^T$. The vector $\mathbf{c} = \mathbf{h} \star \mathbf{w}$ is the effective channel of order $L_c = L_h + L_w$. The symbol $\star$ represents discrete time convolution and L_h and L_w are the orders of the channel and TEQ respectively. It is assumed that $2L_c < N$ holds, where N is the FFT size [22]. This assumption makes sure that the

autocorrelation matrix $E[\mathbf{x}_n\mathbf{x}_{n-l}^T]$ of the input to the channel defined in the next Section, contains only one diagonal of nonzero entries. The importance of this assumption will become clear in the next section. Due to baseband nature of the ADSL transmission, all quantities are taken as real, generalization to the complex case is straightforward [9].

3.4 SAAM

The autocorrelation sequence of the effective channel, $\mathbf{c}$ is given by

$$R_{cc}(l) = \sum_{k=0}^{L_c} c(k)c(k-l) \tag{3.4.1}$$

when the effective channel $\mathbf{c}$ has zero taps outside a window of size $(v+1)$, its autocorrelation values should be zero outside a window of size $(2v+1)$, i.e.,

$$R_{cc}(l) = 0, \forall\ |l| > v$$

The length of the non-zero autocorrelation is proportional to the length of the non-zero impulse response sequence of a channel. This is demonstrated in Figure (3.5). In the top left plot, the channel impulse response sequence has $v_1 + 1 = 10$ contiguous non-zero values and is zero outside. The autocorrelation of this channel is shown in the top right plot for non-negative lags starting from lag 0. In the lower left plot, the channel impulse response sequence has $v_2 + 1 = 5$ contiguous non-zero values and is zero outside. The autocorrelation of this channel is shown in the bottom right plot again for non-negative lags starting from lag 0. The autocorrelations of channel 1 and channel 2 are zero from lags v_1+1 and v_2+1 onward respectively. In multicarrier systems the channel can be of maximum length $v+1$. Therefore, minimizing the (non-negative)

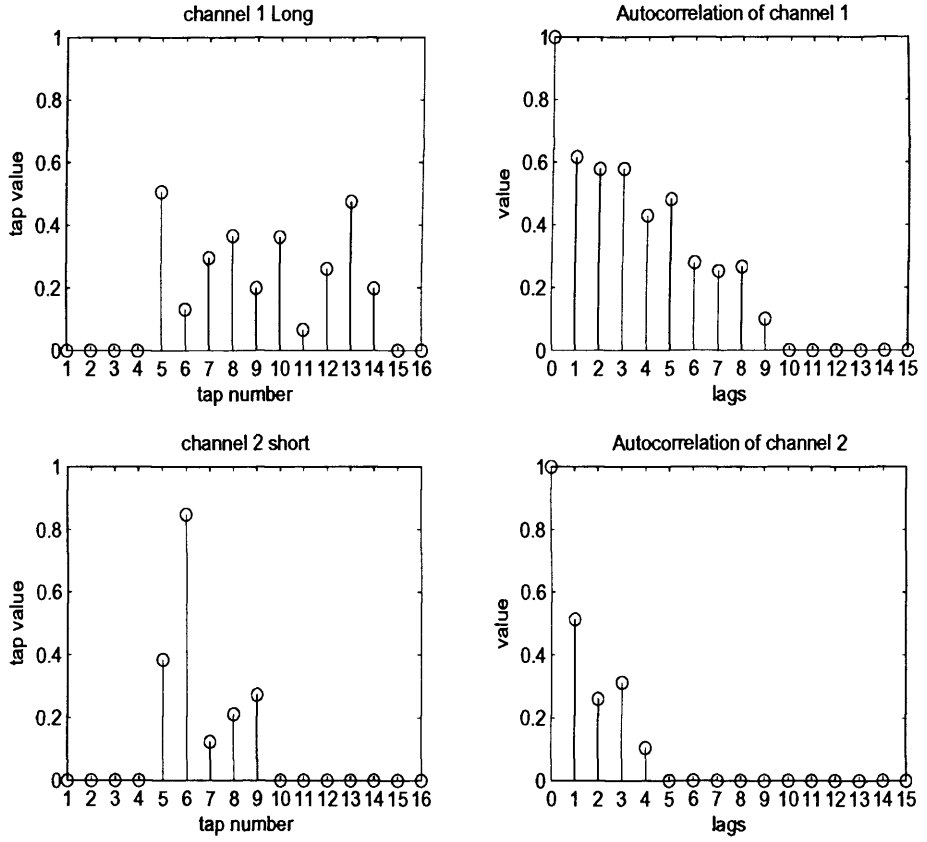

Figure 3.5. Two channel impulse response sequences and their corresponding autocorrelations.

autocorrelation of a channel for lags $v+1$ and onward, should give a shortened channel of required length i.e., $v+1$.

Therefore, a cost function, J_{v+1} based on the sum of absolute values of the auto-correlation of the effective channel is suggested. The reasons for taking absolute values have been explained in Section (3.2.3). This is in contrast to the cost function of [22] based on the sum of squared autocorrelation values for the same lags. We have

$$J_{v+1} = \sum_{l=v+1}^{L_c} |R_{cc}(l)| \tag{3.4.2}$$

The trivial (anti)solution of $\mathbf{w} = 0$ can be avoided by imposing a norm constraint on the equalizer i.e., $\|\mathbf{w}\|_2^2 = 1$. The optimization problem can then be stated as

$$\mathbf{w}^{opt} = \arg_{\mathbf{w}} \min_{\|\mathbf{w}\|_2^2=1} J_{v+1}$$

The autocorrelation sequence of the output $y(n)$ is given by

$$\begin{aligned} R_{yy}(l) &= E[y(n)y(n-l)] \\ &= E[(\mathbf{c}^T\mathbf{x}_n + \mathbf{w}^T\mathbf{v}_n)\ (\mathbf{x}_{n-l}^T\mathbf{c} + \mathbf{v}_{n-l}^T\mathbf{w})] \end{aligned} \tag{3.4.3}$$

where $\mathbf{x}_n = [x(n), x(n-1), \ldots, x(n-L_c)]^T$ and $\mathbf{v}_n = [v(n), v(n-1), \ldots, v(n-L_w)]^T$. The noise correlation matrix becomes

$$E[\mathbf{v}_n\mathbf{v}_{n-l}^T] = \begin{bmatrix} R_{vv}(l) & \ldots & R_{vv}(l+L_w) \\ \vdots & \ddots & \vdots \\ R_{vv}(l-L_w) & \ldots & R_{vv}(l) \end{bmatrix} \tag{3.4.4}$$

where $R_{vv}(l) = E[v(n)v(n-l)]$. The noise sequence $v(n)$ is assumed i.i.d. Therefore, the matrix in Equation (3.4.4) is a Toeplitz matrix with only one diagonal of nonzero entries depending upon the value of l, and hence becomes a shifting matrix. The matrices $E[\mathbf{x}_n\mathbf{v}_{n-l}^T] = 0$ and $E[\mathbf{v}_n\mathbf{x}_{n-1}^T] = 0$ since the signal $x(n)$ and the noise $v(n)$ are uncorrelated. If $2L_c < N$ holds, then the Toeplitz matrix $E[\mathbf{x}_n\mathbf{x}_{n-l}^T]$ has a shifting effect too. Now we can simplify Equation (3.4.3) to [22]

$$\begin{aligned} R_{yy}(l) &= \sum_{k=0}^{L_c} c(k)c(k-l) + \sigma_v^2 \sum_{k=0}^{L_w} w(k)w(k-l) \\ &= R_{cc}(l) + \sigma_v^2 R_{ww}(l) \end{aligned} \tag{3.4.5}$$

So that the cost function in Equation (3.4.2) can be approximated and denoted as $\hat{J}_{v+1}$

$$\begin{aligned} \hat{J}_{v+1} &= \sum_{l=v+1}^{L_c} |R_{yy}(l)| \\ &= \sum_{l=v+1}^{L_c} |R_{cc}(l) + \sigma_v^2 R_{ww}(l)| \end{aligned} \tag{3.4.6}$$

In most situations, the TEQ length $(L_w + 1)$ is shorter than the cyclic prefix length, v. In such situations, $R_{ww}(l)$ does not exist for the stated lags in Equation (3.4.6). Even if the TEQ is larger than the cyclic prefix, the second term being added is very small due to its multiplication with σ_v^2. The noise variance σ_v^2 is usually small for ADSL channels [22]. Therefore, it is assumed that under practical scenarios, the hat on J_{v+1} can be dropped so that $\hat{J}_{v+1} \cong J_{v+1}$. For this cost function an estimate of the length of the channel $\mathbf{h}$ is needed to determine $L_c = L_h + L_w$, which is fortunately known because the CSA test loops have almost all of their energy in 200 consecutive taps [70].

3.5 Blind Adaptive Algorithm

The steepest gradient-descent algorithm to minimize J_{v+1} is

$$\begin{aligned}\mathbf{w}^{new} &= \mathbf{w}^{old} - \mu\nabla_{\mathbf{w}}\left(J_{v+1}\right) \\ &= \mathbf{w}^{old} - \mu\nabla_{\mathbf{w}}\left(\sum_{l=v+1}^{L_c} |E[y(n)y(n-l)]|\right)\end{aligned} \tag{3.5.1}$$

where μ is the step size and $\nabla_{\mathbf{w}}$ is the gradient evaluated at $\mathbf{w} = \mathbf{w}^{old}$. A Moving Average (MA) implementation is used to realize the instantaneous cost function

$$J_{v+1}^{inst}(k) = \sum_{l=v+1}^{L_c}\left|\sum_{n=kN_{avg}}^{(k+1)N_{avg}-1}\frac{y(n)y(n-l)}{N_{avg}}\right| \tag{3.5.2}$$

Here N_{avg} is a design parameter which determines a tradeoff between the algorithm complexity and a good estimate of the expectation. The stochastic gradient-descent algorithm of Equation (3.5.1), therefore, can be written as (3.5.3) which, using Equation (3.3.2), takes the form of Equation (3.5.4).

$$\begin{aligned}\mathbf{w}^{k+1} = \mathbf{w}^{k} - \mu\sum_{l=v+1}^{L_c}&\left\{sign\left(\sum_{n=kN_{avg}}^{(k+1)N_{avg}-1}\frac{y(n)y(n-l)}{N_{avg}}\right)\right\} \\ &\times\left\{\nabla_{\mathbf{w}}\left(\sum_{n=kN_{avg}}^{(k+1)N_{avg}-1}\frac{y(n)y(n-l)}{N_{avg}}\right)\right\}\end{aligned} \tag{3.5.3}$$

$$\begin{aligned}\mathbf{w}^{k+1} = \mathbf{w}^{k} - \mu\sum_{l=v+1}^{L_c}&\left\{sign\left(\sum_{n=kN_{avg}}^{(k+1)N_{avg}-1}\frac{y(n)y(n-l)}{N_{avg}}\right)\right\} \\ &\times\left\{\left(\sum_{n=kN_{avg}}^{(k+1)N_{avg}-1}\frac{y(n)\mathbf{r}_{n-l} + y(n-l)\mathbf{r}_n}{N_{avg}}\right)\right\}\end{aligned} \tag{3.5.4}$$

$$\mathbf{w}^{k+1} = \frac{\mathbf{w}^{k+1}}{\|\mathbf{w}^{k+1}\|_2^2} \tag{3.5.5}$$

The function $sign(\cdot)$ is defined in Equation (3.2.2). The equalizer vector $\mathbf{w}$ must be normalized at every iteration to ensure that $\|\mathbf{w}\|_2^2 = 1$. The complexities of the SAM-MA and SAAM-MA algorithms have been calculated in the Tables (3.1) and (3.2) respectively. It is evident that introduction of the *sign* function in Equation (3.5.4) has reduced the computational complexity of the SAAM as compared to the SAM algorithm.

Steps	# multiplications	# addition/subtractions
(a)N_{avg} times $y(n-l)\mathbf{r}_n$	$N_{avg}.\{L_w+1\}$	-
(b)N_{avg} times $y(n)\mathbf{r}_{n-l}$	$N_{avg}.\{L_w+1\}$	-
(c)(a+b)	-	$N_{avg}.\{L_w+1\}$
(d)N_{avg} times $y(n)y(n-l)$	N_{avg}	-
(e)sum (d) outputs	-	$N_{avg}-1$
(f)output (e)× output (c)	L_w+1	-
(g)Sub-total for (L_c-v) lags	$(L_c-v)\{N_{avg}(2L_w+3)+L_w+1\}$	$(L_c-v)\{N_{avg}(L_w+2)-1\}$
(h)2μ× output of (g)	L_w+1	-
(i)$\mathbf{w}^k$ - (h)	–	L_w+1
(j)Total	$(L_c-v)\{N_{avg}(2L_w+3)+L_w+1\}+L_w+1$	$(L_c-v)\{N_{avg}(L_w+2)-1\}+L_w+1$

Table 3.1. Complexity of SAM-MA.

3.6 Properties of the SAAM cost function

Some properties of the SAAM cost function will be mentioned in Chapter 4 where another autocorrelation based channel shortening algorithm will be suggested.

Steps	# multiplications	# addition/subtractions
(a)N_{avg} times $y(n-l)\mathbf{r}_n$	$N_{avg}.\{L_w+1\}$	-
(b)N_{avg} times $y(n)\mathbf{r}_{n-l}$	$N_{avg}.\{L_w+1\}$	-
(c)(a+b)	-	$N_{avg}.\{L_w+1\}$
(d)N_{avg} times $y(n)y(n-l)$	N_{avg}	-
(e)sum (d) outputs	-	$N_{avg}-1$
(f)Sub-total for (L_c-v) lags	$(L_c-v)\{N_{avg}(2L_w+3)\}$	$(L_c-v)\{N_{avg}(L_w+2)-1\}$
(g)$\mu\times$ output of (f)	L_w+1	-
(h)$\mathbf{w}^k$ - (g)	–	L_w+1
(i)Total	$(L_c-v)\{N_{avg}(2L_w+3)\}+L_w+1$	$(L_c-v)\{N_{avg}(L_w+2)-1\}+L_w+1$

Table 3.2. Complexity of SAAM-MA.

3.7 "Left" Initialization

For blind equalizers based upon the Constant Modulus Algorithm (CMA), it has been suggested that the location of the single spike initialization should be driven according to the center of the mass of the channel impulse response [71]. This results in a better Mean Squared Error (MSE) performance of the receivers. If the channel impulse response is reasonably symmetric, a center spike is most appropriate. Also without any *a prior* knowledge about the channel impulse response, a center spike is a good strategy. This is motivated by being able to concentrate on the equalization of the minimum as well as the non-minimum phase response of the channel. On the other hand, if the channel impulse response is asymmetric, then the initial spike location should be moved in the direction of the center of mass. The equalizer can, therefore, be "left", "center", or "right" initialized. Blind equalization does not imply "blind" equalizer design [71]. In Figure (3.6), the zeros of the

CSA loop 1 channel are shown. It is clear that most of the zeros lie within the unit circle at a radius of approximately 0.985, while only a few lie outside the unit circle. Therefore, CSA loop channels are *quasi* minimum phase channels [4]. They have the center of mass of their

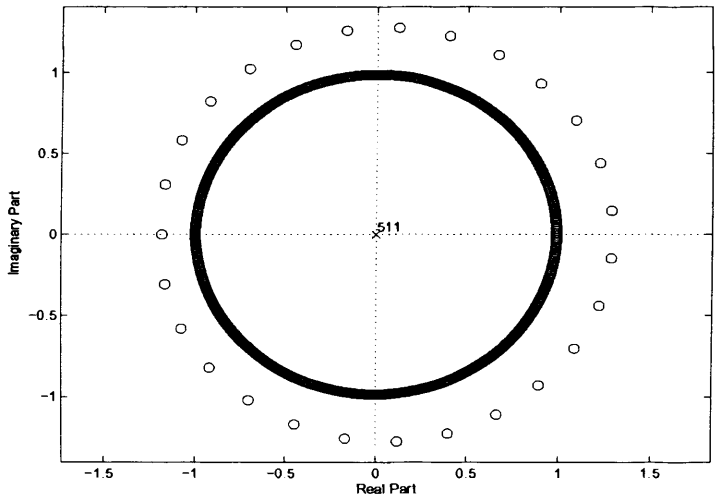

Figure 3.6. Pole-zero diagram of CSA loop 1.

impulse response on the "left" as shown by the plot of the impulse response of the CSA loop 1 channel in Figure (3.7). Using this knowledge, the "left" initialization strategy is suggested alongside the SAAM-cost function. Specifically, the first spike is initialized to unity. The "left" initialization has also been simulated in [72, 73] for the TEQ design algorithms for ADSL channels. The results presented in the next Section show that "left" initialization gives better performance in terms of achievable bit rates.

3.8 Simulation Results

Standard ADSL downstream transmission parameters were chosen: CP was 32, the FFT size was 512, the equalizer length was 16, the averaging window size N_{avg} was 32, and the channel was CSA test loop 1 available

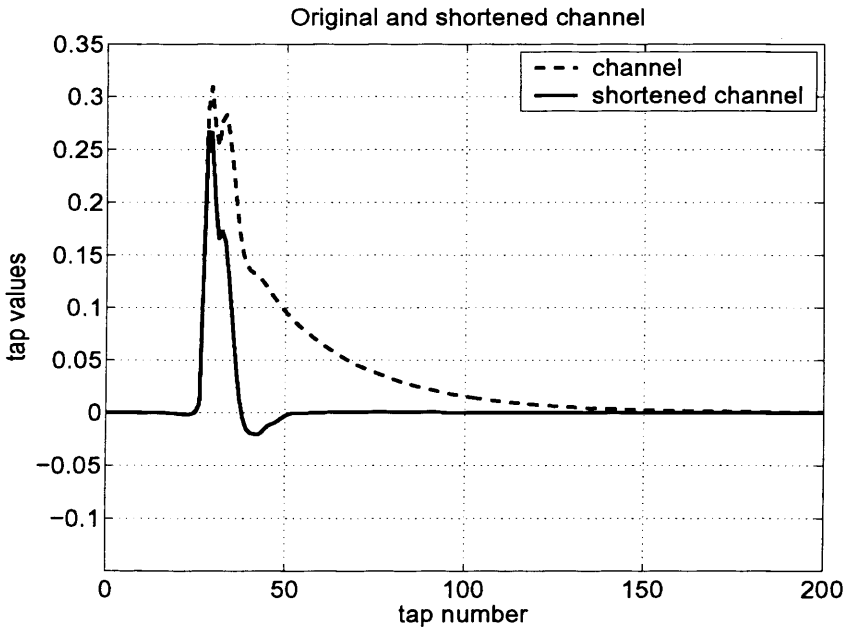

Figure 3.7. Original and the shortened channel.

at [70]. The 4-QAM signalling was used on all of the sub-carriers. These parameters were also chosen so as to compare the results with those of SAM in [22]. For the case of Gaussian-mixture modeling, the signal to Gaussian noise power was such that $\sigma_x^2\|\mathbf{h}\|^2/\sigma_v^2 = 40$ dB. This is a typical value of SNR in ADSL environments. A total of 75 symbols comprising of 544 samples each were used. The moving average implementation of the SAAM algorithm as given in Equation (3.5.4) with unit norm constraint on the equalizer vector $\mathbf{w}$ was employed. For a point-to-point system with bit loading, the achievable bit rate for a fixed probability of error (typically 10^{-7} in DSL) is the performance metric. The SNR gap Γ is given by

$$\Gamma = \Gamma_{gap} + \gamma_m - \gamma_c \tag{3.8.1}$$

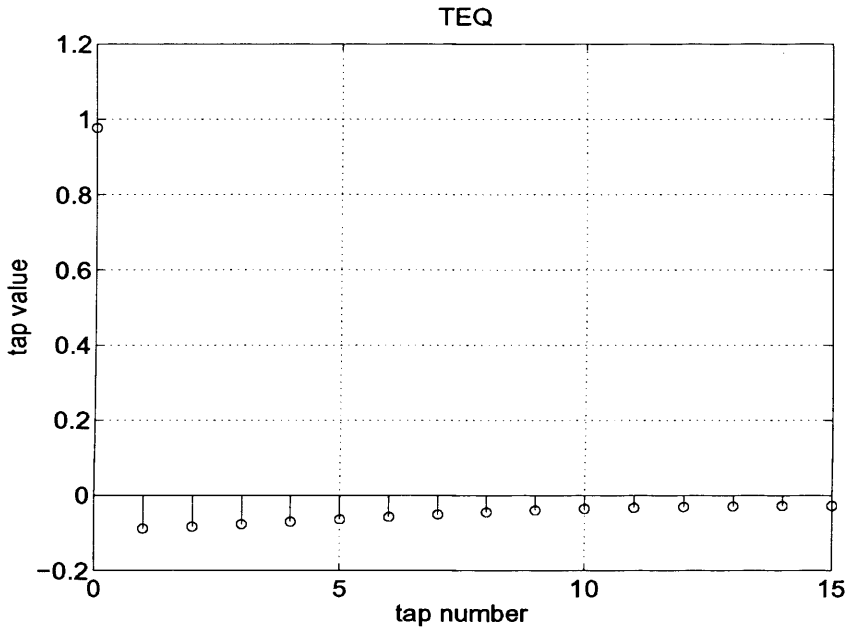

Figure 3.8. 16-tap TEQ.

The bit rate on each subcarrier is determined using noise margin γ_m = 6dB and the coding gain γ_c = 4.2dB. The value of Γ_{gap} = 9.8dB is used which corresponds to a probability of error 10^{-7} and the QAM modulation used across the subcarriers. The bit rate on each subcarrier i is calculated based on

$$b_i = \log_2 \left(1 + 10^{((SNR_i - \Gamma)/10)}\right) \tag{3.8.2}$$

The subchannel SNR, SNR_i in Equation (3.8.2) is found by using the subchannel SNR model described in Equation (2.2.17) and includes the channel noise as well as the distortion due to ICI and ISI caused by the energy of the channel outside the $v + 1$ length. This definition can be used to assess the performance of the TEQ algorithms. To use this model, the maximal energy point of the shortened channel is used as the starting index of the $v + 1$ length window of the desired channel.

The bit rate is computed with the formula

$$rate = \left(\sum_{i=1}^{N/2} b_i \right) \cdot \frac{F_s}{N+v}$$

where $F_s = 2.208$ MHz is the sampling frequency. SAM, SAM-optimized (SAM-opt), SAAM with Center spike initialization (SAAM-C), SAAM with "left" (first spike) initialization (SAAM-L), and the maximum SSNR algorithm (MSSNR) of [21] are simulated. The step sizes used for the adaptive algorithms are 5, 1.05, 0.0003, and 0.00016 respectively, empirically chosen to give the best performance. For simulations in α-stable noise, the geometric-SNR (G-SNR) definition defined in Section (3.2.4) is used, instead of the standard SNR definition, due to infinite variance of SαS distributions. The dispersion of the noise for a given value of α is changed and the achievable bit rate is calculated. The remainder of the explanation is related to the individual figures. The impulse responses of the original and the shortened channel with SAAM-L are shown in Figure (3.7). The equalizer designed after the SAAM algorithm converges is shown in Figure (3.8). In Figure (3.9), the learning curve of the SAAM cost function and the bit rate as a function of the averaging block number are shown. It is noteworthy that the bit rate approaches the maximum SSNR solution of [21] and that the cost function and the bit rate are a smooth function of each other i.e., the SAAM minima and the bit rate maxima appear to be located in close proximity. Careful selection of parameters for the reported SAM algorithm also leads to the same performance under AWGN (see Figure (3.10) continues curve). I shall call this algorithm as SAM-optimized (SAM-opt). Figure (3.10) shows under AWGN, the achievable bit rate

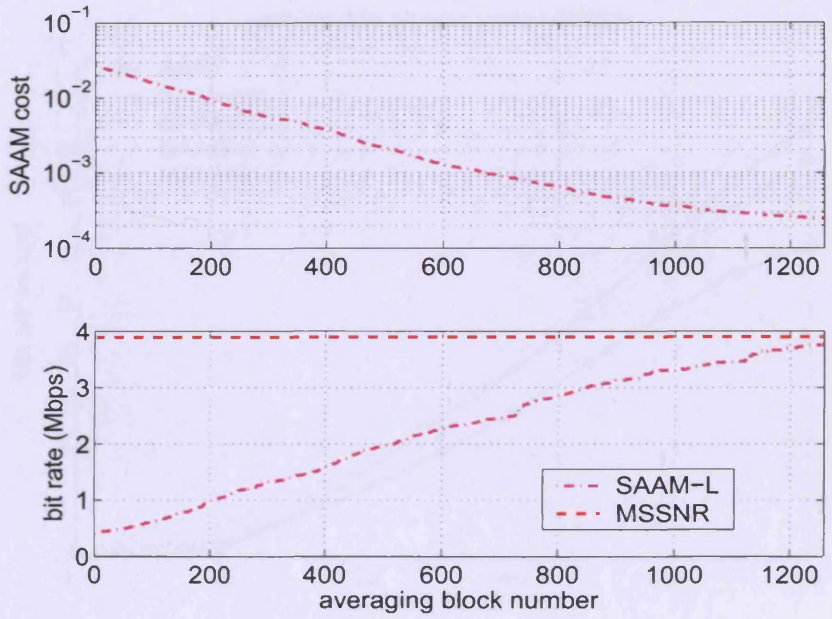

Figure 3.9. SAAM cost and bit rate versus averaging block number at 40dB SNR.

versus SNR for the respective algorithms. The performance of SAAM-C is slightly below that of SAM-opt, this is expected because robust algorithms are not optimal for the pure AWGN environment. They are designed for special conditions (impulsive noise here). However, SAAM-L outperforms SAM-opt, showing existence of a good initialization strategy for such channels.

In Figure (3.11) the effect of impulsive noise on the quasi-achievable bit rate (quasi because the same bit rate calculation, to a first approximation, on the basis that the impulses occur infrequently, is used. These results are for an impulsive contribution of 1% only) is simulated. The value of k is changed from 10 to 100 to simulate the amplitude of the impulsive spikes from 20 dB to 40dB, while keeping p their contribution factor at 1%. The signal to Gaussian noise ratio is 40dB. As expected with increasing k the degradation in the SAM-opt algorithm is more

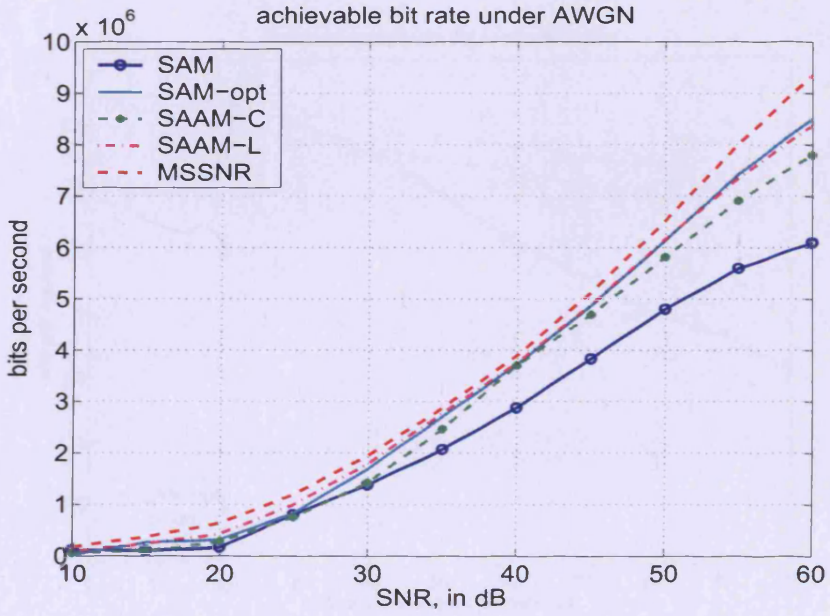

Figure 3.10. Achievable bit rate versus SNR for white noise.

than in the other two algorithms. To illustrate it more, the convergence behavior is shown in Figure (3.12) applying impulses of 40dB higher than the AWGN and at a contribution factor of 1%. This is the typical level of impulse noise in ADSL environments where the spikes can totally eliminate the signal for a hundred of microseconds [59,74]. It is evident from Figure (3.12) that the behavior of the SAM-opt algorithm deteriorates, whereas that of SAAM-C and SAAM-L remains smooth and less affected achieving higher bit rates.

Figure (3.13) shows the achievable bit rate by SAAM in Gaussian noise at 40dB G-SNR versus averaging block/iteration number. In Figures (3.14) and (3.15) the achievable bit rate versus G-SNR is shown at different values of α. The values of α were 2, 1.95, 1.9 and 1.7. As noted earlier, for the ADSL impulsive noise the value of α stays above 1.9. The above tested range was to show the robustness of the proposed

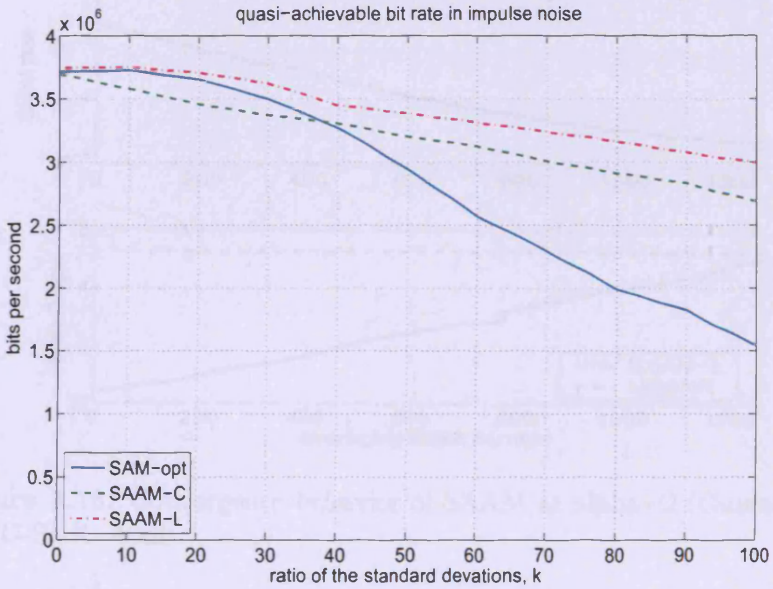

Figure 3.11. Quasi-achievable bit rate versus ratio of standard deviations of two noise components, p=1%, SNR=40dB.

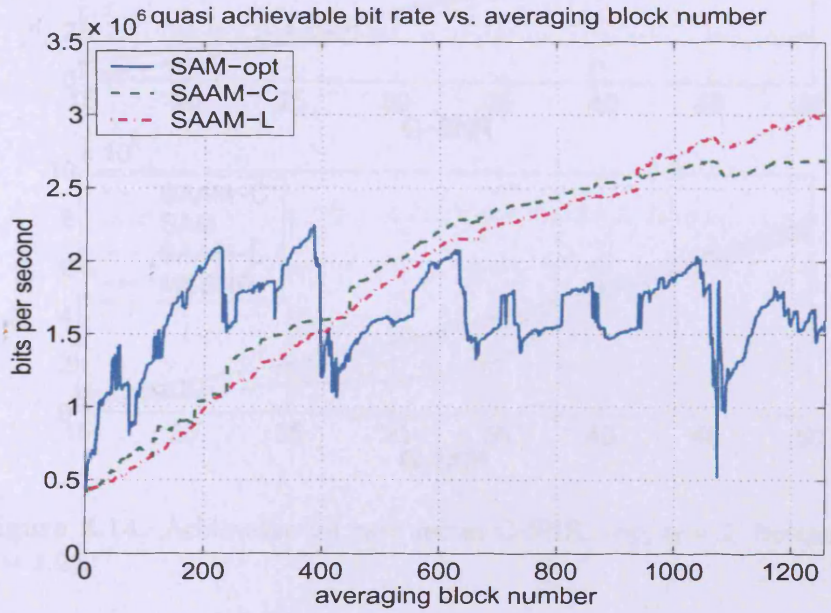

Figure 3.12. Quasi-achievable bit rate versus averaging block number, at 40dB SNR and at k=100 (40dB), impulse noise contribution p=1%

.

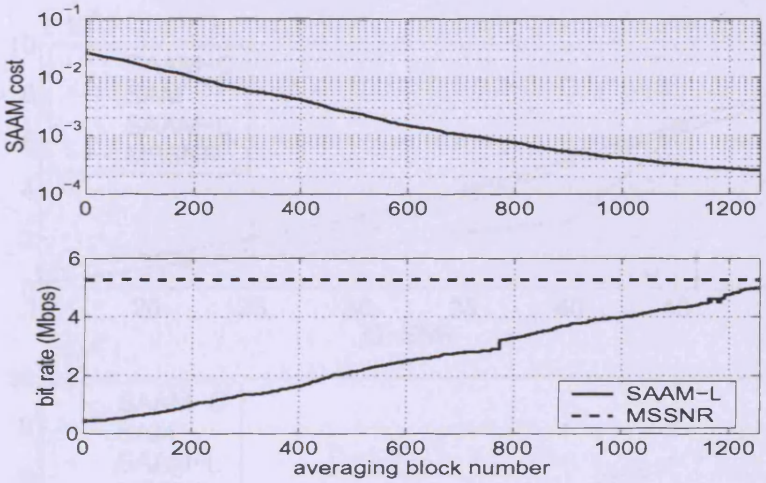

Figure 3.13. Convergence behavior of SAAM at alpha=2 (Gaussian) and G-SNR=40dB.

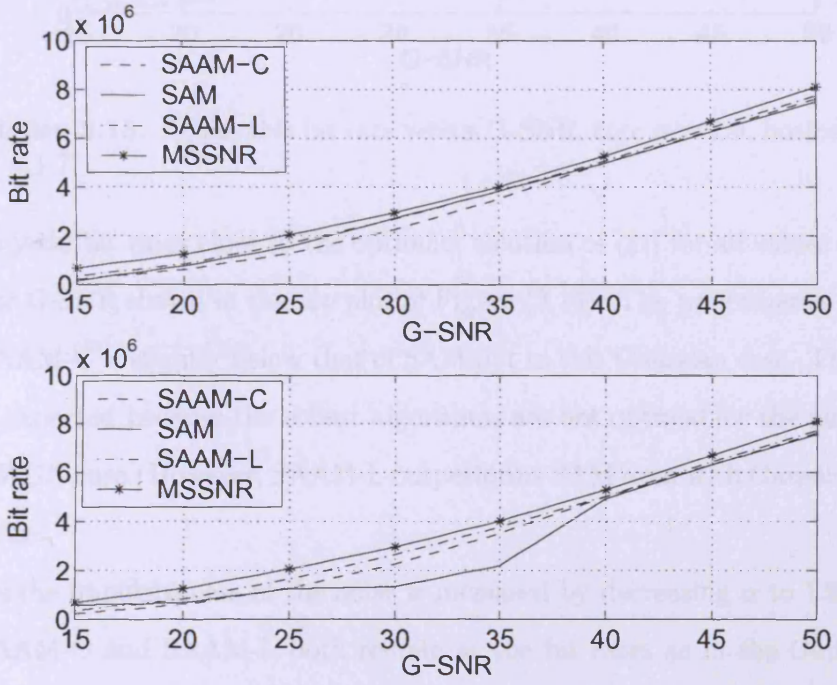

Figure 3.14. Achievable bit rate versus G-SNR, top; $\alpha = 2$, bottom; $\alpha = 1.95$.

new algorithm SAAM to even an increased range of impulsiveness.

At $\alpha = 2$ i.e., the Gaussian noise case, all the three algorithms are seen

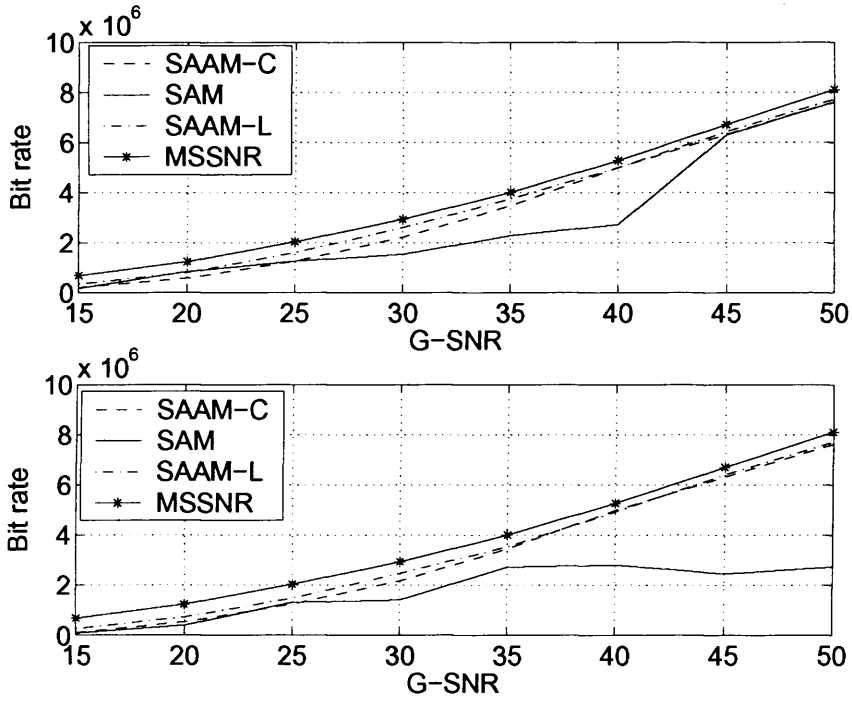

Figure 3.15. Achievable bit rate versus G-SNR, top; $\alpha = 1.9$, bottom; $\alpha = 1.7$.

to yield bit rates close to the optimum solution of [21] for all values of the G-SNR shown in the top plot of Figure (3.14). The performance of SAAM-C is slightly below that of SAM-opt in this Gaussian case. This is expected because the robust algorithms are not optimal for the pure AWGN case. However, SAAM-L outperforms SAM even with Gaussian noise.

As the impulsiveness of the noise is increased by decreasing α to 1.95, SAAM-C and SAAM-L both remain at the bit rates as in the Gaussian case, while SAM-opt degrades to low bit rates. It is particular to note in the bottom plot in Figure (3.14) that SAM-opt is not showing any degradation at higher G-SNRs. Increasing G-SNR at fixed α means decreasing the dispersion, γ. Figure (3.2) showed the effect of changing dispersion on the pdf of an SαS distribution, while keeping

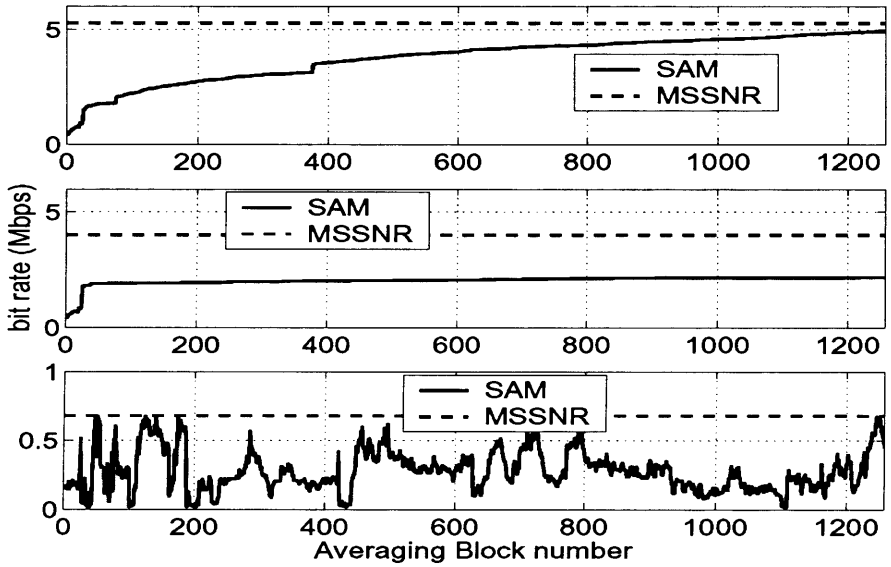

Figure 3.16. Convergence of SAM at alpha=1.95, top; G-SNR=40dB, middle; G-SNR=35dB, bottom; G-SNR=15dB.

α fixed. It is evident that less dispersion (higher G-SNR) means fewer outliers in the noise exist while most of the noise samples are concentrated around the zero mean. Even these reduced number of outliers have small strengths. This has been explained further in Figure (3.16), where the convergence of SAM-opt at $\alpha = 1.95$ and the G-SNR values of 15dB, 35dB and 40dB respectively, is shown. With the increase of the G-SNR (decrease of γ) the achievable bit rate performance of SAM gets better.

The same trend of Figure (3.14) is observed in the top plot of Figure (3.15), SAAM-C and SAAM-L remain at their optimum bit rates while SAM-opt degrades. This time the point on the G-SNR axis, where SAM-opt returns to its optimum bit rate has moved towards the right to a higher G-SNR value of 45dB. In the bottom plot of Figure (3.14), SAM had returned to its optimum bit rate at G-SNR=40dB while now it is still degraded at this value of G-SNR. This can be explained by

looking at Figure (3.1). Decreasing α while fixing G-SNR increases the strength and the number of outliers which cause degradation of the SAM algorithm. The consequence is that if the α of the stable noise is low, SAM-opt requires high signal to noise ratios to give its optimum bit rates. Increasing impulsiveness further has degraded SAM to the extent that it cannot return to its optimum bit rate even at 50dB G-SNR as shown in the bottom plot of Figure (3.15). SAAM-C and SAAM-L are not affected by this high degree of impulsiveness. SAAM-L is respectively showing higher data rates than SAAM-C, and showing the benefits of left-initialization of the blind adaptive TEQ for ADSL channels.

3.9 Conclusions

The proposed algorithm SAAM has proven to be robust for operations in environments with a range of degree of impulsiveness. The computational complexity of SAAM is also lower than SAM. Noting the quasi minimum phase nature of ADSL channels, a "left" initialization strategy was suggested for the blind adaptive channel shortening equalizers. Simulation results show that SAAM approaches the maximum shortening signal-to-noise ratio (MSSNR) solution [21] in Gaussian noise. SAAM is also robust to additive white non-Gaussian noise. Further studies on SAM have also been undertaken showing that the bit rates achieved by SAM in Gaussian noise can be further improved upon those previously reported.

Chapter 4

SINGLE LAG AUTO-CORRELATION MINIMIZATION

SAM [22] is an attractive blind adaptive channel shortening algorithm which minimizes the sum of the squared autocorrelations of the effective channel outside of a CP-length window. The drawback with SAM is that it has a significantly higher computational complexity and it does not have any stopping criterion (to be explained in Section 4.6) to freeze the TEQ when the SSNR of the effective channel reaches its maximum. Identical channel shortening can be achieved by minimizing the square of only a single autocorrelation[1]. The proposed single lag autocorrelation minimization (SLAM) algorithm has, therefore, relatively low complexity. The autocorrelation minimization is constrained with a novel stopping criterion so that the adaptation of the SLAM algorithm only maximizes the SSNR of the effective channel or minimizes ISI energy and it avoids the opposite. The simulations have shown that SLAM achieves higher bit rates than SAM for a range of SNRs for the

[1]There are potentially degenerate cases where minimizing only a single autocorrelation does not lead to channel shortening to the required width (private correspondence with the second author of [22]). This is discussed in Section (4.7).

8 CSA loop channels.

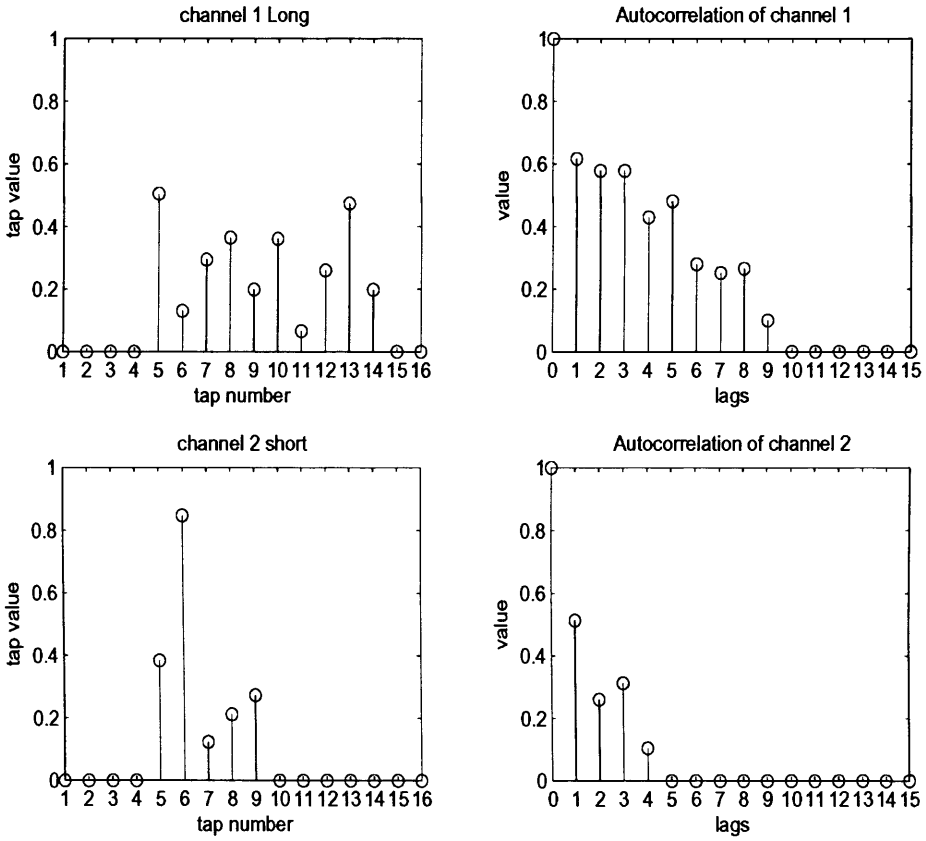

Figure 4.1. Two channel impulse response sequences and their corresponding autocorrelations.

4.1 Motivation

Figure (4.1) is a reproduction of Figure (3.5). In the top left plot, the channel impulse response sequence has $v_1 + 1 = 10$ contiguous non-zero values and is zero outside. The autocorrelation of this channel is shown in the top right plot for non-negative lags starting from lag 0. In the lower left plot, the channel impulse response sequence has $v_2 + 1 = 5$ contiguous non-zero values and is zero outside. The autocorrelation of this channel is shown in the bottom right plot again for non-negative

lags starting from lag 0. The autocorrelations of channel 1 and channel 2 are zero from lags equal to and greater than $v_1 + 1$ and $v_2 + 1$ respectively. Therefore, minimizing the non-zero autocorrelation of a channel only at the lag $v+1$ should give a shortened channel of length i.e., $v+1$. The impulse response sequences of the two channels shown have only positive taps, as an example, the SAM and the SLAM algorithms can shorten channels with negative taps.

4.2 System Model

The same system model shown in Figure (3.4) is used. The same assumptions for the signal and noise as in Section (3.3) are used. The transmitted baseband sequence $x(n)$ is assumed to be white, zero-mean and WSS. This unit variance, $\sigma_x^2 = 1$, source sequence is transmitted through the linear finite-impulse response (FIR) channel $\mathbf{h} = [h(0)h(1), \ldots, h(L_h)]^T$. Here $v(n)$ is a zero-mean, i.i.d., noise sequence uncorrelated with the source sequence and has a variance σ_v^2. The received signal $r(n)$ at the input of the TEQ is

$$r(n) = \sum_{k=0}^{L_h} h(k)x(n-k) + v(n) \tag{4.2.1}$$

and $y(n)$, the output of the TEQ is given by

$$y(n) = \sum_{k=0}^{L_w} w(k)r(n-k) = \mathbf{w}^T\mathbf{r}_n \tag{4.2.2}$$

where $\mathbf{w} = [w(0)w(1), \ldots, w(L_w)]^T$ is the impulse response vector of the TEQ and $\mathbf{r}_n = [r(n)\ r(n-1)\ \ldots\ r(n-L_w)]^T$. The vector $\mathbf{c} = \mathbf{h} \star \mathbf{w}$ is the effective channel of order $L_c = L_h + L_w$. The symbol $\star$ represents

discrete time convolution and L_h and L_w are the orders of the channel and TEQ respectively. It is assumed that $2L_c < N$ holds, where N is the FFT size [22]. It means that the length of the effective channel is less than half the FFT size. Due to the baseband nature of the ADSL transmission, all quantities are taken as real; generalization to the complex case is straightforward [9].

4.3 SLAM

The autocorrelation sequence of the effective channel, $\mathbf{c}$, is given by

$$R_{cc}(l) = \sum_{k=0}^{L_c} c(k)c(k-l) \tag{4.3.1}$$

When the effective channel $\mathbf{c}$ has zero taps outside a contiguous window of size $(v+1)$, its autocorrelation value at a lag of $v+1$ is always zero, i.e.,

$$R_{cc}(l) = 0, \quad l = v+1$$

Therefore, a cost function, J_{slam}, based upon minimizing the square of the auto-correlation of the effective channel at lag $l = v+1$ is suggested, i.e.,

$$J_{slam} = |R_{cc}(l)|^2, \; l = v+1 \tag{4.3.2}$$

The trivial solution can be avoided by imposing a norm constraint on the TEQ i.e., $\|\mathbf{w}\|_2^2 = 1$. The optimization problem can then be stated as in [22]

$$\mathbf{w}^{opt} = \arg_{\mathbf{w}} \min_{\|\mathbf{w}\|_2^2=1} J_{slam}$$

As explained in Section (3.4), the autocorrelation sequence of the output $y(n)$ of the TEQ is related to the autocorrelation sequence of the

effective channel as

$$R_{yy}(l) = R_{cc}(l) + \sigma_v^2 R_{ww}(l) \tag{4.3.3}$$

An approximation to the cost function in Equation (4.3.2), denoted by $\hat{J}_{slam}$ is given by

$$\begin{aligned} \hat{J}_{slam} &= |R_{yy}(l)|^2, \qquad l = v+1 \\ &= |R_{cc}(l)|^2 + 2\sigma_v^2 R_{cc}(l) R_{ww}(l) \\ &\quad + \sigma_v^4 |R_{ww}(l)|^2 \end{aligned} \tag{4.3.4}$$

In most situations, the TEQ length $(L_w + 1)$ is shorter than the cyclic prefix length, v. In such cases, $R_{ww}(l)$ does not exist for the stated lag in Equation (4.3.4). Therefore, both the noise terms in Equation (4.3.4) vanish entirely. Even if the TEQ is longer than the cyclic prefix, the second and third terms being added are very small due to their multiplication with σ_v^2 and σ_v^4. The noise variance σ_v^2 is usually small for ADSL channels [22]. Therefore, it is assumed that under practical scenarios $\hat{J}_{slam} \cong J_{slam}$ as in Equation (4.3.2). Another notable difference of SLAM with SAM is that for the SLAM cost function, the knowledge of order of the channel $\mathbf{h}$ to determine L_c is not needed, as is required by SAM in [22]. The SLAM algorithm only requires the output of the TEQ and is, in that sense, blind.

4.4 Adaptive Algorithm

The steepest gradient-descent algorithm to minimize J_{v+1} is

$$\begin{aligned} \mathbf{w}^{new} &= \mathbf{w}^{old} - \mu \nabla_{\mathbf{w}} \left(J_{v+1} \right) \\ &= \mathbf{w}^{old} - \mu \nabla_{\mathbf{w}} \left(\left| E[y(n)y(n-l)] \right|^2 \right), \quad l = v+1 \end{aligned} \tag{4.4.1}$$

where μ is the step size and $\nabla_{\mathbf{w}}$ denotes the gradient evaluated at $\mathbf{w} = \mathbf{w}^{old}$.

4.4.1 Moving Average Implementation

A moving average implementation is used to realize the instantaneous cost function

$$J_{v+1}^{inst}(k) = \left| \sum_{n=kN_{avg}}^{(k+1)N_{avg}-1} \frac{y(n)y(n-l)}{N_{avg}} \right|^2, \quad l = v+1 \tag{4.4.2}$$

Here N_{avg} is a design parameter which determines a tradeoff between the algorithm complexity and a good estimate of the expectation. The stochastic gradient-descent algorithm, can then be written as (4.4.3) which, using Equation (4.2.2), takes the form of Equation (4.4.4).

$$\begin{aligned} \mathbf{w}^{k+1} = \mathbf{w}^{k} - 2\mu & \left\{ \sum_{n=kN_{avg}}^{(k+1)N_{avg}-1} \frac{y(n)y(n-l)}{N_{avg}} \right\} \\ & \times \left\{ \nabla_{\mathbf{w}} \left(\sum_{n=kN_{avg}}^{(k+1)N_{avg}-1} \frac{y(n)y(n-l)}{N_{avg}} \right) \right\} \end{aligned} \tag{4.4.3}$$

$$\mathbf{w}^{k+1} = \mathbf{w}^k - 2\mu \left\{ \sum_{n=kN_{avg}}^{(k+1)N_{avg}-1} \frac{y(n)y(n-l)}{N_{avg}} \right\} \times \left\{ \sum_{n=kN_{avg}}^{(k+1)N_{avg}-1} \left(\frac{y(n)\mathbf{r}_{n-l} + y(n-l)\mathbf{r}_n}{N_{avg}} \right) \right\} \quad (4.4.4)$$

$$\mathbf{w}^{k+1} = \frac{\mathbf{w}^{k+1}}{\|\mathbf{w}^{k+1}\|_2^2} \quad (4.4.5)$$

where

$$l = v + 1$$

4.4.2 Auto Regressive Implementation

Another way of implementing the SLAM algorithm is by using the Auto-Regressive (AR) estimates. Let

$$\mathbf{a}^n = (1-\rho)\mathbf{a}^{n-1} + \rho y(n) \begin{bmatrix} r(n-v-1) \\ \vdots \\ r(n-v-1-L_w) \end{bmatrix}$$

$$b^n = \mathbf{w}^T \mathbf{a}^n$$

$$\mathbf{c}^n = (1-\rho)\mathbf{c}^{n-1} + \rho y(n-v-1) \begin{bmatrix} r(n) \\ \vdots \\ r(n-L_w) \end{bmatrix}$$

where $0 < \rho < 1$ is a forgetting factor and is a design parameter. Using these AR estimates and Equation (4.2.2), the update rule of Equation

Steps	# multiplications	# addition/subtractions
(a)N_{avg} times $y(n-l)\mathbf{r}_n$	$N_{avg}.\{L_w+1\}$	-
(b)N_{avg} times $y(n)\mathbf{r}_{n-l}$	$N_{avg}.\{L_w+1\}$	-
(c)(a+b)	-	$N_{avg}.\{L_w+1\}$
(d)N_{avg} times $y(n)y(n-l)$	N_{avg}	-
(e)sum (d) outputs	-	$N_{avg}-1$
(f)$2\mu\times$ output of (e)	1	-
(g)output (f)$\times$ output (c)	L_w+1	-
(h)$\mathbf{w}^k$ - (g)	–	L_w+1
(i)Total	$N_{avg}.\{2L_w+3\}+L_w+2$	$N_{avg}.\{L_w+2\}+L_w$

Table 4.1. Complexity of SLAM-MA.

(4.4.1) can be written as

$$\begin{aligned}\mathbf{w}^{n+1} &= \mathbf{w}^n - 2\mu\{E[y(n)y(n-l)]\} \\ &\quad .\{E[y(n)\mathbf{r}_{n-l} + y(n-l)\mathbf{r}_n]\} \\ &\cong \mathbf{w}^n - 2\mu\, b^n.\{\mathbf{a}^n + \mathbf{c}^n\} \qquad (4.4.6)\end{aligned}$$

$$\mathbf{w}^{n+1} = \frac{\mathbf{w}^{n+1}}{\|\mathbf{w}^{n+1}\|_2^2} \qquad (4.4.7)$$

The advantage of AR implementation is that the TEQ is updated at every time instant rather than at every N_{avg}^{th} time instant as is the case with the MA implementation. The complexity of SAM-MA calculated in Table 3.1 was $(L_c-v)\{N_{avg}(2L_w+3)+L_w+1\}+L_w+1$ multiplications plus one division for renormalization. The computational complexity of the MA implementation of SLAM (SLAM-MA), AR implementation of SLAM (SLAM-AR), and AR implementations of SAM (SAM-AR) are calculated in the Tables 4.1, 4.2, and 4.3 respectively. The calculations

Steps	# multiplications	# addition/subtractions
(a)$\mathbf{a}^n$	$2L_w + 3$	$L_w + 1$
(b)$\mathbf{c}^n$	$2L_w + 3$	$L_w + 1$
(c)(a)+(b)	-	$L_w + 1$
(d)$\mathbf{b}^n$	$L_w + 1$	L_w
(e)$2\mu\times$ (d)	1	-
(f)output (e) $\times$ output (c)	$L_w + 1$	-
(g)$\mathbf{w}^n$ - (f)	$-$	$L_w + 1$
(i)Total	$6L_w + 9$	$5L_w + 4$

Table 4.2. Complexity of SLAM-AR.

Steps	# multiplications	# addition/subtractions
(a)$\mathbf{a}^n$	$2L_w + 3$	$L_w + 1$
(b)$\mathbf{c}^n$	$2L_w + 3$	$L_w + 1$
(c)(a)+(b)	-	$L_w + 1$
(d)$\mathbf{b}^n$	$L_w + 1$	L_w
(e)output (d) $\times$ output (c)	$L_w + 1$	-
(f)Sub-total for ($Lc-v$) lags	$(L_c - v).\{6L_w + 8\}$	$(L_c - v).\{4L_w + 3\}$
(g)$2\mu\times$ (f)	$(L_c - v).\{6L_w + 8\} + L_w + 1$	-
(h)$\mathbf{w}^n$ - (g)	$-$	$L_w + 1$
(i)Total	$(L_c - v).\{6L_w + 8\} + L_w + 1$	$(L_c - v).\{4L_w + 3\} + L_w + 1$

Table 4.3. Complexity of SAM-AR.

shown in these Tables clearly show the implementation advantage of SLAM over the SAM algorithm. For ADSL downstream case, $L_h = 512$, the typical value of $L_w = 16$ and $v = 32$. This gives $L_c - v = 499$. Therefore, the complexity of SLAM is about 1/500 times that of SAM for ADSL downstream transmission environment parameters.

4.5 Properties of the SLAM cost function

As for other blind equalization algorithms, e.g., CMA; SLAM's cost can be expected to be multimodal. In general, the SLAM cost surface will have local minima. As in [22] for SAM, an example is presented here to demonstrate the existence of global and local minima of SLAM. Consider the following theorem.

Theorem 4.5.1. *The SLAM cost function is invariant to the operation* $\boldsymbol{w} \rightarrow \overline{\boldsymbol{w}}$, *where* $\overline{\boldsymbol{w}}$ *denotes* $\boldsymbol{w}$ *with the order of its elements reversed.*

Proof: Consider the autocorrelation sequence of the combined channels $\mathbf{c}_1 = \mathbf{h} \star \mathbf{w}$ and $\mathbf{c}_2 = \mathbf{h} \star \overline{\mathbf{w}}$, where $\star$ denotes convolution.

$$\begin{aligned}
\mathbf{R}_{c_1 c_1} &= \mathbf{c}_1 \star \overline{\mathbf{c}_1} = (\mathbf{h} \star \mathbf{w}) \star \overline{(\mathbf{h} \star \mathbf{w})} \\
&= \mathbf{h} \star \mathbf{w} \star \overline{\mathbf{h}} \star \overline{\mathbf{w}} \\
&= (\mathbf{h} \star \overline{\mathbf{w}}) \star (\overline{\mathbf{h}} \star \mathbf{w}) \\
&= \mathbf{c}_2 \star \overline{\mathbf{c}_2} = \mathbf{R}_{c_2 c_2}
\end{aligned}$$

Since the autocorrelation sequence is invariant to reversing the order of the elements of $\mathbf{w}$, the SLAM cost is also invariant to such a switch. Theorem (4.5.1) means if there is a good minima of the SLAM cost surface, say at $\mathbf{w}_0$, there will also be another minimum at $\overline{\mathbf{w}}_0$. Even though the SLAM cost will be the same, the achievable bit rate will not be the same for the two TEQ settings. This flipped $\overline{\mathbf{w}}_0$, therefore, is not necessarily as good as $\mathbf{w}_0$. Another consequence is that the SLAM cost surface is symmetric with respect to $\mathbf{w} \rightarrow \overline{\mathbf{w}}$; therefore, there will be minima, maxima, or saddle points along the subspace $\mathbf{w} = \overline{\mathbf{w}}$.

To demonstrate this as in [22], consider the following example. The

channel is $\mathbf{h} = [1, 0.5, 0.3]$, the cyclic prefix length is 1 (making the length of the required channel 2), there is no noise, the TEQ $\mathbf{w}$ has three taps, and the unit norm constraint $\|\mathbf{w}\|_2 = 1$ is used. The equalizer, then must lie on the unit sphere; therefore the equalizer is represented in spherical coordinates: $w_0 \triangleq w_x = \cos(\theta)\sin(\phi), w_1 \triangleq w_z = \cos(\phi), w_2 \triangleq w_y = \sin(\theta)\sin(\phi)$. In this case $\mathbf{w} \rightarrow \overline{\mathbf{w}}$ is equivalent to switching w_x and w_y, which is equivalent to reflecting θ over $\pi/4$ or $5\pi/4$, and $\mathbf{w} \rightarrow -\mathbf{w}$ is equivalent to the combination of reflecting ϕ over $\pi/2$ and adding π to θ.

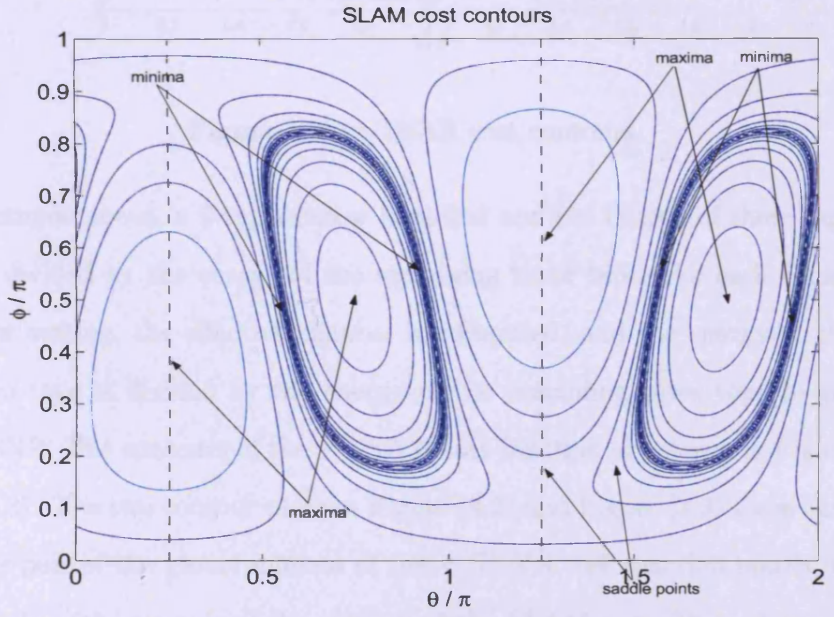

Figure 4.2. SLAM cost contours. The dashed lines are the plane of symmetry of the SLAM cost function.

A contour plot of the SLAM cost function is shown in Figure (4.2). The axes represent normalized values of the spherical coordinates θ and ϕ. The contours are logarithmically scaled. There are four minima, but they all have equivalent values of the SLAM cost due to the equivalence relations $\mathbf{w} \rightarrow \overline{\mathbf{w}}$ and $\mathbf{w} \rightarrow -\mathbf{w}$. For the 5-tap effective channel in the

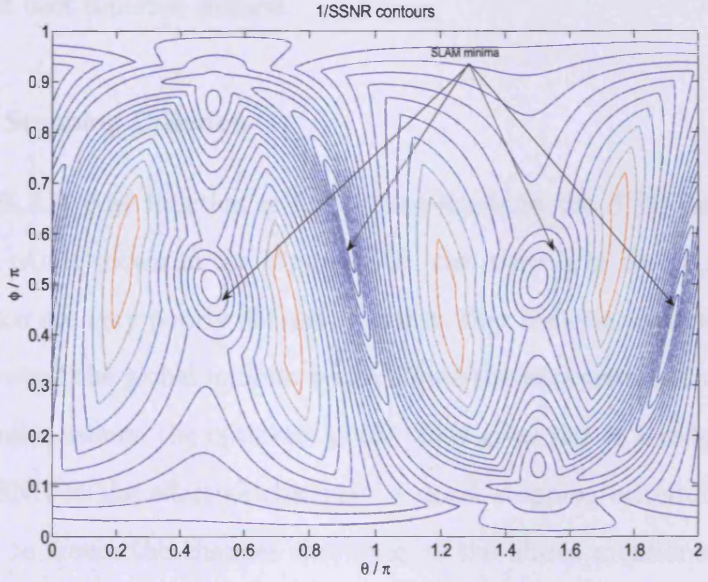

Figure 4.3. 1/SSNR cost contours.

example above, a 2-tap window is picked and the energy of these taps is divided by the energy of the remaining three taps. For each equalizer setting, the effective channel is computed, and the energy of the two taps is divided by the energy of the remaining three taps to get SSNR. The contours of the $1/SSNR$ cost function are shown in Figure (4.3). The two contour plots in Figure (4.2) and Figure (4.3) show that the pair of the global minima of the $1/SSNR$ cost function match up nicely with one pair of the minima of the SLAM cost. Thus, if a pair of the minima of the SLAM cost have a high value of $1/SSNR$, it will be the pair of local minima in terms of the achievable bit rate. The global minima can be found by switching to the other pair of minima of SLAM simply by reversing the order of taps in $\mathbf{w}$. The SAAM cost function suggested in the previous chapter is based on minimizing the autocorrelation, therefore, analysis presented here applies similarly to

SAAM cost function surface.

4.6 Stopping Criterion

The SLAM cost function is highly non-linear in the TEQ parameter space. As is shown in the Figure (4.2), the minima of the SLAM cost function are very poorly defined. It seems that the cost surface is shallow around the global minima which allows the parameters of the TEQ to wander around the optimum point. This gives rise to a reduction in the SSNR of the effective channel. A novel stopping criterion is proposed to freeze the channel shortener at the above mentioned point. Specifically the energy of the taps of the TEQ, except the first tap, is examined and when the sum of the energy of these taps reaches a threshold, the adaptation of the TEQ is stopped. The stopping criterion seems intuitive, also there have been studies in the literature showing the importance of initialization tactics and equalizer parameter constraints for the blind adaptive equalizers to ensure convergence only to the global minima [75]. The proposed stopping criterion which constrains the TEQ parameters does not add any extra computational complexity as the norm of the TEQ is being taken at every iteration. Simulations have shown the effectiveness of the stopping criterion.

4.7 Simulations

The standard parameters of an ADSL downstream transmission were simulated as in [22]. Both MA and AR implementations of the SLAM algorithms were simulated. The value of N_{avg} and ρ for the MA and AR implementations of SLAM were 32 and 1/100 respectively. The step

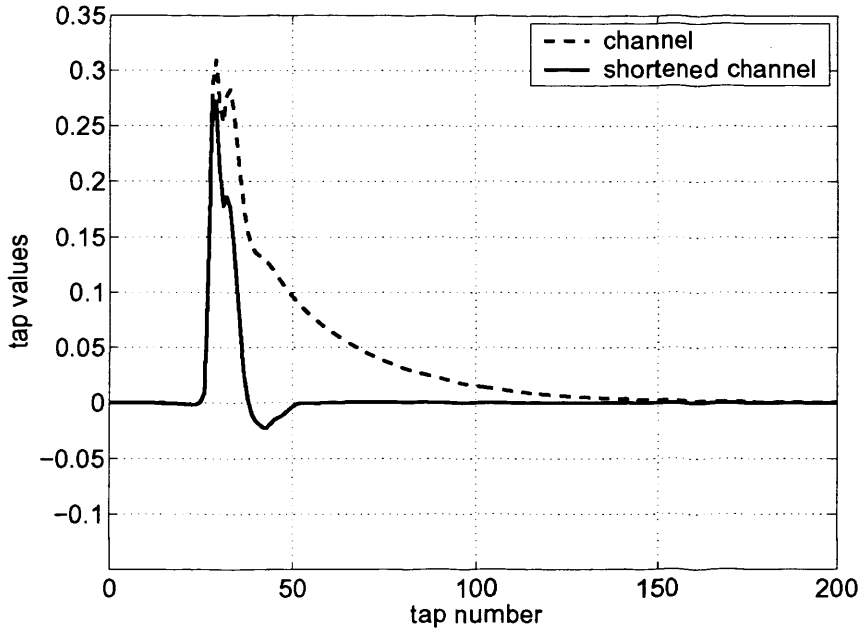

Figure 4.4. Original and the shortened channel.

sizes used for both implementations were 150 and 12 respectively. The value of the *threshold* = 0.044 was fairly same for all the 8 CSA loop channels. Left initialization with the first spike of the TEQ initialized to unity was used. MA and AR implementations of the SAM algorithm are also shown for comparison purposes. Achievable bit rate for a fixed probability of error was chosen as the performance metric. The details of how the bit rate is calculated have already been given in Section (3.8). The bit rate on each subcarrier is determined using noise margin γ_m = 6dB and the coding gain γ_c = 4.2dB. The value of Γ_{gap} = 9.8dB is used which corresponds to a probability of error 10^{-7} and the QAM modulation used across the subcarriers. SLAM is also compared with the MSSNR solution of [21]. The remainder of the explanation relates to the figures mentioned individually.

Figures (4.4) and (4.5) show the shortening effect on the original chan-

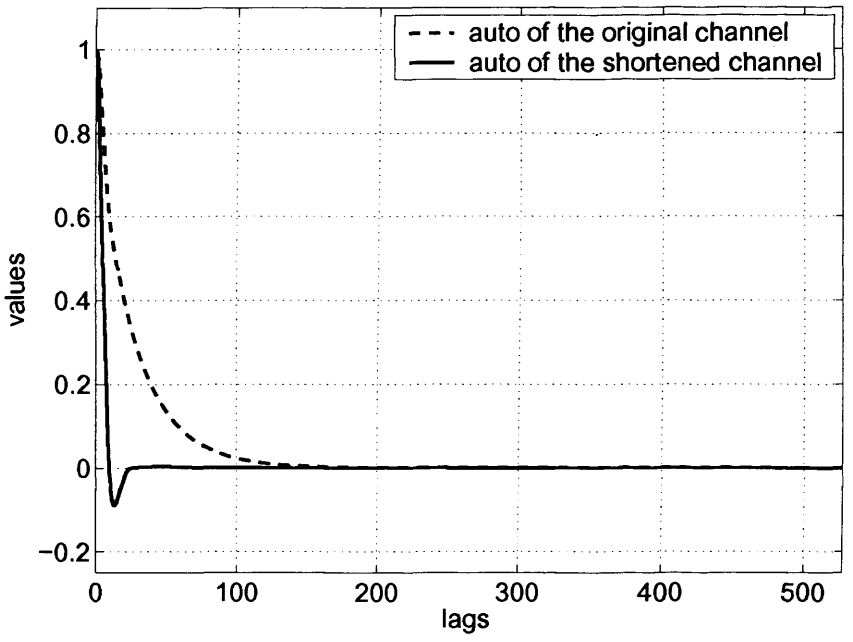

Figure 4.5. Autocorrelation of the original and the shortened channel for non-negative lags.

nel and its autocorrelation. Figure (4.6) shows the 16-tap TEQ designed after the SLAM algorithm converges. Figure (4.7) in its top plot shows the SSNR of the effective channel versus averaging block/iteration number. The middle plot shows the achievable bit rate versus iteration number for SLAM and SAM algorithms without stopping criterion. Decrease in the bit rates after achieving the peak bit rates is evident for both the algorithms. The bottom plot shows the SLAM cost versus the iteration number. As was noted with SAAM, the SLAM cost function and the bit rate are also a smooth function of each other i.e., the SLAM minima and the bit rate maxima appear to be located in close proximity. All the results in these plots were for an SNR=40dB. In Figure (4.8), the same plots have been reproduced. This time the novel stopping criterion is used for the SLAM algorithm. It is clear that the TEQ adaptation has been frozen once the peak bit rates have been

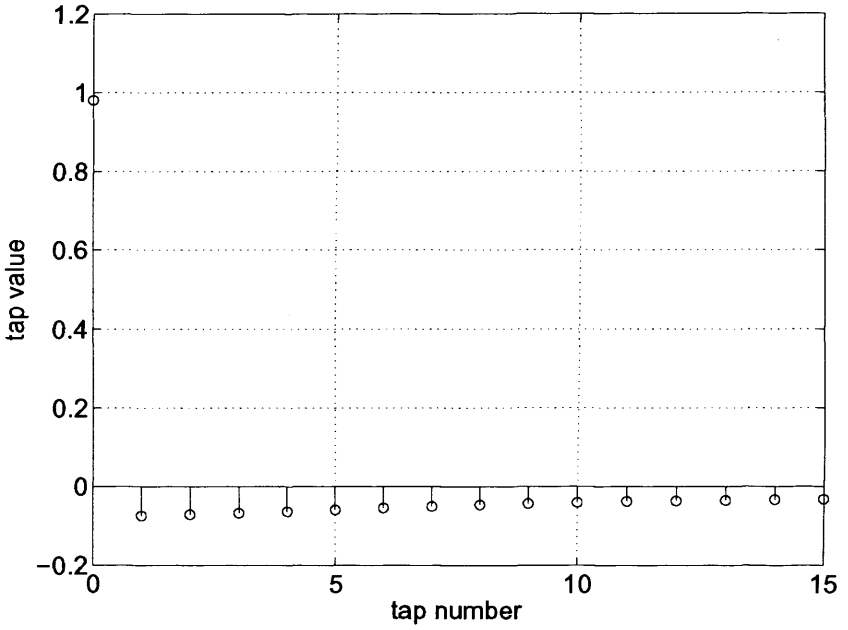

Figure 4.6. TEQ coefficients.

achieved. Figure (4.9) shows the bit rates versus a range of SNRs for white as well as Near End Crosstalk (NEXT) noise. The upstream signal is the source of the NEXT noise for the downstream transmission. The NEXT noise is generated by the code available at [70] which is based on the specification given in [60]. NEXT noise was generated by exciting a coupling filter with spectrum $|H_{next}(f)|^2 = H_0 H_{mask}(f) f^{3/2}$ with white noise. The constant H_0 was chosen so that the variance of the NEXT was σ_v^2, with σ_v^2 chosen to achieve the desired SNR [22]. The filter H_{mask} is an ADSL upstream spectral mask that passes frequencies between 28 and 138 KHz. SLAM approaches the MSSNR bit rates and outperforms SAM for the whole range of the SNRs. The behavior of the SLAM algorithm is almost the same for white as well as NEXT noise.

In Figure (4.10), the data rates achieved by SLAM for the 8 CSA loop

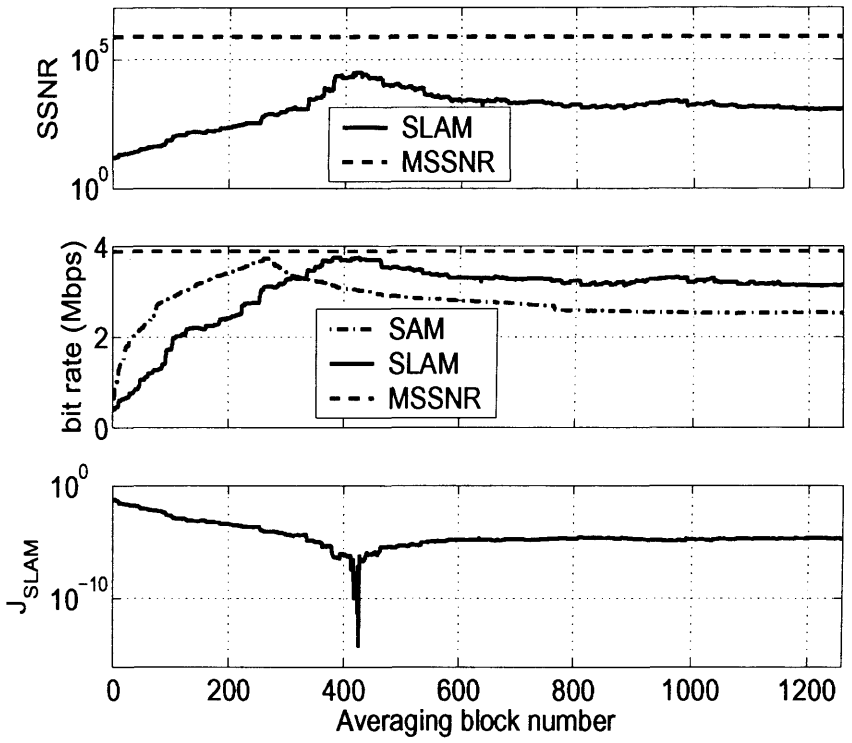

Figure 4.7. SAM, SLAM(-MA), and MSSNR simulated at SNR=40dB. top; SSNR versus iteration number. middle; Bit rates achieved by SAM, SLAM-MA (no stopping criterion used), and MSSNR versus iteration number. bottom; SLAM cost versus iteration number.

channels are shown. The results of the AR implementation of SLAM have been shown in Figures (4.11) and (4.12).

If all the contiguous $\tau + 1$ taps of a channel impulse response sequence are only positive and the channel is zero outside this width of $\tau + 1$, its non-negative autocorrelation values are always zero from the lag equal to and greater than $\tau + 1$. In this case the SAM as well as the SLAM cost will be zero at the same time. However, if the contiguous $\tau+1$ taps of the channel impulse response sequence are more frequently positive and negative, then there is a possibility that its non-negative autocorrelation is zero at some lag lower than $\tau + 1$ and non-zero for higher lags. It again becomes zero for lags equal to and greater than $\tau + 1$.

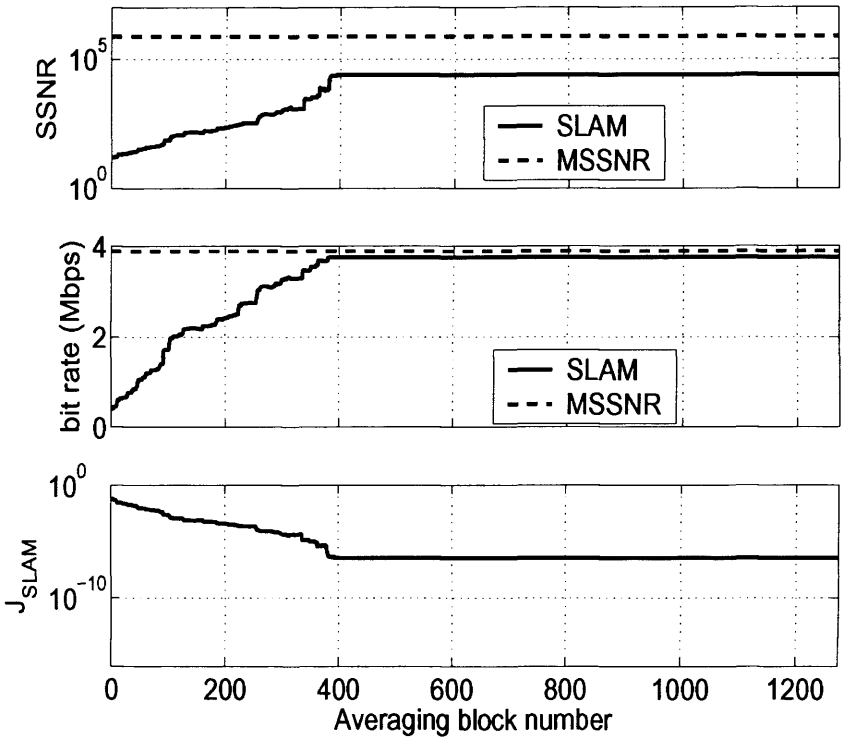

Figure 4.8. SAM, SLAM(-MA), and MSSNR simulated at SNR=40dB. top; SSNR versus iteration number. middle; Bit rates achieved by SAM, SLAM-MA (with stopping criterion), and MSSNR versus iteration number. bottom; SLAM cost versus iteration number.

In this case, the statement does not hold that the channel is zero after the width equal to the lag of the first zero autocorrelation. In the nutshell, it would mean that the SLAM cost is zero but the channel is not shortened. Nevertheless, simulations show that SLAM does similarly well for the CSA loop channels, for which SAM has been simulated. A SLAM channel shortening example is shown in Figure (4.13) where upstream filtering has been included in the channel.

4.8 Conclusions

The SLAM algorithm proposed in this chapter inherits all the merits of the SAM algorithm of [22] while at the same time considerably reduces

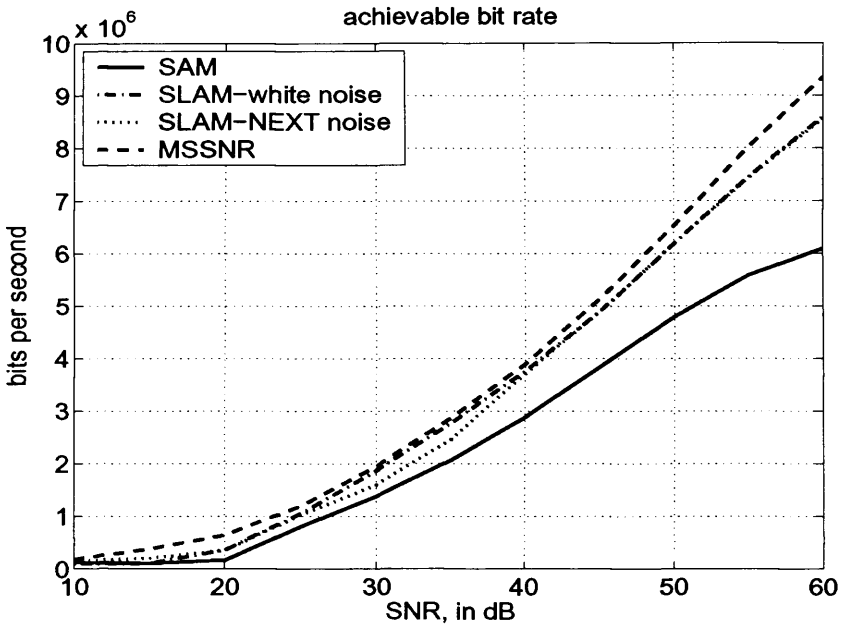

Figure 4.9. Achievable bit rate versus SNR for white and NEXT noise.

its complexity. Moreover, SLAM does not need a knowledge of the order of the original channel to calculate the cost function. The intuitive stopping criterion freezes the TEQ parameters at the peak achievable bit rates and stops them from wandering. The simulations have been performed for all 8 CSA loop channels. SLAM, with the stopping criterion, achieves better bit rates than SAM for a range of SNRs and for both white as well as NEXT noise.

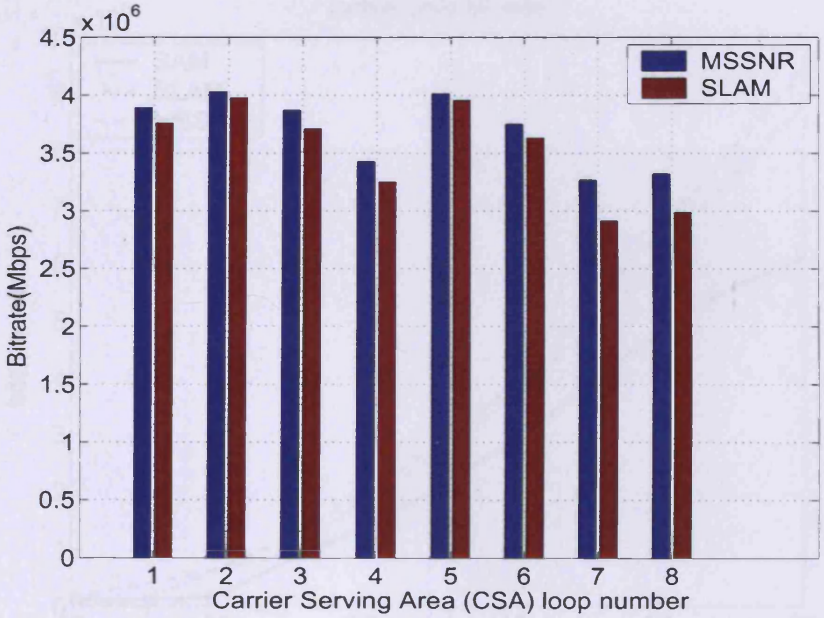

Figure 4.10. Achievable bit rates at 40dB SNR for 8 CSA loops.

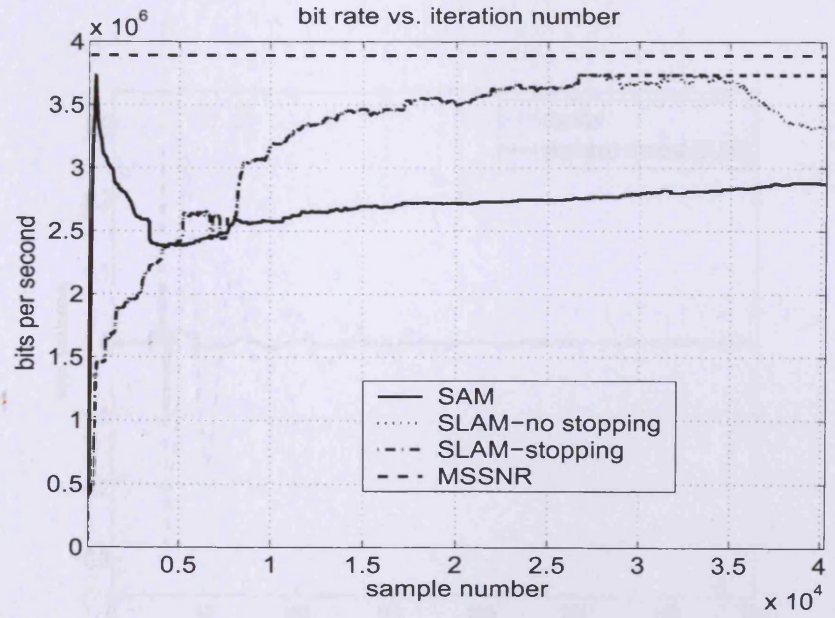

Figure 4.11. Achievable bit rate versus iteration number at 40dB SNR. Without stopping criterion applied, both SAM and SLAM(-AR) start decreasing the bit rate.

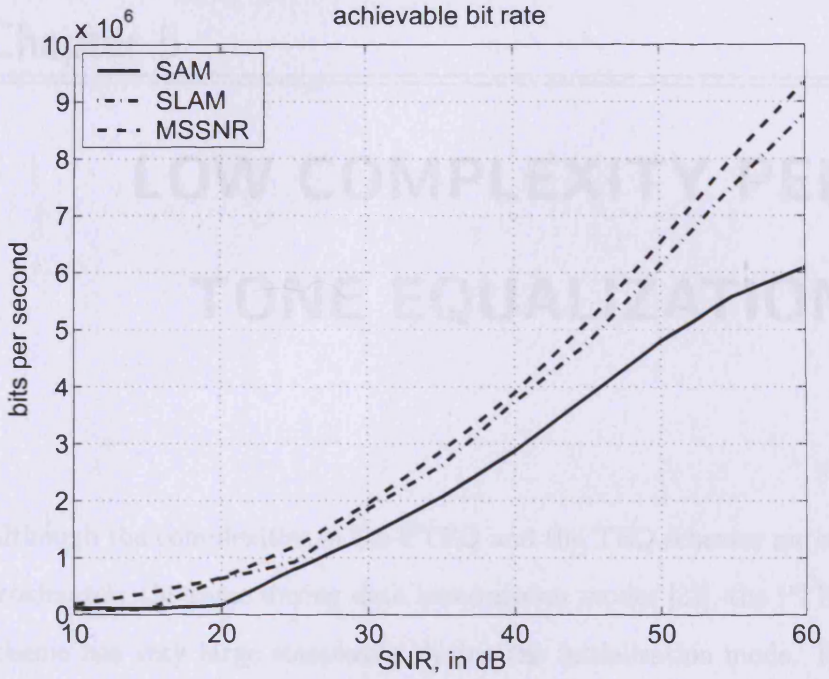

Figure 4.12. Achievable bit rate versus SNR for SAM, SLAM(-AR) and MSSNR.

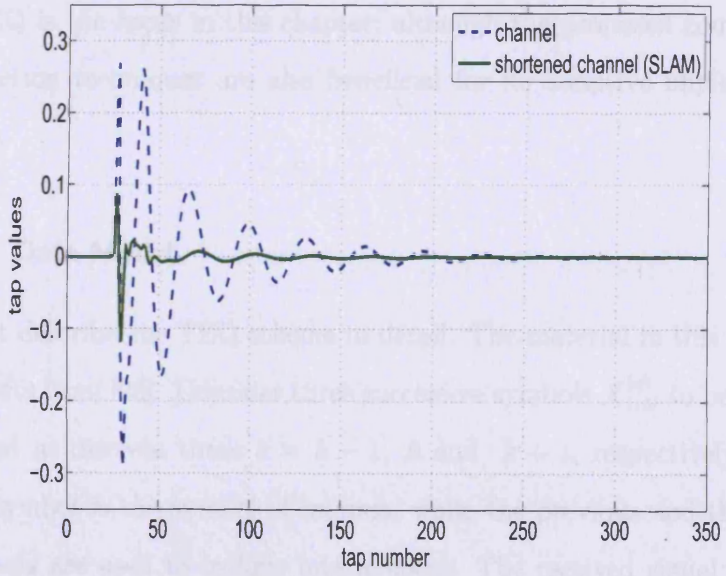

Figure 4.13. Original and the shortened channel. The upstream filters have applied to the original channel.

Chapter 5

LOW COMPLEXITY PER TONE EQUALIZATION

Although the complexities of the PTEQ and the TEQ schemes are approximately the same during data transmission modes [23], the PTEQ scheme has very large complexity during the initialization mode. For DMT-based systems, this scheme requires initialization of $T \times N/2$ filter taps instead of only T taps as in the TEQ scheme. This problem is addressed in this chapter. The direct non-adaptive initialization of the PTEQ is the focus in this chapter; although the proposed complexity reduction techniques are also beneficial for its adaptive implementations.

5.1 Data Model

I first describe the TEQ scheme in detail. The material in this section benefits from [23]. Consider three successive symbols $X_{1:N}^{(c)}$ to be transmitted at discrete times $c = k-1$, k and $k+1$, respectively. The kth symbol is the symbol of interest, while the previous and the next symbols are used to include interferences. The received signal can be

specified in vector form as:

$$\overbrace{\begin{bmatrix} r_{k\cdot s+v-T+2+\delta} \\ \vdots \\ r_{(k+1)\cdot s+\delta} \end{bmatrix}}^{\mathbf{r}} = \left[\begin{array}{c|ccc|c} & \mathbf{h} & 0 & \dots & \\ \mathbf{O}_{(1)} & & \ddots & & \mathbf{O}_{(2)} \\ & \dots & 0 & \mathbf{h} & \end{array}\right] \cdot \begin{bmatrix} \mathbf{P} & \mathbf{O} & \mathbf{O} \\ \mathbf{O} & \mathbf{P} & \mathbf{O} \\ \mathbf{O} & \mathbf{O} & \mathbf{P} \end{bmatrix}$$

$$\cdot \begin{bmatrix} \mathcal{I}_N & \mathbf{O} & \mathbf{O} \\ \mathbf{O} & \mathcal{I}_N & \mathbf{O} \\ \mathbf{O} & \mathbf{O} & \mathcal{I}_N \end{bmatrix} \cdot \overbrace{\begin{bmatrix} \mathbf{X}_{1:N}^{(k-1)} \\ \mathbf{X}_{1:N}^{(k)} \\ \mathbf{X}_{1:N}^{(k+1)} \end{bmatrix}}^{\mathbf{X}} + \overbrace{\begin{bmatrix} n_{k\cdot s+v-T+2+\delta} \\ \vdots \\ n_{(k+1)\cdot s+\delta} \end{bmatrix}}^{\mathbf{n}} \tag{5.1.1}$$

which can also be written as

$$\mathbf{r} = \mathbf{H} \cdot \mathbf{X} + \mathbf{n} \tag{5.1.2}$$

where

$$\mathbf{P} = \left[\begin{array}{c|c} \mathbf{O} & \mathbf{I}_v \\ \hline \multicolumn{2}{c}{\mathbf{I}_N} \end{array}\right] \tag{5.1.3}$$

which adds the cyclic prefix. Here $s = N+v$ is the length of the symbol including the prefix and k denotes the symbol index. Furthermore, r_l denotes the received signal, and n_l zero mean additive noise with l being the sample index. The vector $\mathbf{h} = [h_L \dots h_0 \dots h_{-K}]$ is the channel impulse response in reverse order. The $\mathcal{I}_N$ matrices are $N \times N$ IFFT matrices [23]. $\mathbf{O}_{(1)}$ and $\mathbf{O}_{(2)}$ are zero matrices of size $(N+T-1) \times (N+v-T+1-L+v+\delta)$ and $(N+T-1) \times (N+v-K-\delta)$ respectively. These sizes show that the first sample for the symbol of interest has been

collected after a delay of K. This zero reference delay K corresponds to the head $[h_{-K} \dots h_{-1}]$ and the tail $[h_{v+1} \dots h_L]$ which maximizes the energy in $[h_0 \dots h_v]$ [23]. Therefore $K+1$ is the synchronization point. A blind method to estimate K has been suggested in Section (5.2). If K' is the estimate of K, then the parameter δ is the synchronization error, given by

$$\delta = K' - K \tag{5.1.4}$$

The standard receiver with a TEQ is based on the following operation:

$$\begin{bmatrix} Z_1^{(k)} \\ \vdots \\ Z_N^{(k)} \end{bmatrix} = \begin{bmatrix} D_1 & 0 & \cdots \\ 0 & \ddots & 0 \\ \vdots & 0 & D_N \end{bmatrix} \cdot \underbrace{\mathcal{F}_N \cdot (\mathbf{R} \cdot \mathbf{w})}_{1\ FFT}$$

where

$$\mathbf{R} = \begin{bmatrix} r_{k\cdot s+v+1+\delta} & r_{k\cdot s+v+\delta} & \cdots & r_{k\cdot s+v-T+2+\delta} \\ r_{k\cdot s+v+2+\delta} & r_{k\cdot s+v+1+\delta} & \cdots & r_{k\cdot s+v-T+3+\delta} \\ & \ddots & \ddots & \\ r_{(k+1)\cdot s+\delta} & r_{(k+1)\cdot s-1+\delta} & \cdots & r_{(k+1)\cdot s-T+1+\delta} \end{bmatrix}$$

and $\mathbf{w}_{T\times 1} = [w_0 w_1, \dots, w_{T-1}]^T$ is the real T-tap TEQ, $\mathcal{F}_N$ an $N \times N$ FFT-matrix, D_i the complex 1-tap FEQ for tone i, $\mathbf{R}$ an $N \times T$ Toeplitz matrix of received samples for the current symbol k, and $Z_i^{(k)}$ is the final output for tone i and symbol k. The PTEQ scheme is based on transferring the TEQ operations to the frequency domain. For a single tone i,

$$Z_i^{(k)} = D_i \cdot row_i(\mathcal{F}_N) \cdot (\mathbf{R} \cdot \mathbf{w}) = \underbrace{row_i(\mathcal{F}_N \cdot \mathbf{R})}_{T\ FFTs} \cdot \underbrace{\mathbf{w} \cdot D_i}_{\mathbf{w}_i} \tag{5.1.5}$$

Now $\mathbf{w}_i$ is a complex T-tap PTEQ for tone i. From Equation (5.1.5), it seems that T FFTs are needed instead of one FFT per symbol. Because of the Toeplitz structure of $\mathbf{R}$, these FFTs can be calculated efficiently by a sliding FFT [23]. One full FFT has to be calculated for the first column of $\mathbf{R}$ and the $(T-1)$ remaining FFTs can be deduced from it. Using this property of the sliding FFT, the so called modified PTEQ equalizer for each tone i has as its inputs the ith output of the FFT of the first column of the matrix $\mathbf{R}$ and $(T-1)$ real difference terms. From now on this modified PTEQ equalizer will be called the PTEQ equalizer and will be denoted by $\mathbf{v}_i = [v_{i,0} \dots v_{i,T-1}]^T$.

The block diagrams of the TEQ/FEQ scheme and the PTEQ scheme are given in Figure (5.1) specialized to the case $N = 4$, $T = 3$. As shown in Equation (5.1.1), $(N+T-1)$ samples are collected related to symbol period k in the $(N+T-1) \times 1$ vector $\mathbf{r}^{(k)}$, note that these collected samples form the entries of the Toeplitz matrix $\mathbf{R}$. The PTEQ equalizer for the ith tone, denoted by the $T \times 1$ vector $\mathbf{v}_i$, has as its inputs the ith output of the FFT, denoted by $[\mathbf{0}_{1\times T-1}, \mathcal{F}_N(i,:)] \cdot \mathbf{r}^{(k)}$, and $(T-1)$ difference terms, denoted by $[\mathbf{I}_{T-1}, \mathbf{0}_{(T-1)\times(N-T+1)}, -\mathbf{I}_{T-1}] \cdot \mathbf{r}^{(k)}$, where $\mathbf{I}_n$ is the $n \times n$ identity matrix, $\mathbf{0}_{n\times m}$ is the $n \times m$ all zero matrix, and $\mathcal{F}_N(i,:)$ is the ith row of the $N \times N$ FFT matrix $\mathcal{F}_N$. The optimal PTEQ equalizer, which gives rise to maximum SNR on each tone i, can be computed by finding the MMSE-PTEQ by minimizing the following

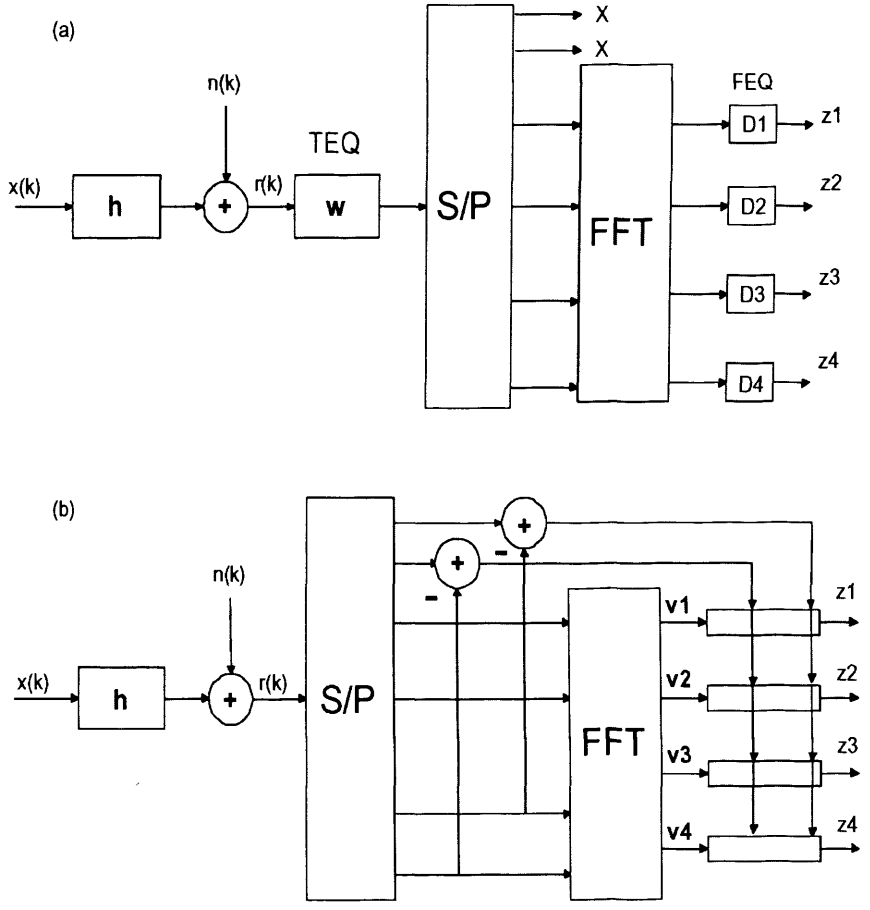

Figure 5.1. Comparison of TEQ/FEQ and PTEQ schemes for N=4, T=3 (a) The TEQ/FEQ scheme (b) The PTEQ scheme.

cost function [23]:

$$\min_{\mathbf{v}_i} J(\mathbf{v}_i)$$

$$= \min_{\mathbf{v}_i} E\left\{\left|\overline{\mathbf{v}}_i^T \cdot \underbrace{\left[\begin{array}{c|c|c} \mathbf{I}_{T-1} & \mathbf{O} & -\mathbf{I}_{T-1} \\ \hline \mathbf{O} & & \mathcal{F}_N(i,:) \end{array}\right]}_{\mathbf{F}_i} \cdot \mathbf{r}^{(k)} - X_i^{(k)}\right|^2\right\}$$

where $\overline{\mathbf{v}}_i = [v_{i,T-1} \ldots v_{i,0}]^T$. Where the column vector $\overline{\mathbf{z}}_i^k = \mathbf{F}_i \cdot \mathbf{r}^{(k)}$, contains $(T-1)$ required difference terms in reverse order in its first $(T-1)$ entries, and the ith value of the single FFT in its last entry. The MMSE solution is then given by

$$\overline{\mathbf{v}}_i = E\{(\overline{\mathbf{z}}_i^k)^H(\overline{\mathbf{z}}_i^k)\}^{-1} E\{(\overline{\mathbf{z}}_i^k)^H(X_i^k)\}$$

This optimum PTEQ equalizer calculation is based on the assumption that the channel model and the signal and noise covariance matrices are known as in [23]. The complexities of the TEQ/FEQ scheme and the PTEQ scheme during data transmission are comparable and are of the order of F_sT, where F_s is the sampling frequency [23].

5.2 Synchronization

In what follows, it is shown that the expected value of the power of the first difference term is proportional to the energy of the channel impulse response outside of a length v window, plus a noise gain term. The value of this energy depends upon the value of K'. When this value is minimized or in other words when the energy is maximized in a window of length v, $K' = K$ and consequently $\delta = 0$. The proof

follows the outlines of the cost function analysis presented in [38]. The following are assumed

1. The IFFT outputs are uncorrelated.
2. $N \geq (L + K + 1)$, The FFT length is at least as large as the channel impulse response length.
3. Noise autocorrelation function $R_n(l) = 0$ for $l > N$.
4. Noise is uncorrelated with data.

The first difference term is given by

$$Diff_1 = r(v + K') - r(v + N + K') \tag{5.2.1}$$

The expected value of the power of the first difference term is given by

$$J_1 = E\left(r(v + K') - r(v + N + K')\right)^2 \tag{5.2.2}$$

Next consider the following definitions:

$$\begin{aligned} \mathbf{x}_j &= [x(j), x(j-1), \ldots, x(j-(L+K+1)+1)] \\ \mathbf{x}_j' &= \mathbf{x}_j - \mathbf{x}_{j+N} \end{aligned} \tag{5.2.3}$$

$$
\begin{aligned}
J_1 &= E[|\mathbf{h}^T\mathbf{x}_{v+K'} - \mathbf{h}^T\mathbf{x}_{v+N+K'} + n_{v+K'} - n_{v+N+K'}|^2] \\
&= E[|\mathbf{h}^T\mathbf{x}'_{v+K'}|^2] + E[n_{v+K'} - n_{v+N+K'}|^2] \\
&= \mathbf{h}^T \underbrace{E[\mathbf{x}'_{v+K'}(\mathbf{x}'_{v+K'})^h]}_{\mathbf{A}_x^{v+K'}} \mathbf{h} + E[|n_{v+K'}|^2] + E[|n_{v+N+K'}|^2] \\
&\quad -2E[(n_{v+K'})(n_{v+N+K'})] \\
&= \mathbf{h}^T \underbrace{E[\mathbf{x}'_{v+K'}(\mathbf{x}'_{v+K'})^h]}_{\mathbf{A}_x^{v+K'}} \mathbf{h} + 2\sigma_n^2 \qquad (5.2.4)
\end{aligned}
$$

Where assumption (4) has been used in going from the first to the second line. Assumption (3) has been used in moving from the second to the third line and then to the fourth line. Note that

$$
\begin{aligned}
\mathbf{x}'_{v+K'} = \; & [x(v+K') - x(v+N+K') \\
& x(v+K'-1) - x(v+N+K'-1), \ldots, \\
& x(v+K' - (L+K+1)+1) \\
& -x(v+N+K' - (L+K+1)+1)]^T
\end{aligned}
$$

The values of x that enter additively have the highest index of $(v+K')$, whereas the values of x that enter with a minus sign have the smallest index of $(v+N+K' - (L+K+1)+1)$. If assumption (2) holds i.e., $N \geq L+K+1$, then the highest index in the first group will be lower than the lowest index in the second group. Now if assumption (1) above holds, then $\mathbf{A}_x^{v+K'}$ will be diagonal. Furthermore, the middle v terms in Equation (5.2.4) are all zero due to the addition of the cyclic prefix in the transmitted signal. Thus

$$
\mathbf{A}_x^{v+K'} = 2\sigma_x^2[diag(\mathbf{1}_{K'\times 1}, \mathbf{0}_{v\times 1}, \mathbf{1}_{(L+K+1-v-K')\times 1})] \qquad (5.2.5)
$$

Substituting in (5.2.4),

$$J_1 = 2\sigma_x^2 \left(\sum_{j=1}^{K'} |h_j|^2 + \sum_{j=v+K'+1}^{K+L+1} |h_j|^2 \right) + 2\sigma_n^2 \qquad (5.2.6)$$

It is straightforward to show that the expected value of the power of the second difference term is given by

$$J_2 = 2\sigma_x^2 \left(\sum_{j=1}^{K'-1} |h_j|^2 + \sum_{j=v+K'}^{K+L+1} |h_j|^2 \right) + 2\sigma_n^2 \qquad (5.2.7)$$

and so on.

Depending upon the parameter K', there are three cases

- if $K' > K$, suppose $K' = K + 1$, which means $\delta = +1$, J_1 is proportional to the energy of the channel impulse response from its tap 1 to $(K + 1)$ plus the energy in the taps after a window of length v plus a noise gain term. Likewise, J_2 is proportional to the energy of the channel impulse response from its tap 1 to K plus the energy in the taps after a window of length v plus a noise gain term, and so on, for higher difference terms.

- if $K' = K$, which means $\delta = 0$, J_1 is proportional to the energy of the channel impulse response from its tap 1 to K plus the energy in the taps after a window of length v plus a noise gain term. Likewise, J_2 is proportional to the energy of the channel impulse response from its tap 1 to $(K - 1)$ plus the energy in the taps after a window of length v plus a noise gain term, and so on, for higher difference terms.

- if $K' < K$, suppose $K' = K - 1$, which means $\delta = -1$, J_1 is

proportional to the energy of the channel impulse response from its tap 1 to $(K-1)$ plus the energy in the taps after a window of length v plus a noise gain term. Likewise, J_2 is proportional to the energy of the channel impulse response from its tap 1 to $(K-2)$ plus the energy in the taps after a window of length v plus a noise gain term, and so on, for higher difference terms.

The points summarized above give an inside look into the construction of the difference terms especially at different synchronization errors in the system. These are further elaborated in Section (5.3).

The timing synchronization in OFDM systems corresponds to finding a delay which maximizes the energy in the impulse response of the channel in a window of length $v+1$. There are many timing synchronization algorithms developed for multicarrier systems [76]. These schemes estimate the channel impulse response as is realized within a DMT system by consistently transmitting the same DMT symbol during initialization and generating the multicarrier signal without guard band insertion. At the receiver, an FFT is performed and the outputs are corrected to remove the QAM modulation. Finally, the IFFT applied to the corrected signal yields a noisy estimate of the channel impulse response from which the symbol timing is extracted by searching for the maximal energy of the impulse response in a window of length $(v+1)$ [76].

It was shown in Equation (5.2.6) that depending upon the synchronization delay, the expected value of the power of the first difference term is proportional to the energy of the channel impulse response outside a window of length v. This energy would be minimum (or the energy in a length v would be maximum) when $K' = K$. Thus, K can be

estimated by minimizing J_1 over the symbol timing delay d

$$K' = \min_{0 \le d \le s-1} \sum_{k=1}^{\mathcal{K}} (r(k \cdot s + v + d) - r(k \cdot s + v + N + d))^2 \quad (5.2.8)$$

by transmitting $\mathcal{K}$ symbols. The good thing about this approach is that it is blind and also does not require any FFT and IFFT operation to obtain the synchronization parameter as required by the methods mentioned in [76].

There are two very close variants of the above proposed synchronization method. In [77] the redundancy in the cyclic extension is used to find a timing estimate. It uses the correlation between all of the CP samples and the last v samples in the data portion of the OFDM symbol. This effectively means using v number of difference terms instead of only one as in Equation (5.2.8) to find the timing estimate. A multipath channel smears out the correlation output and the peak often does not correspond to an ISI-free sampling position. Therefore this method is optimal only for a single ray channel [78].

The algorithm presented in [78] is based on an ensemble correlation that is computed across identically positioned samples belonging to several OFDM symbols. This effectively means using only one difference term to find the timing estimate. This method exactly corresponds to the method proposed above in Equation (5.2.8) except that this and the method in [77] have been given for the case when the cyclic prefix is longer than the channel. The good thing about the method in Equation (5.2.8) is it provides a good symbol timing estimate within the framework of the PTEQ scheme. This estimate can be used with 2-tap PTEQ proposed in the next Section for the low complexity equalization

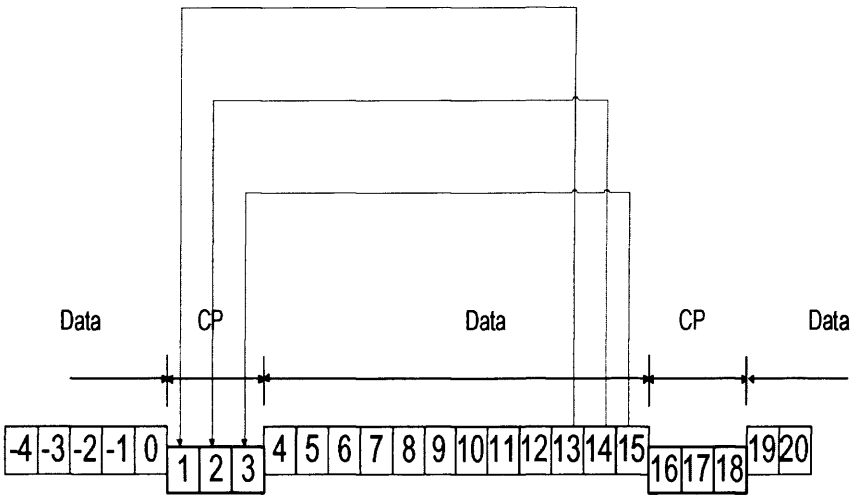

Figure 5.2. Illustration of the PTEQ difference terms in a multicarrier system. N=12, CP=3. If T=CP+1=4, then T-1=CP=3, and if $\delta = 0$, the difference terms are, [r(3)-r(15)], [r(2)-r(14)], and [r(1)-r(13)].

of the multicarrier systems.

5.3 Difference Terms–elaborated

The concepts presented in Section (5.2) are further explained diagrammatically in Figure (5.2). Assume a length 9 channel
i.e., $\mathbf{h} = [h_1\ h_2\ h_3\ h_4\ h_5\ h_6\ h_7\ h_8\ h_9]^T$, where $[h_1\ h_2\ h_3]^T$ constitutes the head of the channel and $[h_4\ h_5\ h_6\ h_7\ h_8\ h_9]^T$ is the channel spread from its peak to the end. Obviously, the value of the CP used in Figure (5.2) is less than the spread of the channel. If perfect synchronization is assumed, then the first difference term $[r(3) - r(15)]$ in Figure (5.3) would be zero if h_1, h_2, h_3, h_7, h_8 and h_9 are zero. It has been suggested in [79,80] that the ISI and ICI caused by insufficient CP are a function of the FFT of the head (which in our example is $[h_1\ h_2\ h_3]^T$) and the tail (which in our example is $[h_8\ h_9]^T$) of the channel impulse response. It is evident that the first difference term energy is proportional to the

energy of the undesirable part of the channel plus the energy of one tap of the desirable or acceptable part of the channel. The second difference term $[r(2) - r(14)]$ would be zero if h_1, h_2, h_6, h_7, h_8 and h_9 are zero. With one additional term, there are two more taps i.e., $[h_6\ h_7]^T$, from the acceptable part of the channel and also the h_3 part of the head has not been taken into account. The third difference term $[r(1) - r(13)]$ would be zero if h_1, h_5, h_6, h_7, h_8 and h_9 are zero. Therefore, the third difference term energy contains $[h_5\ h_6\ h_7]^T$ from the acceptable part of the channel leaving behind only the first tap and as before, the $[h_3\ h_2]^T$ part of the head has not been taken into account. It is clear that as the number of difference terms used is increased, the useful information to calculate the interference is decreased. There is another point to note here. From the nature of the exponentially decaying impulse responses of the CSA channels, the magnitudes of the difference terms tend to increase with their number. For example, at $\delta = 0$, their magnitudes increase with second, third difference term and so on.

If there is negative synchronization error in the system, the position of the head and tail that contribute to ISI and the resulting ICI changes in proportion to the synchronization error. Suppose $\delta = -1$ in the above example, the head and tail of the channel that give rise to interference are $[h_1\ h_2]^T$ and $[h_7\ h_8\ h_9]^T$ respectively. This time the tail is longer than that for the case of perfect synchronization. The first difference term $[r(2) - r(14)]$ would be zero if h_1, h_2, h_6, h_7, h_8 and h_9 are zero. It is evident that the first difference term energy is proportional to the energy of the undesirable part of the channel plus the energy of one tap of the desirable or acceptable part of the channel. The second difference term $[r(1) - r(13)]$ would be zero if h_1, h_5, h_6, h_7, h_8 and h_9 are

$$r(3) = h1\,x(6) + h2\,x(5) + h3\,x(4) + h4\,x(3) + h5\,x(2) + h6\,x(1) + h7\,x(0) + h8\,x(-1) + 9\,x(-2)$$

$$= h1\,x(6) + h2\,x(5) + h3\,x(4) + \boxed{h4\,x(15) + h5\,x(14) + h6\,x(13)} + h7\,x(0) + h8\,x(-1) + h9\,x(-2)$$

$$r(15) = h1\,x(18) + h2\,x(17) + h3\,x(16) + \boxed{h4\,x(15) + h5\,x(14) + h6\,x(13)} + h7\,x(12) + h8\,x(11) + h9\,x(10)$$

$$r(2) = h1\,x(5) + h2\,x(4) + h3\,x(3) + h4\,x(2) + h5\,x(1) + h6\,x(0) + h7\,x(-1) + h8\,x(-2) + h9\,x(-3)$$

$$= h1\,x(5) + h2\,x(4) + \boxed{h3\,x(15) + h4\,x(14) + h5\,x(13)} + h6\,x(0) + h7\,x(-1) + h8\,x(-2) + h9\,x(-3)$$

$$r(14) = h1\,x(17) + h2\,x(16) + \boxed{h3\,x(15) + h4\,x(14) + h5\,x(13)} + h6\,x(12) + h7\,x(11) + h8\,x(10) + h9\,x(9)$$

$$r(1) = h1\,x(4) + h2\,x(3) + h3\,x(2) + h4\,x(1) + h5\,x(0) + h6\,x(-1) + h7\,x(-2) + h8\,x(-3) + h9\,x(-4)$$

$$= h1\,x(4) + \boxed{h2\,x(15) + h3\,x(14) + h4\,x(13)} + h5\,x(0) + h6\,x(-1) + h7\,x(-2) + h8\,x(-3) + h9\,x(-4)$$

$$r(13) = h1\,x(16) + \boxed{h2\,x(15) + h3\,x(14) + h4\,x(13)} + h5\,x(12) + h6\,x(11) + h7\,x(10) + h8\,x(9) + h9\,x(8)$$

Figure 5.3. Construction of Difference terms.

zero. Again as noted above, with the increase in the number of difference terms used, the useful information to calculate the interference is decreased.

If the channel length is smaller than or equal to CP, the transmission is (ISI+ICI) free. In such cases, the PTEQ scheme reduces to con-

ventional equalization in OFDM/DMT systems where equalization is performed with 1-tap FEQ (say 1-tap PTEQ) and it will not use any difference terms. If the spread of the channel energy is greater than the CP, the advantages of 1-tap FEQ equalization do not hold anymore. In such cases, one difference term can be used along with the first tap of the PTEQ, as explained in the previous paragraphs. Two columns of $\mathbf{R}$ would be needed now. This reduces the initialization complexity and the memory requirements of the PTEQ scheme as only $(2 \times N/2)$ equalizer coefficients have to be initialized as compared to $(T \times N/2)$ coefficients. During data transmission, the complexity of the PTEQ scheme is of the order of $F_s T$ [23]. Therefore, this observation also reduces the computational complexity of the PTEQ scheme during data transmission mode. Simulations for ADSL CSA Loop channels show that this 2-tap PTEQ gives maximum achievable bit rates comparable to the case with $(CP + 1)$ tap PTEQ at $\delta = 0$ and is also robust to a reasonable range of negative synchronization errors. For larger negative delays, few additional difference terms are needed as they are not that insignificant at these delays.

In the case of positive synchronization error, the effect on the bit rate is more severe. Positive synchronization error corresponds to processing the received block in an FFT window which is a mixture of two transmitted blocks. Consequently, there is very strong intercarrier and inter symbol interference $(ISI + ICI)$ from the next symbol even if the channel length is smaller than the CP. If the channel length is larger than the CP, there is additional interference from the previous symbol. As in the above two cases, the same analysis based on head and tail of the channel contributing to the interferences can be applied.

The difference is that now first and onward difference terms are significant. Interestingly, the difference terms having number greater than the synchronization error suddenly drop in magnitude. Simulations have shown that for positive synchronization errors, proportional difference terms are required to keep data rates at the maximum value. However, such values of δ would not be used in any practical system [44, 81].

5.4 Simulations

The length two MMSE-PTEQ is implemented by modifying the Matlab code available at [70]. The same method of calculating bit rate is used as explained in previous chapters. However, the signal to noise ratio SNR_i, on each tone i is now based on the estimation of mean square error between input-output data for each tone i. The total bit rate in Equation (3.8.3) is summed over the used tones only. The used tones are $(38 - 255)$ and 4-QAM constellation is used on each of the used tones. The FFT size used is $N = 512$, the CP length is $v = 32$, the power of the transmitted signal is 23dBm and AWGN has $psd_n = -140$dBm/Hz. The equalizer is trained with 511 symbols [70]. CSA loop 1 and 4 with NEXT from 8 disturbers are considered. The synchronization error δ is determined by the relative distance from the first sample index of the channel impulse response window of $(v + 1)$ samples with maximum energy. The effect of δ on the achievable bit rate is simulated. Figure 5.4 shows the achievable bit rate for different lengths of PTEQ equalizer for a range of synchronization errors.

In the case of perfect synchronization i.e., $\delta = 0$, the data block selected for the FFT corresponds exactly to the transmitted IFFT block [81,82], provided the channel length is less than CP. Only one-tap PTEQ would

have been sufficient to equalize the symbols. Because now the channel length is greater than the CP, there is interference (ISI+ICI). An equalizer of length two achieves the same data rates as obtained by a length 33 equalizer. This is because the first difference term gives us a measure of this interference and as we use more difference terms the useful information about this interference is lost. Hence, there is no added benefit in using these redundant difference terms.

This PTEQ equalizer of length 2 gives maximum bit rates until a syn-

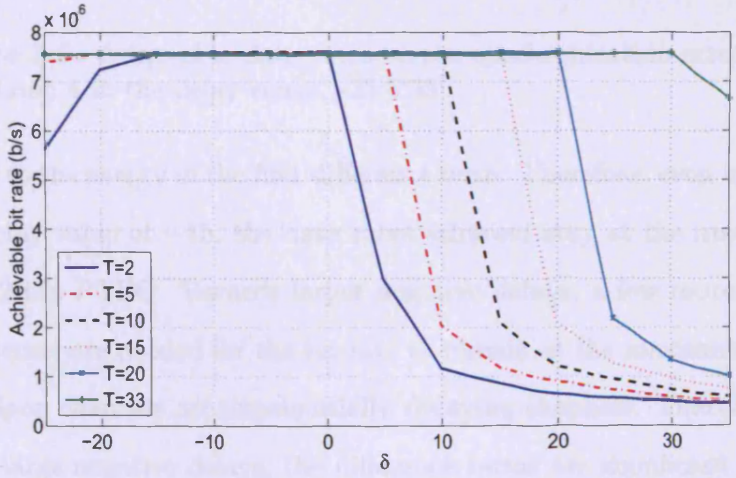

Figure 5.4. Achievable data rates versus synchronization error, δ for CSA Loop 1 in the delay range [-25:5:35].

chronization delay of approximately -15. For negative delays, all the samples in the FFT window belong to the same quasi-periodically extended symbol, if the value of the CP is enough to mitigate the effects of the channel delay spread plus the synchronization error [81,82]. If this is the case the only effect is the phase rotation which can be handled by the 1-tap FEQ (or 1-tap PTEQ). In DMT-based ADSL systems, CP inserted is insufficient, so there will be ISI and the resulting ICI in the received symbol. The value of this interference (ISI+ICI) is propor-

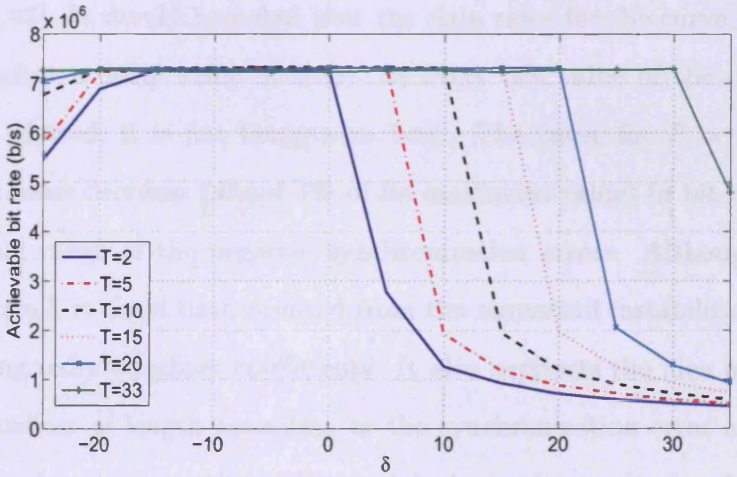

Figure 5.5. Achievable data rates versus synchronization error, δ for CSA Loop 4 in the delay range [-25:5:35].

tional to the energy in the first difference term. Therefore, even up until the delay value of -15, the data rates achieved stay at the maximum for a 2-tap PTEQ. Towards larger negative delays, a few more difference terms are needed for the bit rate to remain at the maximum. The CSA loop channels are exponentially decaying channels. Therefore, at these large negative delays, the difference terms are significant due to longer and significant tails contributing to the interference. Also the first few additional difference terms do not lose their useful information towards the interference calculation. For positive synchronization errors, the PTEQ length is proportional to the error due to the reasons given above.

A 2-tap TEQ has also been suggested in [40] for ADSL CSA loops. A plot similar to Figures (5.4) and (5.5) has been shown in [27] showing that a 3 tap TEQ is sufficient to give maximum bit rates over a fairly long range of delays. The non-symmetrical behavior of an OFDM system with respect to positive and negative delays has also been shown

in [82,83]. It should be noted that the data rates for the curve $T = 33$ drop after a delay value of +33. As every 5th value of the delay is being plotted, it is not being seen here. The curve for $T = 33$ also shows some decrease (about 1% of its maximum value) in bit rates in the mid range of the negative synchronization errors. Although it is very small, it could have resulted from the numerical instability of calculating more equalizer coefficients. It also supports the idea of using an equalizer of length according to the synchronization error and not necessarily a long equalizer. Figure 5.5 shows the results for the CSA loop 4 and similar explanation applies.

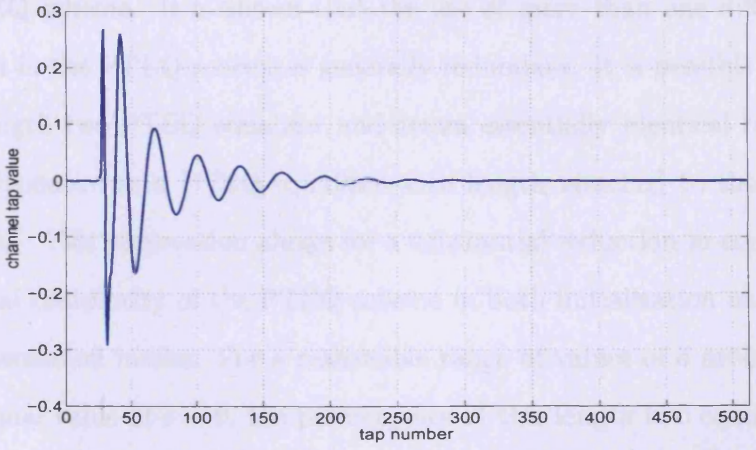

Figure 5.6. Normalized CSA Loop 1 impulse response with upstream filtering.

The synchronization method proposed in the Equation (5.2.8) is simulated to find the synchronization delay for CSA loop channels 1 and 4. Upstream filtering has been included in the channel impulse responses. The normalized CSA 1 channel impulse response is shown in Figure (5.6). The optimum synchronization point for this channel which maximizes channel energy in a window of length $(v + 1)$ is at tap number

27. The proposed method successfully finds the optimum synchronization point for both of the channels. If on the other hand, the difference terms used are equal to the value of CP according to the [77] method, the synchronization delay is wrongly found to be 40.

5.5 Conclusions

In this chapter a low complexity per tone equalization (PTEQ) scheme for discrete multitone (DMT)-based systems has been proposed. A low complexity blind synchronization method is also suggested which is intuitively based on the construction of the difference terms of the PTEQ scheme. It is shown that the use of more than one difference term in the PTEQ scheme is generally redundant. It is possible to use a length two PTEQ equalizer and attain essentially identical bit rate performance as a PTEQ equalizer with length matched to the cyclic prefix. This observation allows for a substantial reduction in computational complexity of the PTEQ scheme in both initialization and data transmission modes. For a reasonable range of values of δ around the optimal value of $\delta = 0$, the performance of this length two equalizer is relatively insensitive to the choice of δ. Therefore, the proposed length two PTEQ equalizer is robust to a range of negative synchronization delays in the system. For positive synchronization delays, however, the required PTEQ equalizer length is proportional to the synchronization error, which is a consequence of strong intercarrier interference ICI in the received signal. As noted above, it is always advisable to avoid late synchronization in multicarrier communication systems.

Chapter 6

CONCLUSIONS AND FURTHER RESEARCH

In this chapter general conclusions are drawn and suggestions for further research are given.

The implementation complexity of a multicarrier communication system is generally less than that of a single carrier system for the same amount of delay spread. This reduction in complexity is to a large extent due to the use of the CP which eliminates the need for an equalizer except for a single FEQ at each subchannel. However, to reduce the bandwidth efficiency loss due to insertion of CP, channel shortening or partial equalization in the form of a TEQ is introduced. The complexity of this partial equalization should, therefore, be kept low in order to keep the superiority of the multicarrier systems over single carrier systems. The throughput loss due to the insertion of the CP can further be reduced indirectly by applying channel shortening algorithms which are blind and do not need training. Furthermore, channel shortening should be made robust to the impulsive noise impairment found in ADSL channels.

Chapter 3 proposes a robust blind adaptive channel shortening algorithm called SAAM. SAAM is based on the concept of property restoral.

In particular, it restores the span of the autocorrelation of the received data input of the TEQ to a short range. The motivation of SAAM is if the channel is short, the autocorrelation of its output should also be short. The algorithm does more than just channel shortening. It makes channel shortening robust to impulsive noise and is also less complex than another similar algorithm SAM. The algorithm achieves bit rates close to those of the MSSNR algorithm of [21] in AWGN conditions. To assess the robustness of the SAAM algorithm, the impulsive noise has been modelled as Gaussian-mixture and as α-stable distributions. Due to the *quasi* minimum phase nature of the channel impulse response of ADSL, a "left" initialization scheme is suggested which further enhances the convergence performance of SAAM. It is found that SAM in its original version requires a large value of the learning parameter i.e., the step size. Its performance can also be improved by applying a suitable smaller step size. The SAAM algorithm uses the l_1-norm of the autocorrelation outside the window of interest and is robust to a greater degree of impulsiveness found in ADSL channels. Alternatively, [68] proposes to use the log of the autocorrelation in a so called *zero statistics* framework. This method can be used to tackle very high impulsive noise. Future work could involve a comparison of such schemes.

SAM can boast of its merits in terms of channel shortening. It is adaptive so has relatively less complexity as compared to other channel shortening algorithms requiring matrix inversions. It is blind so channel shortening benefits in terms of throughput loss saving become twofold. The use of the term blind is a little debatable for SAM as it does require a prior knowledge about the length of the channel impulse response. It

converges faster than another blind adaptive channel shortening algorithm MERRY and can track channel variations within a symbol because it can update once per sample while MERRY updates once every symbol. Another important feature of SAM opposed to MERRY is that, it is independent of the transmission delay Δ. Therefore, an exhaustive search for the optimal transmission delay is not needed. However, SAM has higher complexity than MERRY. SAM also does not have a stopping criterion to freeze the TEQ when the SSNR of the effective channel reaches its maximum or the maximum ISI cancellation point has been reached. Chapter 4 addresses the complexity reduction and convergence issues with SAM [22]. The main argument of this chapter is that effectively identical channel shortening can be achieved by minimizing a single autocorrelation. The proposed SLAM algorithm has, therefore, relatively low complexity. It does not require, a priori, the knowledge of the length of the original channel. Therefore, the SLAM algorithm fully qualifies to be called a blind algorithm. A novel stopping criterion is proposed which freezes the adaptation of the TEQ when maximum SSNR has been achieved. The stopping criterion does not add complexity to the algorithm, and as such, it can be used with SAM as well.

Chapter 5 discusses the alternate equalization scheme called PTEQ for multicarrier systems. Van Acker et al. [23] proposed the PTEQ scheme, in which equalization is performed with a T-tap equalizer for each tone separately after the FFT-demodulation. This scheme enables true signal-to-noise ratio optimization to be implemented for each tone. The resulting capacity of the PTEQ scheme is always higher and a smoother function of the synchronization delay as compared to the

TEQ scheme [23]. The computational and memory requirements of the PTEQ scheme are proportional to the length of the equalizer used. Although the complexities of the PTEQ and the TEQ schemes are approximately the same during data transmission modes [23], the PTEQ scheme has very large complexity during the initialization mode. Its memory requirements are also comparatively very high. A low complexity PTEQ scheme is, therefore, proposed. It is shown that the use of more than one difference term in the PTEQ scheme is generally redundant, given the perfect synchronization. The length of the equalizer is equal to the number of difference terms used plus one. The PTEQ scheme assumes knowledge of the channel impulse response for its reported lease square solution. In this case synchronization point is known and it is possible to use only a length two PTEQ equalizer and attain essentially identical bit rate performance as a PTEQ equalizer with length matched to the cyclic prefix. This observation allows for a substantial reduction in computational complexity of the PTEQ scheme in both initialization and data transmission modes. In this way the equalization complexity can be traded off with the synchronization complexity in the system. Simulations also show that for a reasonable range of values of synchronization error, δ around the optimal values of $\delta = 0$, the performance of this length two equalizer is relatively insensitive. For positive synchronization errors, however, the required PTEQ equalizer length is proportional to the synchronization error, which is a consequence of strong intercarrier interference ICI in the received signal. A low complexity blind synchronization method is also suggested which is intuitively based on the construction of the difference terms of the PTEQ scheme.

The channel shortening algorithms presented in Chapters 3, 4 and 5 are applied to downstream ADSL transmission environments. They are equally applicable to shorten the upstream channels where the direction of transmission is from the subscriber to the telephone exchange. The derivations of the SAAM and the SLAM algorithms have given for the real case. Their extensions to the complex cases are straightforward. Therefore, these algorithms can be potentially applied to the wireless channels in OFDM. PTEQ has already been applied to the wireless channels in [41]. In wireless channels the difference terms are no longer real and it further increases the complexity of the PTEQ scheme. This underlines the importance of our 2-tap PTEQ scheme. MIMO systems are receiving more attention in the context of ADSL as well as OFDM [20, 84]. It is possible to extend the concepts presented in the thesis to the MIMO systems, and this is the subject of ongoing and future research.

Appendix A

ACHIEVABLE BIT RATE

In multicarrier systems, the achievable bit rate R in bits per second is determined based on

$$R = \frac{F_s}{N+v} \cdot \sum_{i=used\ carriers} \log_2\left(1 + \frac{SNR_i^{MFB}}{\Gamma}\right) \tag{A.1.1}$$

where $F_s = 2.208$ MHz is the sampling frequency for downstream ADSL transmission, N is the symbol duration without CP and v is the length of CP. SNR gap Γ is assumed constant across all subcarriers. It corresponds to achieving Shannon channel capacity and is given by

$$\Gamma = \Gamma_{gap} + \gamma_m - \gamma_c \tag{A.1.2}$$

where γ_m and γ_c denote desired noise (system) margin and coding gain respectively. The value of Γ_{gap} is 9.8 dB assuming QAM is used and a probability of symbol error of 10^{-7}. The SNR in each subchannel i is defined as

$$SNR_i^{MFB} = \frac{S_{x,i}|H_i|^2}{S_{n,i}} \tag{A.1.3}$$

where $S_{x,i}$, $S_{n,i}$ are the transmitted signal and channel noise power respectively, and H_i is the channel gain, in the ith subchannel. It is the maximum achievable SNR and hence is denoted as the matched filter

bound (MFB). Note that Equation (A.1.1) is used when the length of the channel is not greater than the length of the CP plus unity.

When channel impulse response length is longer than (CP+1), the TEQ is used to shorten the channel. The performance of the TEQ in terms of achievable bit rate is found by changing the definition of SNR_i. It is given by

$$SNR_i = \frac{S_{x,i}|H_i^{signal}|^2}{S_{x,i}|H_i^{ISI}|^2 + S_{n,i}|H_i^{noise}|^2} \tag{A.1.4}$$

Here H_i^{signal}, H_i^{ISI}, and H_i^{noise} are the gains of the signal path h_i^{signal}, ISI path h_i^{ISI} and the noise path h_i^{noise} in the ith subchannel respectively. Specifically, H^{signal} is the N-point FFT of h^{signal} which is the effective/shortened channel multiplied by a window which has magnitude one for a (CP+1) length and zero elsewhere. H^{ISI} is the N-point FFT of h^{ISI} which is the effective/shortened channel multiplied by a window which has magnitude zero for a (CP+1) length and one elsewhere. The index of the (CP+1) window is determined by the synchronization parameter used by the algorithm. The algorithms SAAM and SLAM do not depend upon the value of the synchronization parameter. For these algorithms, the index which maximizes the energy of the (CP+1) window is used to evaluate their achievable bit rates. H_i^{noise} is the N-point FFT of the TEQ.

However in the PTEQ scheme, for a given synchronization parameter, the value of SNR_i, on each tone i is based on the estimation of the mean square error between the input-output data for tone i and the bit rate is calculated by using Equation (A.1.1).

The material in this Appendix has benefitted from [29].

BIBLIOGRAPHY

[1] R. V. Nee and R. Prasad, *OFDM For Wireless Multimedia Communications.* Boston, London: Artech House Publishers, 2000.

[2] B. L. Evans, "Equalizer Design to Maximize Bit Rate in ADSL Transceivers," *Lecture on ADSL Transceivers.* Dept. of Electrical and Comp. Eng. The University of Texas at Austin [Online July 16, 2006] Available: http://www.ece.utexas.edu/~bevans/projects/adsl/index.html.

[3] P. S. Chow, J. M. Cioffi, and J. A. C. Bingham, "A practical discrete multitone transceiver loading algorithm for data transmission over spectrally shaped channels," *IEEE Trans. on Commun.*, vol. 43, no. 234, pp. 773–775, Feb./Mar./Apr. 1995.

[4] A. V. Oppenheim, R. W. Schafer, and J. R. Buck, *Discrete-Time Signal Processing, 2nd edition.* Prentice-Hall, 1989.

[5] J. A. C. Bingham, *ADSL, VDSL, and Multicarrier Modulation.* New York, US: John Wiley & Sons, Inc., 2000.

[6] D. D. Falconer and F. R. Magee, "Adaptive channel memory truncation for maximum likelihood sequence estimation," *Bell Sys. Tech. Journal*, pp. 1541–1562, Nov. 1973.

[7] G. D. Forney, "Maximum-likelihood sequence estimation of digital sequences in the presence of intersymbol interference," *IEEE Trans. on Info. Theory*, vol. 18, pp. 363–378, May 1972.

[8] I. Medvedev and V. Tarokh, "A channel-shortening multiuser detector for DS-CDMA systems," in *Proceeding of the 53rd Veh. Tech. Conf.*, pp. 1834–1838. vol. 3, Rhodes, Greece, May 2001.

[9] R. K. Martin, "Blind, Adaptive Equalization for Multicarrier Receivers," Ph. D. Thesis, Cornell University, US 2004.

[10] S. I. Husain and J. Choi, "Single correlator based UWB receiver implemetation through channel shortening equalizer," in *2005 Asia-Pacific Conf. on Commun.*, pp. 610–614. Perth, Western Australia, Oct. 2005.

[11] M. Kallinger and A. Mertins, "Room impulse response shortening by channel shortening concepts," in *Proc. IEEE Asilomar Conf. on Signals, Systems and Comp.*, pp. 898–902. Pacific Grove, CA, Nov. 2005.

[12] J. A. C. Bingham, "Multicarrier modulation for data transmission: An idea whose time has come," *IEEE Commun. Magazine*, vol. 28, no. 5, pp. 5–14, May 1990.

[13] R. D. J. van Nee, G. A. Awater, M. Morikura, H. Takanashiand, M. A. Webster, and K. W. Halford, "New high-rate wireless LAN standards," *IEEE Commun. Magazine*, vol. 37, no. 12, pp. 82–88, Dec. 1999.

[14] The Inst. of Electrical and Electronics Engineers, "Air Interface for

Fixed Broadband Wireless Access Systems, MAC and Additional PHY Specifications for 2-11 GHz IEEE Std. 802.16a,". 2003 Edition.

[15] The European Telecomm. Standards Inst., "Radio Broadcasting System, Digital Audio Broadcasting (DAB) to Mobile, Portible, and Fixed Receivers,". ETS 300 401, 19951997.

[16] The European Telecomm. Standards Inst., "Digital Video Broadcasting (DVB); Framing Structure, Channel Coding and Modulation for Digital Terrestrial Television,". ETSI EN 300 744 V1.4.1, 2001 Edition.

[17] D. H. Layer, "Digital radio takes to the road," *IEEE Spectrum*, vol. 38, pp. 40–46, July 2001.

[18] S. Galli, A. Scaglione, and K. Dostert, "Broadband is power: Internet access through the power line network," *IEEE Commun. Magazine (special issue)*, vol. 41, no. 5, pp. 82–118, May 2003.

[19] T. Starr, J. M. Cioffi, and P. T. Silverman, *Understanding Digital Subscriber Line Technology.* Englewood Cliffs NJ: Prentice-Hall, 1999.

[20] H. Bölcskei, "MIMO-OFDM wireless systems: Basics, perspectives, and challenges," *May 2006 Report.* Communication Technology Laboratory ETH Zurich 8092 Zurich, Switzerland.

[21] P. J. W. Melsa, R. C. Younce, and C. E. Rohrs, "Impulse response shortening for discrete multitone transceivers," *IEEE Trans. Commun.*, vol. 44, pp. 1662–1672, Dec. 1996.

[22] J. Balakrishnan, R. K. Martin, and C. R. Johnson, "Blind, adaptive channel shortening by sum-squared auto-correlation minimization

(SAM)," *IEEE Trans. Signal Processing*, vol. 51, no.12, pp. 3086–3090, Dec. 2003.

[23] K. V. Acker, G. Leus, M. Moonen, O. van de Wiel, and T. Pollet, "Per tone equalization for DMT-based systems," *IEEE Trans. Commun.*, vol. 49, no. 1, pp. 109–119, Jan. 2001.

[24] J. S. Chow and J. M. Cioffi, "A cost-effective maximum likelihood receiver for multicarrier systems," in *Proc. IEEE Int. Conf. Commun.*, pp. 948–952. vol. 2, June, 1992.

[25] J. S. Chow, J. M. Cioffi, and J. A. C. Bingham, "Equalizer training algorithms for multicarrier modulation systems," in *Proc. IEEE Int. Conf. on Commun.*, pp. 761–765. Geneva, Switzerland, May 1993.

[26] M. V. Bladel and M. Moeneclaey, "Time-domain equalization for multicarrier communication," in *Proc. IEEE Global Telecomm. Conf.*, pp. 167–171. Nov. 1995.

[27] M. Milošević, "Maximizing Data Rate Of Discrete Multitone Systems Using Time Domain Equalization Design," Ph. D. Thesis, The University of Texas at Austin 2003.

[28] J. F. V. Kerchove and P. Spruyt, "Adapted optimization criterion for FDM-based DMT-ADSL equalization," in *Proc. IEEE Int. Conf. Commun.*, pp. 1328–1334. June 1996.

[29] G. Arslan, B. L. Evans, and S. Kiaei, "Equalization for discrete multitone receivers to maximize bit rate," *IEEE Trans. Signal Processing*, vol. 49, pp. 3123–3135, Dec. 2001.

[30] G. Strang, *Linear Algebra and Its Applications.* Harcourt Brace Jovanovich, Publishers, San Diego, CA, 1988.

[31] C. Yin and G. Yue, "Optimal impulse response shortening for discrete multitone transceivers," *Electronics Letters*, vol. 34, pp. 35–36, Jan. 1998.

[32] R. Schur, J. Speidel, and R. Angerbauer, "Reduction of guard interval by impulse compression for DMT modulation on twisted pair cables," in *IEEE Global Telecomm. Conf.*, pp. 1632–1636. San Francisco, USA, Nov. 2000.

[33] B. Lu, L. D. Clark, G. Arslan, and B. L. Evans, "Fast time-domain equalization for discrete multitone modulation systems," in *Proc. IEEE Digital Signal Processing Workshop.* Hunt, TX, Oct. 2000.

[34] R. Schur and J. Speidel, "An efficient equalization method to minimize delay spread in OFDM/DMT systems," in *Proc. IEEE Int. Conf. Commun.*, pp. 1481–1485. June 2001.

[35] A. Tkacenko and P. P. Vaidyanathan, "Noise optimized eigenfilter design of time-domain equalizers for DMT systems," in *Proc. IEEE Int. Conf. Commun.*, pp. 54–58. May 2002.

[36] A. Tkacenko and P. P. Vaidyanathan, "Eigenfilter design of MIMO equalizers for channel shortening," in *Proc. IEEE Int. Conf. Commun.*, pp. 2361–2364. May 2002.

[37] M. G. Troulis and S. Sesia, "A spectrally flat time domain equalizer for rate improvement of multicarrier systems," in *Proc. IEEE Int. Conf. Commun.*, pp. 1803–1807. May 2002.

[38] R. K. Martin, J. Balakrishnan, W. A. Sethars, and C. R. Johnson, "A blind, adaptive TEQ for multicarrier systems," *IEEE Signal Processing Letters*, vol. 9, pp. 341–343, Nov. 2002.

[39] R. K. Martin, J. M. Walsh, and C. R. Johnson, "Low complexity MIMO blind adaptive channel shortening," in *Proc. In. Conf. on Acoustics, Speech, and Signal Processing.* Montreal, Quebec, May 2004.

[40] G. Arslan, "Equalization for Discrete Multitone Transceivers," Ph. D. Thesis, University of Texas at Austin, 2000.

[41] G. Leus and M. Moonen, "Per-tone equalization for MIMO OFDM systems," *IEEE Trans. on Signal Processing, Special Issue on Signal Processing for MIMO Wireless Commun. Systems*, vol. 51, no. 11, pp. 2965–2975, Nov. 2003.

[42] I. Berhumi, G. Leus, and M. Moonen, "Per-tone equalization for OFDM over doubly-selective channels," in *Proc. Int. Conf. on Commun.*, pp. 2642–2647. Paris, France, June 2004.

[43] K. V. Acker, G. Leus, M. Moonen, and T. Pollet, "RLS-based initialization for Per-Tone equalizers in DMT receivers," *IEEE Trans. Commun.*, vol. 51, no. 6, June 2003.

[44] R. K. Martin and C. R. Johnson, "Blind, adaptive, Per Tone equalization for multicarrier receivers," in *Conference on Information Sciences and Systems.* Princeton University, Mar. 2002.

[45] M. Ding, R. Redfern, and B. L. Evans, "A dual-path TEQ structure for DMT ADSL systems," in *Proc. Int. Conf. on Acoustics, Speech, and Signal Processing*, pp. 2573–2576. April, 2002.

[46] M. Milosevic, L. F. C. Pessoa, and B. L. Evans, "Simultaneous multichannel time domain equalizer design based on the maximum composite shortening SNR," in *Proc. IEEE Asilomar Conf. on Signals, Systems and Comp.*, pp. 1895–1899. vol. 2, Pacific Grove, CA, November 2002.

[47] M. de Courville, P. Duhamel, P. Madec, and J. Palicot, "Blind equalization of OFDM systems based on the minimization of a quadratic criterion," in *Proc. Int. Conf. Commun.*, pp. 1318–1321. Dallas, TX, June 1996.

[48] C. F. Gauss, "Gottingische gelehrte anzeigen," pp. 321–327, 1821. reprinted in Werke Bd. 4, pp. 98-117, 1880.

[49] A. Papoulis, *Probability, Random Variables, and Stochastic Processes.* McGraw-Hill, 3rd edition, 1991.

[50] T. C. Chuah, "Robust Techniques For Multiuser CDMA Communications In Non-Gaussian Noise Environments," Ph. D. Thesis, University of Newcastle upon Tyne, UK, 2002.

[51] S. A. Kassam and H. V. Poor, "Robust techniques for signal processing: A survey," *IEEE Proc.*, vol. 73, pp. 433–481, 1985.

[52] B. Aazhang and H. V. Poor, "Performance of DS/SSMA communications in impulsive channels-Part I: Linear correlation receivers," *IEEE Trans. Commun.*, vol. 35, pp. 1179–1188, 1987.

[53] A. D. Spaulding, "Locally optimum and suboptimum detector performance in a non-Gaussian interference environment," *IEEE Trans. Commun.*, vol. 33, pp. 509–517, 1985.

[54] T. K. Blankenship, D. M. Krizman, and T. Rappaport, "Measurements and simulation of radio frequency impulsive noise in hospital and clinics," in *IEEE Proc. Veh. Tech. Conf.*, pp. 1942–1946, 1997.

[55] P. L. Brocket, M. Hinich, and G. R. Wilson, "Nonlinear and non-Gaussian ocean noise," *J. Acoust. Soc. Am.*, vol. 82, pp. 1386–1394, 1987.

[56] J. H. Fennick, "Amplitude distributions of telephone channel noise and a model for impulse noise," *Bell Syst. Tech. J.*, vol. 48, pp. 3243–3263, 1969.

[57] D. Middleton, "Non-Gausian noise models in signal processing for telecommunications: New methods and results for class A and class B noise models," *IEEE Trans. Inform. Theory*, vol. 45, pp. 1129–1149, 1999.

[58] J. Cook, "Wideband impulsive noise survey of the access network," *BT Technical Journal*, vol. 11, no. 3, pp. 155–162, 1993.

[59] I. Mann, S. Mclaughlin, W. Henkel, R. Kirkby, and T. Kessler, "Impulse generation with appropriate amplitude, length, inter-arrival, and spectral characteristics," *IEEE J. Select. Areas in Commun.*, vol. 20, no. 5, pp. 155–162, June 2002.

[60] "Asymmetric Digital Subscriber Line (ADSL) Metallic Interface," American National Standard T1.413-1995, printed from: The accompanying CDROM in [19].

[61] H. V. Poor and M. Tanda, "Multiuser detection in impulsive channels," *Ann. Telecommun.*, vol. 54, pp. 392–400, 1999.

[62] K. Vastola, "Threshold detection in narrow-band non-Gaussian noise," *IEEE Trans. Commun*, vol. 32, pp. 134–139, 1984.

[63] A. T. Georgiadis, "Adaptive Equalisation for Impulsive Noise Environments," PhD thesis, Edinburgh University, UK, 2000.

[64] C. L. Nikias and M. Shao, *Signal Processing with Alpha-Stable Distributions and Applications.* New York: Wiley, 1995.

[65] E. E. Kuruoğlu, "Signal Processing in α-Stable Noise Environments: An L_p-Norm Approach," Ph. D. Thesis, University of Cambridge, UK, 1998.

[66] B. W. Stuck and B. Kleiner, "A statistical analysis of telephone noise," *The Bell System Technical Journal*, vol. 53, no. 7, pp. 1263–1320, Sep. 1974.

[67] B. W. Stuck, "Minimum error dispersion linear filtering of scalar symmetric stable processes," *IEEE Trans. Auto. Control*, vol. 23, pp. 507–509, 1978.

[68] J. G. Gonzalez, D. W. Griffith, and G. R. Arce, "Zero-order statistics: A signal processing framework for very impulsive environments," in *Proc. IEEE Signal Proc. Workshop on Higher Order Statistics.* Banff, Alberta, Canada, 1997.

[69] J. M. Chambers, C. L. Mallows, and B. W. Stuck, "A method for simulating stable random variables," *J. Amer. Stat. Assoc.*, vol. 71, pp. 340–346, 1976.

[70] G. Arslan and M. Ding and B. Lu and Z. Shen and B. L. Evans. MATLAB DMTTEQ Toolbox 3.1, Univ. Texas, Austin, May 10, 2003,

[Online.] Available: http://www.ece.utexas.edu/~bevans/projects/adsl/dmtteq/dmtteq.html.

[71] S. Haykin, *Unsupervised Adaptive Filtering, Blind Deconvolution.* New York, US: John Wiley & Sons, Inc., 2000.

[72] M. Ding, "Channel Equalization To Achieve High Bit Rates In Discrete Multitone Systems," Ph. D. Thesis, The University of Texas at Austin, 2004.

[73] M. Webster and R. Roberts, "Finite length equalization for FFT-based multicarrier systems an error-whitening viewpoint," in *Proc. of the* 31^{th} *Asilomar Conference on Signals, Systems and Computers*, pp. 555–559. Nov. 1997.

[74] H. Dai and H. V. Poor, "Crosstalk mitigation in DMT VDSL with impulse noise," *IEEE Trans. Circuits and Systems–I: Fundamental theory and applications*, vol. 48, no. 10, pp. 1205–1213, Oct. 2001.

[75] Z. Ding and R. A. Kennedy, "On the whereabouts of local minima for blind adaptive equalizers," *IEEE Trans. Circuits and Systems–II: Analog and Digital Signal Processing*, vol. 39, no. 2, pp. 119–123, Feb. 1992.

[76] T. Pollet and M. Peeters, "Synchronization with DMT modulation," *IEEE Commun. Magazine*, pp. 80–86, 1999.

[77] J. J. van de Beek, M. Sandell, and P. O. Borjesson, "ML estimation of time and frequency offset in OFDM systems," *IEEE Trans. Signal Processing*, vol. 45, no.7, July 1997.

[78] K. Ramasubramanian and K. Baum, "An OFDM timing recovery scheme with inherent delay-spread estimation," in *Proc. of IEEE GLOBECOM*, pp. 3111–3115. Nov. 2001.

[79] T. Pollet, H. Steendam, and M. Moeneclaey, "Performance degration of multi-carrier systems caused by an insufficient guard interval duration," in *International Workshop on Copper Wire Access Systems (CWAS '97), Bridging the Last Copper Drop.* Budapest, Oct. 1997.

[80] W. Henkel, G. Taubock, P. Ödling, P. O. Börjesson, and N. Petersson, "The cyclic prefix of OFDM/DMT–An analysis," in *International Zurich Seminar on Broadband Communications Access-Transmission-Networking.* ETH Zurich Switzerland, Feb. 2002.

[81] M. Engels, *Wireless OFDM Systems, How to make them work?* Boston: Kluwer Academic Publishers, 2002.

[82] L. Hanzo, W. Webb, and T. Keller, *Single- and Multi-carrier Quadrature Amplitude Modulation, Principles and applications for Personal Communications, WLANs, and Broadcasting.* Chichester, U.K.: Wiley–IEEE press, 2000.

[83] Y. Mostofi and D. C. Cox, "Analysis of the effect of timing synchronization errors on pilot-aided OFDM systems," in *37th Asilomar Conf. on Signals, Systems and Computers.* Monterey, California, November 2003.

[84] G. Ginis and J. M. Cioffi, "Vectored transmission for digital subscriber line systems," *IEEE Journal on Select. Area in Commun.*, pp. 1085–1104, June 2002.